La Rivista del Nuovo Cimento (2023) 46:521–618
https://doi.org/10.1007/s40766-023-00047-4

REVIEW PAPER

Clusters in light nuclei: history and recent developments

Ivano Lombardo[1,2] · **Daniele Dell'Aquila**[3,4]

Received: 25 June 2023 / Accepted: 28 August 2023 / Published online: 9 November 2023
© The Author(s) 2023

Abstract
In this review, we discuss recent advancements in the study of clustering phenomena occurring in light nuclei, and their influence on nuclear structure, dynamics, and astrophysics. In the introduction, we outline the historical steps leading to the concept of α-clusterization in nuclei and provide a comprehensive description of the evolution of nuclear models capable to describe clustering aspects in nuclear systems and of the main experiments and discoveries leading to the development of this research field. We also describe some spectroscopic techniques that are used to establish the clustered nature of a given nuclear state. Some relevant experimental and theoretical findings recently reported both in experimental and theoretical works are discussed in the text. We put emphasis on recent achievements and remaining problems in the description of the structure of light isotopes, from helium to neon, including both self- and non-self-conjugate nuclei. Particular attention to the implication in the nuclear astrophysics context and to clustering effects in the dynamics of nuclear reactions is pursued all along the review.

Keywords Clusters in nuclei · Alpha-clustering · Nuclear molecules · Nuclear spectroscopy · Cluster models

1 Introduction

The static properties and the dynamical evolution of many-body systems in nature are determined by the properties of the *potential energy* of the system. In particular,

✉ Daniele Dell'Aquila
daniele.dellaquila@unina.it

Ivano Lombardo
ivano.lombardo@ct.infn.it

1 Dipartimento di Fisica e Astronomia "E. Majorana", Università di Catania, Via S. Sofia 64, 95123 Catania, Italy

2 INFN, Sezione di Catania, Via S. Sofia 64, 95123 Catania, Italy

3 Dipartimento di Fisica "E. Pancini", Università di Napoli Federico II, Via Cintia, 80126 Naples, Italy

4 INFN, Sezione di Napoli, Via Cintia, 80126 Naples, Italy

physical systems find more *convenient* reaching stages characterized by lower values of the corresponding potential energy, resulting in a gain in *stability*. A genuine effect of this aspect is represented by the common tendency of the elementary constituents of a system to congregate in sub-units, often indicated as *clusters*. This peculiar and *ubiquitous* phenomenon, which is commonly referred as *clustering*, is present in a large varieties of physical systems and in an extremely broad range of length scales: in astrophysics, with the clusters of stars and galaxies; in the micro-physics domain, with clustering of atoms and molecules; and even in social science and biology, where several human or animal behaviors can be explained in terms of sub-aggregation of independent subjects.

The aim of this report is to review some recent results linked to the occurrence of α-clustering in atomic nuclei. This subject is very broad, involving the structure of light nuclei, the presence of molecular-like structures formed in nuclear reactions, the occurrence of cluster decay from very heavy nuclei, the impact on astrophysics of clustering, the structure of hyper-nuclei, and many other aspects that have been well referred and discussed at general conferences on Nuclear Physics and, in particular, in the well-known series of International Conferences on Clustering Aspects on Nuclear Structure and Reactions (started in 1969, with 11 editions up to now) and, more recently, in the Status of Art on Nuclear and Cluster Physics (SOTANCP) Workshop. Excellent books and review papers on clustering are also available in the literature (among the others, see. e.g., [1–9]), forming a complete introduction to all the topics related to clustering in nuclear physics. In the present review, we will discuss some of the published results coming from the last 5 years of experimental and theoretical studies on clustering in light nuclei; even if we tried to be as inclusive as possible, we are aware that we could have missed some important findings and we apologize in advance for this. The review is preceded by an extended historical note on clustering that (we believe) could represent a stimulating starting point for much more broad historical and biographical investigations, and by an introduction to (some of) the models, techniques, and strategies commonly adopted in the discussion of clustering aspects in light nuclei.

2 Clustering in nuclei: a historical overview

The origins of the cluster model for the atomic nucleus are commonly traced back to the very beginning of nuclear physics. Soon after the discovery of alpha radioactivity by Becquerel, and Marie and Pierre Curie, and after the identification that α particles were nuclei of ^{4}He atoms (Rutherford, see e.g., [10]), several scientists supposed that nuclei could be composed of α particles, stably residing inside the atomic nucleus. An example of a nuclear model of this type was proposed by George Gamow in 1930 [11]. With the large body of data coming from nuclear reactions during the 30s, and the breakthrough discovery of the existence of the neutron (Chadwick, 1932), such naive approaches were quickly abandoned, in favor of a more reliable vision of the nucleus as constituted by *protons* and *neutrons* (e.g., Fermi gas model [12], and Liquid Drop Model (1935) [13]). In 1935, Werner Heisenberg proposed a theory of α–α interactions that included in a qualitative way the presence of exchange forces and

considered the possible analogy with interactions between atoms of noble gasses [14]. This α–α interaction was then used to describe the behavior of nuclei, and the results were compared with predictions made using nucleon–nucleon interactions. Since both the approaches had their limits in the description of data, Heisenberg deduced that a more solid description of nuclei could be characterized by an intermediate behavior between the two models. In 1936, Bethe and Bacher [15] critically reviewed the coeval nuclear models using α particles as constituents, arriving at the conclusion that the adverse arguments against the α model were more effective than the favorable ones.

A change of perspective occurred in 1937, the *golden year* of α-clustering in nuclei. It was in this year, in fact, that Wilfried Wefelmeier, a German physicist,[1] clearly noted the extra-stability, in terms of binding energy, of $N = Z$ even–even nuclei, as ^{12}C, ^{16}O, ^{20}Ne, and proposed that they could be considered as formed by α particles arranged, in a molecular-like fashion, to form peculiar and regular geometries [17]. Wefelmeier attached, even on an epistemological basis, the considerations of Bethe and Bacher, and underlined that the α-like particles at the basis of his model were *transient* units, with a short-lived identity, but nevertheless dynamically influencing the whole structure of the nucleus. In a biographic note, Carl Friedrich von Weizsäcker[2] recognized the priority of the alpha geometric model of the nucleus to Wefelmeier and indicates, possibly, one of the causes of the progressive reduction of Wefelmeier's scientific activities: the insurgence of a progressive disease leading to his death at only 35 years [16]. Wefelmeier did not limit the applicability of the α model of the nucleus just to self-conjugate nuclei, but applied it also for heavy nuclei [17, 18]; in this framework, he tried to explain the different branching ratio toward α- or β-decay in actinide and transuranic nuclei, evidenced by Lise Meitner [19], considering the different shapes predicted by his model.[3] A beautiful overview of the Wefelmeier's model is described in [23]. Curiously, in his main article on α-clustering in nuclei [17], Wefelmeier warmly thanked his old mentor in Bern, Rudolph Signer, at that time non-tenured professor of inorganic chemistry, who, some decades after, would have become one of the fathers of the discovery of the DNA double helix. It is, therefore, possible that some of the seeds of the α model of the nucleus were planted during the discussions between Wefelmeier and Signer in Bern in the period 1935–1936,

[1] Wefelmeier was essentially a *freelance* scientist, with a complex and introvert personality, often in contrast with the academic and politic institutions in the Germany of his time. In the obituary dedicated to him by C.F. von Weizsacker [16], he noted: *"In science, he was distinguished by complete originality of questions, productive imagination and constant vivid display of rich empirical material. He was born to be an outsider.* [...] *In 1937, when I convinced him to work for a period in our institute, I told him: "You are a corsair. But don't you think that having served some time in the regular army can also help you in this profession?" He accepted this point of view, came and stayed for 6 years."* (translated from the German). Curiously, Wefelmeier was not formed as a physicist, but he studied Chemistry and Economic science [16].

[2] The first textbook on nuclear physics introducing for the first time the cluster model of the nucleus was the famous Weizsacker's "*Die Atomkerne—Grundlagen und Anwendungen ihrer Theorie*" (Akademische Verlagsgesellschaft, Leipzig 1937).

[3] Despite the solicitations of von Weizsacker, Otto Hahn refused three times to meet Wefelmeier to discuss with him on possible theoretical explanation of fission (based on the "kernwurst" model introduced by Wefelmeier). No citation to Wefelmeier's works is reported in the subsequent articles by Hahn and Meitner, even if Otto Frisch found some concepts of the Wefelmeier's model very useful to understand the parameters of fissile nuclei [20]. For a detailed historical perspective of physics in Berlin at the end of 30s and on the discovery of fission, see also [21, 22].

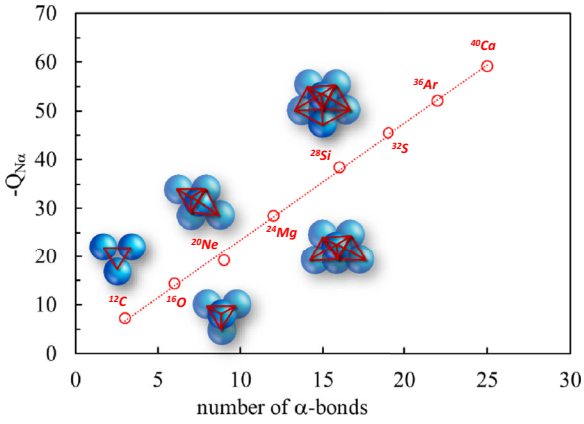

Fig. 1 An artistic overview of the α cluster model by Wefelmeier, Wheeler and Hafstad–Teller. Geometrical arrangements of clusters in self-conjugate nuclei are pictorially indicated in correspondence to the number of bonds between α particles. The almost linear relationship between the number of bonds and the energy needed to disintegrate a self-conjugate nucleus into its $N\alpha$ cluster is indicated by the dotted line. See also [25]

and, subsequently, germinated with more thorough discussions in Berlin with von Weizsacker. Almost contemporary to Wefelmeier's work, John Archibald Wheeler developed also his cluster model of the nucleus [24], with many concepts borrowed from the Chemistry world and several contact points with Wefelmeier's work.

In the same period, a young student of the Fermi school, Ugo Fano (at that time visiting researcher at Leipzig), considered, for the first time, the effect of the Pauli exclusion principle on the behavior of the wave function of one extra-nucleon in Wefelmeier's model: the density distribution of the odd-nucleus should be far away from the concentration of α clusters [26]. If the alpha particles constituted an elongated regular structure, as indicated by Wefelmeier for nuclei with $Z \approx 71$, the orientation of the orbital angular momentum of the odd proton should have stayed along the longitudinal axis of the figure, explaining the positive value of the quadrupole moment [26, 27]. Similar arguments were applied also to explain the known trend of magnetic moments [28]. After the pioneering works of Wefelmeier, Wheeler, and Fano, at the end of the 30's, there was a strong development of the α model of the nucleus: Hafstad and Teller [29] and Dennison [30] were able to predict the existence and the position of some excited states in self- and non-self-conjugate nuclei, reinforcing the idea that the regularity of the observed binding energies in light nuclei should be ascribed to the number of bonds between two α-particles (see Fig. 1).

The only nucleus slightly deviating from the astonishing linear trend of the α-binding energy as a function of the number of bonds was ^{20}Ne (see Table 1): the trigonal bi-pyramid arrangement accounted for 9 bonds, while the agreement with the other points would have been a bit better if a number of 8 effective bonds was considered. Indeed, Wefelmeier suggested that the bond connecting the two alphas at the opposite vertex of the bi-pyramid would be much less effective than the others because of the large distance involved and the shadowing effect due to the distribution of the remaining three αs in the central plane.

Interestingly, this model was extended also to non-self-conjugate nuclei, as ^{56}Fe: in such case, 13 α particles should form a centered icosahedron with 42 bonds, with the remaining four neutrons playing a minor role in the overall structure of the nucleus. Indeed, the observed alpha binding per bond is not so far (just 15% smaller) from the value observed for lighter self-conjugate nuclei, giving support to the model [27].

Table 1 Geometrical configurations proposed by [17, 31, 32] for the first self-conjugate nuclei

Nucleus	N. of α-s	Configuration	N. bonds	α-binding energy (MeV)	α-binding energy per bond (MeV)
^{8}Be	2	Straight line	1	−0.092	−0.092
^{12}C	3	Triangle	3	7.275	2.425
^{16}O	4	Tetrahedron	6	14.437	2.406
^{20}Ne	5	Trigonal bipyramid	9	19.167	2.130
^{24}Mg	6	Tetragonal bipyramid (octahedron)	12	28.483	2.374
^{28}Si	7	Pentagonal bipyramid	16	38.467	2.404
^{32}S	8	Sphenoidal bipyramid	19	45.415	2.390

The number of bonds is indicated together with the α-binding energy and the α-binding energy per bond

In deriving their alpha model, Wefelmeier, Wheeler, and Hafstad and Teller clearly considered the α clusters inside nuclei as short-lived structures: after a certain time interval, they would dissolve inside the nucleus and then, from nucleons inside the nucleus, another α-particle can be formed, and so on [33]. In this context, it was fundamental to estimate, in a semi-classical way, the degree of stability (and the corresponding lifetime) of an α-like particle in the nucleus, in comparison with the period of vibration or rotation of excited nuclei [27]. A first attempt of this type was made by Wheeler [24], who defined the *lability* of an α cluster in a given vibrational state of a nucleus as the time required by such a cluster to exchange a proton or a neutron with its surroundings moving in opposite phase. Semi-classical considerations based on the Rayleigh formula for normal modes of vibrations led Wheeler to observe that the survival time of the cluster was well larger than the typical vibration time of the nucleus. This finding suggested the impact of α clustering in determining the structure of excited states of nuclei. Another great merit of Wheeler was the introduction of the Resonating Group Model of a nucleus at the end of the 30s [34], with the possibility of expressing the wave function of a nucleus as a linear combination of different clustered structures contributing with different weights to its structure.

In all such considerations, it was early evident that a solid knowledge of the spectroscopy of excited states in ^{8}Be and ^{12}C would have been extremely useful to understand the applicability and the details of the α model. In this context, unfortunately, some contradictions occurred in the 30s, leading to several shortcomings in the interpretation of data. The first excited state of ^{8}Be, i.e., the famous 3.0 MeV broad 2^{+} state, was discovered by Dee and Gilbert [35] in 1936. After some months, Feenberg and Wigner, starting from theoretical considerations, suggested a $J = 2$ nature for such a state [36] and foresaw that the broad width should be associated with an easy disintegration of this state into two α-particles not well bound by the Coulomb barrier. A new experiment on α+^{4}He scattering, made by Samuel Devons in

1939 [37], and the subsequent data analysis in terms of partial waves contributing to the scattering differential cross section, confirmed the $J = 2$ assignment. However, in 1941, Wheeler [38] performed a new comprehensive review of α+^{4}He scattering data, and from a very elegant phase shift inspection based on Complex Analysis, deduced a 0^+ assignment for the first excited state in ^{8}Be, leading to strong difficulties in the description of ^{8}Be α structure on a simple geometrical basis and complicating the groundings of the α model. It is worth noting that Wheeler's results were questioned only at the beginning of 1950, especially by analyzing the behavior of ^{8}Li beta decay data, see [39].

The same discouraging condition affected the spectroscopy of ^{12}C. In 1936, Gilberto Bernardini and Daria Bocciarelli in Florence [40] and Heinz Maier-Leibnitz in Heidelberg [41] analyzed the ^{9}Be(α,n)^{12}C reaction induced by radioactive alpha emitters on a thin ^{9}Be film, finding that several groups of neutrons were observed (Florence and Heidelberg) and that associated gamma radiation was present (Heidelberg). From kinematic analysis, they suggested the occurrence of states at about 4.4 (clearly evident from the neutron analysis of Bernardini and Bocciarelli) and 6.3 MeV (quite a weak neutron group). No solid information on the spin of the state was reported until the 50s [39]; just a tentative 2^+ or 0^+ assignment for the 4.4 MeV state was reported in [27]. The situation was a bit better for the ^{16}O case, thanks to the study of α+^{12}C scattering and on the ^{19}F(p,α)^{16}O reaction [27, 39, 42, 43]. Naturally, with such poor spectroscopic information, all the speculations made with the alpha cluster (or other) models at that time were just tentative and often subject to contradictory discussions.

Anyway, the success of the α model of the nucleus in describing the binding energy of the ground state of self-conjugate nuclei led several authors to investigate in more detail the characteristics of the α+α interaction, as it can be inferred from the elastic scattering of α particles on ^{4}He and from the structure of the ^{8}Be nucleus. In doing this, some of them often applied the "Hartreee model of nuclei" [44] (an independent particle approach, based on the theory of nuclear forces available at that time) to determine the binding energies of self- and non-self-conjugate nuclei with perturbative corrections of increasingly large order, leading to the formation of clusters. Grönblom and Marshak [45], Margenau [46], and Wergeland [47] attempted to introduce, in a quantitative way, the effect of exchange forces in the description of the interaction between multiple α particles, finding that the effect of exchange forces was of the same order of magnitude and with a similar range as the ordinary van der Waals-like attraction; this feature would lead to the lack of additivity of the interactions between three or more α particles, in striking contrast with the atomic physics case. In this sense, the apparent additivity of the energies of the α particle bonds was considered as a fortuitous results of much more complex, and essentially non-additive, interaction effects [45]. Other shortcomings of the α model were related to the difficulty in the description of the so-called $4n + 2$ nuclei: the predictions for a self-conjugate nucleus with two extra-nucleons were different from the ones obtained starting from the subsequent self-conjugate nucleus with two holes [25]. Better success was instead seen in the description of $4n \pm 1$ nuclides [27].

Intense research activities on the emission of light clusters during the slow-neutron-induced fission of ^{235}U were performed during the 40's and the early 50s; an early communication by Richard Present (1941) based on the analysis of potential energy

profiles of fissioning nuclei, indicated as dynamically possible a ternary scission of heavy nuclei in the context of the liquid drop model with deformation. In particular, the work by Ernest Titterton [48] especially focused on *ternary fission* events where an high-energy α particle accompanied the two fission fragments; accurate analysis of emulsions showed that αs were emitted with an average energy of $\simeq$ 15 MeV and with an angular distribution strongly peaked at 90° with respect to the fission axis. It is interesting to notice that (more rare) ternary fission events with the emission of clusters heavier than an α particle (with mass numbers up to 9) were also observed in the same period (see, e.g., the work of [49] at the College de France).

The introduction of the nuclear shell model at the end of the 40s led to an eclipse of the α model. The shell model was in fact much more powerful in the description of the spectroscopy of medium to heavy nuclei, concerning both ground state and excited states properties. Some problems, anyway, were still persisting on the structure of very light nuclei (see, e.g., [50]). A typical example was the structure of the ^{6}Li ground state: since the end of the 40's, it was known that it has $J^\pi = 1^+$, $\mu = 0.822\mu_N$ and a tiny quadrupole momentum. The last feature would point out the presence of four nucleons saturating the 1s shell and the remaining two "valence" nucleons in the 2s shell, with parallel spins coupled to give the $J^\pi = 1^+$ value; with such a structure, that would strongly reflect a α-deuteron cluster structure, the predicted magnetic dipole moment would be $\mu = 0.88\mu_N$, quite close to the experimental value. This scheme was in *total disagreement* with shell model predictions and beautifully pointed out the cluster nature of ^{6}Li; similar arguments were found also for ^{7}Li.

In the same period, much more refined experimental observations of the spectroscopy of light nuclei were reported in the literature. For example, in 1951, Guier et al. [51] investigated at Evanstone the states of ^{12}C produced with the ^{9}Be(α,n) reaction induced using a thin α source bombarding an ultra-thin Be foil. The analysis of neutron groups pointed out the existence of a state close to 7.5 MeV. Two years later, Harries in Oxford [52] performed the same reaction using a cloud chamber to directly detect the electron–positron pairs emitted by the 4.4 MeV state of ^{12}C. The angular distribution of the pairs was in excellent agreement with the predictions from a decay of a 2^+ state. Very interestingly, 7 events of pairs with a total energy of 7.0 ± 0.6 MeV were reported, and since no γ-radiation was seen in the region of 7 MeV, he assigned this state as a candidate 0^+. In the same period, Fred Hoyle, starting from the considerations made by Salpeter and Opik [53], discussed the possibility that the rate of the triple-α process in red giants could strongly be enhanced by the presence of a resonant state in ^{12}C with a 0^+ nature and excitation energy slightly above the 3α threshold (7.27 MeV). At the end of 1953, a dedicated high-resolution experiment of the ^{14}N(d,α) reaction at the Kellogg laboratory (CalTech) by the group of Ward Whaling [54] unequivocally confirmed the existence of the state predicted by Hoyle, at apparent energy of 7.68 MeV.[4] A few years later (1957), again at CalTech, the group of William Fowler [55] investigated the beta decay of ^{12}B, and the "Hoyle state" was quite firmly assigned as 0^+.

[4] To perform this experiment, Whaling used a very large magnetic spectrometer that should be moved from its original hall. To move the spectrometer, he and his collaborators used hundreds of *tennis balls*, under a plate on which the spectrometer sat. "Sure enough, we moved that darn thing down the hall, rolling it", Whaling recalled in an interview given at CalTech.

It was observed at the end of the 50s that the J^π and the position of the Hoyle state and of a number of other excited states in self-conjugate nuclei (as the 6.05 MeV, the second 0^+ state in ^{16}O) were very difficult (or even impossible) to be described in the framework of the shell model. This observation, together with the availability of new data on electron scattering on light nuclei and, consequently, of a more accurate mapping of their density distribution, leads to a resurgence of the cluster model of the nucleus. For example, Dennison [56] tried to describe the known excited states of ^{16}O in the framework of the α model; the difficulties seen in the description of the second 0^+ state of ^{16}O lead Morinaga [57] to suppose the possible existence of a linear-chain of α-particles to describe the structure of this state and also of the Hoyle state in ^{12}C. The search for members of the rotational bands built on the Hoyle state and on the 6.05 MeV state of ^{16}O represented a long hunt in nuclear spectroscopy that is beautifully described, for example, in the series of proceedings of the Cluster conferences.

On a more general theoretical ground, in 1958, a seminal work of Karl Wildermuth and Themis Kanellopoulos [58] at CERN introduced a new cluster model for particles moving independently in a harmonic oscillator potential. In this case, thanks to the intrinsic properties of the potential, the global wave functions can be separated in terms of clusters of particles in relative motion; if interactions are added, the lowermost energy states are expected to be the ones where the clusters are unexcited, but they are in different states of relative motion. One year later, Benjamin Bayman and Aage Bohr [59] demonstrated the strong connections between the cluster model of Wildermuth and Kanellopoulos and the coeval model developed by James Philip Elliott using the $SU(3)$ group theory to investigate the occurrence of collective motions in the framework of the shell model [60]. All these models played a leading role in the theoretical calculation of α particle *spectroscopic amplitudes*, linked to the degree of clusterization of a given state in a nucleus (see Sect. 3 for further discussions).

At the end of the 50s, there was also a renewed interest in understanding the details of α-decay. In 1958, George Igo performed an optical model analysis of α scattering data on medium to heavy nuclei, carefully determining the shape of the potential seen by an α particle from the nuclear surface to outside [61]. One year later, John Rasmussen performed accurate penetrability calculations in the WKB approximation by using the Igo potential and taking also into account the possible presence of the centrifugal barrier [62]. This procedure allowed to re-determine the reduced α widths (see Sect. 6.1), linked to the pre-formation probability of an α particle in the parent nucleus, for a large series of even–even emitters in the $Z = 84$–100 region. The effect of the shell closure at $N = 126$ was clearly demonstrated from the trend of the reduced α width distributions. In 1960, Hans Mang succeeded in reproducing the *relative* trends of the reduced α width distributions for odd and even Polonium and Astatine emitters on the basis of *pure shell model* calculations; the observed problems in the description of the *absolute* values of the widths were attributed to the presence of clustering effects close to the nuclear surface not well taken into account in the conventional configuration mixing used to perform the calculations [63].

The possible reconciliation between shell model calculations and the occurrence of clustering was a problem in fashion during the 60s also for the description of the structure of light self-conjugate nuclei in the framework of the shell model. In general, it was observed that when a residual interaction between nucleons is included, the

solution of the many-body problem for light nuclei could lead to spurious states and missing configurations that can be overcome by considering α-clusterization (see e.g., the discussions in [64, 65] for the ^{16}O case). In the same period, it was proposed also to use the generator coordinate method of Griffin, Hill, and Wheeler [66] to describe the clustered nature of states in light nuclei; a historical example can be found in the paper by Brink and Weiguni [67] for the description of the structure of ^{20}Ne. The Alpha Cluster Model proposed by Brink et al. [68] as an extension of the old work by Margenau [46], was subsequently used to describe the cluster structure of several self-conjugate nuclei (see, e.g., [65, 69]). Another mathematical model for clustering, developed by Yuri Smirnov and collaborators in Moscow, allowed the calculation of electric transitions strengths $E\lambda$; from the comparison with experimental data, a large degree of α clustering in ^{9}Be was seen, with an isolation extent of α clusters well larger than the one typically predictable by shell model calculations [70].

The route toward the understanding of clustering was widened at the end of 50s by an important technical discovery made at the Fermi Institute of the University of Chicago: the development of a new source able to produce Lithium ions [72, 73], subsequently accelerated to 2.1 MeV by a van der Graaf accelerator.[5] With this facility, George Morrison performed in 1961 some studies of (^{6}Li,d) and (^{7}Li,t) reactions at 2.1 MeV on ^{6,7}Li targets that pointed out, for the first time, the possible occurrence of α-*transfer* mechanisms, and suggested this type of reactions as a powerful tool to study the clustering in light nuclei. Several α-*transfer* reactions were studied during the 60s and the 70s, both in the stripping and pick-up modes, leading to the determination of α spectroscopic factors (indicated as S_α and linked to the degree of α clusterization in a given nucleus, see Sect. 3 for theoretical details) in nuclei of the p and sd shells. A detailed discussion of all the experimental S_α values obtained during the 60s and 70s was reported in the review work of Fulbright [74]. The simultaneous development of a theory for particle–particle angular correlations in the sequential decay of unbound excited states allowed also to determine unambiguously the spin and parity of several excited states; one of the pioneer investigations using this technique was made by the group of Artemov and Goldberg at the Kurchatov Institute for the study of α cluster states in ^{16}O [75], followed few years later by similar analyses of the Catania-Saclay group on several oxygen isotopes [76, 77].

During the 60s, four seminal discoveries were made concerning clusters in light nuclei, and we discuss them in more detail in the following:

First, in 1960, the Chalk River group of Bromley and Almqvist [78, 79] observed the presence of broad structures in the excitation functions of cross sections of elastic

[5] This discovery was due to the group of Samuel Allison, director of the Fermi Institute, and in particular to John Edwin Norbeck, at the time young Ph.D. student in Chicago. Norbeck, in particular, was formed as a chemist, with strong interests on radio-chemistry and chemistry of explosives. To obtain a stable Li source, they coated the platinum filament of the source with synthetic β-eucryptite powder. As indicated by Norbeck, the possibility of using natural eucryptite as source of Li ions was suggested in 1955 by Leviant and collaborators in a Proceeding of the USSR Academy of Science. In earlier times (1936), Bernard Kinsey succeeded in producing 1 MeV ^{7}Li beams at Berkeley with a different technique. The high intensity beam ($\simeq$ 10 μA) was driven on Li and Be targets, but no reactions with high-energy ejectiles were registered; indeed, if the energy was been just few hundreds of keV higher, the overcoming of barrier would have lead to plenty of reactions and the discovery of previously unknown radioactive isotopes as ^{13}B and ^{15}C. For discussions on such aspects, see [73].

scattering and reactions between heavy self-conjugate nuclei (especially in $^{12}C+^{12}C$), at energies close to Coulomb barrier. This breakthrough was made possible by the combined use of a newly developed *Tandem* van de Graaf accelerator and high-resolution solid-state detectors. The average widths of the observed structures ($\approx$ 100 keV, with average spacing between peaks of $\approx$ 300 keV) show an intermediate behavior between the typical values expected for compound nucleus resonances and for potential scattering resonances, and this posed several questions in the interpretation of the results. A possible answer, based on the characteristics of the optical model, hypothesized the occurrence of a *secondary* minimum in the $^{12}C+^{12}C$ scattering potential to explain the data, but the origin of such a minimum was still obscure at that time. Another possibility suggested by the Bromley's group was the formation of a *nuclear molecule*, seen as a sort of *dinucleus* made by the two interacting carbon nuclei in close contact, during the early phase of the collision. At the end of the 60s, a paper by Vogt and Michaud [80] illustrated the connections between the α cluster description of a ^{12}C nucleus and the observed structure in the $^{12}C+^{12}C$ reactions; in particular, α–α interactions between the two reacting nuclei would give rise to *doorway states* with characteristics similar to the broad structures seen experimentally. In the same period, Imanishi and co-workers at Tokyo University underlined the fundamental role played by the *inelastic coupling* to excited states in the colliding partners to explain the experimental data [81].

The second breakthrough of the 60s related to clusters in nuclei was the discovery of incomplete fusion phenomena by Harold Britt and Arthur Quinton at the HILAC accelerator in Yale, in 1961 [82]. They investigated the emission of α particles and protons in reactions induced by carbon, nitrogen, and oxygen beams on gold and bismuth targets, at energies around 10 MeV/nucleon. To detect α particles and protons, they used a telescope detector made by a proportional counter followed by a thick

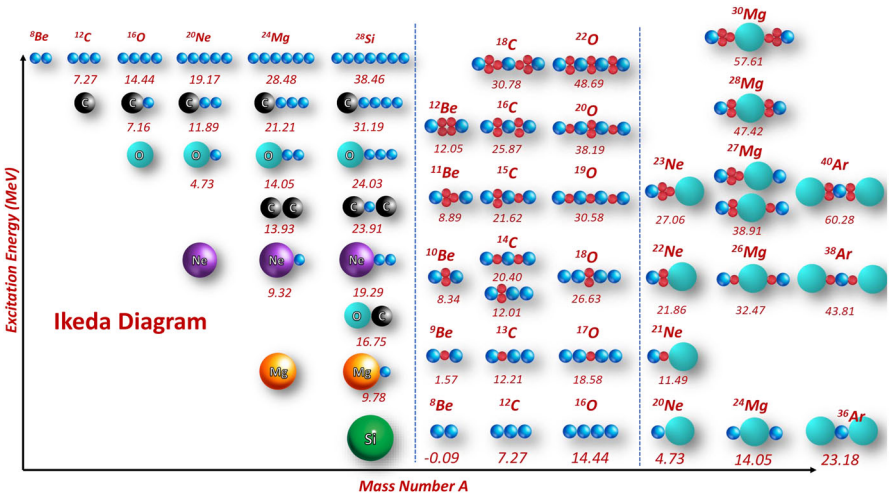

Fig. 2 Artistic view of the Ikeda threshold-rule diagram for self-conjugate nuclei (left) and neutron-rich light isotopes (right). Re-elaborated from [7, 71]

CsI scintillator crystal. The analysis of angular distributions and energy spectra of such light particles indicated the presence of a component associated with a *direct* emission from the projectile and not coming from the evaporation of a compound nucleus. Particles escaping from capture would not participate in the fusion between the colliding partners, giving origin to an incomplete momentum transfer processes, as early recognized in a seminal work by John Alexander and Lester Winsberg at Berkeley [83].

The third important progress of the 60s concerned the development of accurate phenomenological potentials for the description of α–α scattering; these researches were mainly performed by Darriulat et al. [84] and by Ali and Bodmer [85]. In particular, the Ali–Bodmer potential was largely used in subsequent calculations by many models aiming to treat the occurrence of clustering in nuclei.

The fourth breakthrough of the 60s was the publication of the *Ikeda diagram* [71], translating into a quantitative table the idea that strong clustered structure in light nuclei should occur close to the α (or more complex decomposition in self-conjugate nuclei) thresholds, see Fig. 2. In particular, the philosophy itself of the Ikeda diagram indicated that clustering could have a very relevant role in nuclear astrophysics: the presence of near-the-threshold states could in fact have a dramatic impact on the rate of processes involved during the He burning, as it occurs for example in the case of the triple-α fusion with the Hoyle state [86]; it has been recently suggested that cluster states could have a sizeable impact also in heavier burning processes, as for C+C fusion in more violent stellar scenarios [87].

During the same period, several data on elastic scattering of α particles by light-to-medium-mass nuclei were collected experimentally, and three characteristic effects, quite different from the phenomenology seen with proton or deuteron elastic scattering experiments, were observed [88]: a pronounced maximum of the differential cross section at 180°; a general enhancement of differential cross sections in the backward hemisphere, and the presence of broad maxima in the excitation functions collected at backward angles. Some explanations of these phenomena suggested during the 60s considered the possible occurrence of *glory* effects [89, 90], analog of the Mie theory of glory in optics and due to the peculiar α-nucleus potentials, or, alternatively, the presence of α-exchange effects in the target due to the strong clustering characterizing, especially light self-conjugate target nuclei [91, 92].

As a historical curiosity, in 1965, Linus Pauling made a tentative merging of the cluster model and the shell model by introducing the so-called *spheron* model of the nucleus [93]; despite the success in reproducing the presence of magic numbers, this model was not subject to further development by other theorists. At the basis of the model, there were the *spherons*, i.e., nuclear clusters made by two (dineutron), three (^{3}H and ^{3}He) or four (^{4}He) nucleons, formed with a process similar to hybridization, having a diameter adjusted in order to reproduce the correct magic numbers for poly-spherons structures leading to an overall spherical symmetry. Some weaknesses of the model are linked to the use of unbound clusters (dineutrons), the presence of adjusted parameters, and the lack of a fully quantum mechanical derivation of the model starting from reliable nucleon–nucleon interaction. A more refined model of the nucleus, seen as an assembly of light clusters, was later developed by MacGregor at the end of 70s, with the advantage of using a bi-dimensional Ising model to build

up the entire nucleus, avoiding ambiguities given by different possible geometrical setups that could equally describe the nucleus [94].

During the 70s, several authors compared the predictions of the deformed harmonic oscillator (originally introduced by James Nix for calculations of the fission barrier in heavy nuclei, [95]) for medium-light nuclei with the Nilsson model ones. The development of the smoothing method, first introduced by Vilen Strutinsky, allowed to understand the effect of shell closure in the potential energy profiles of light nuclei [96]. In this framework, the seminal work by Larsson and Leander on the structure of medium-mass self-conjugate nuclei, making use of the Nilsson–Strutinsky method, allowed to predict the existence of several secondary minima in the potential energy surface of such nuclei, clearly linked with the occurrence of several possible cluster arrangements [97].

A different approach, searching for a unified description of cluster and shell structure in light nuclei, was introduced in 1973 by Yasuhisa Abe, Jun Hiura and Hajime Tanaka. It took the basis from the *molecular orbital* theory in physical chemistry, and described the structure of light nuclei by means of a linear combination of nuclear orbitals (LCNO) obtained by a self-consistent field [98]. Furthermore, accurate evaluations of polarization effects between clusters indicated a strong stability of α clusters against dissolution in the nuclear medium for all the lighter-most self-conjugate nuclei. The *leaving behind* of the conceptual limitations linked to the applicability of the Born–Oppenheimer approximation in the nuclear cluster world was discussed in details in Ref. [99] and represented an important step in the ripeness of this field of nuclear physics; in this work, by applying such approximation and using the Ali–Bodmer potential for the α–α interaction, it was possible to reconstruct the structure of ^{9}Be in a fully molecular picture.

In the 70s, it was proposed also by Arima, Gillet, and Ginocchio the *Quartet model*, aiming at describing the nucleus as made by α particles residing into orbitals similar to the harmonic oscillator ones and allowing the transition of quartets from an orbital to another to correctly describe the presence of 0^{+} cluster states at large excitation energies [100]; experimental analysis on quartet states in ^{20}Ne were discussed in [101, 102].

In the same period, the presence of broad structures, of the same type of the ones seen in the 60s in elastic scattering and p, α, n, γ reaction channels, was discovered also in the excitation functions of *complete fusion* between self-conjugate nuclei [103]. Also the elastic scattering of identical self-conjugate nuclei (as ^{12}C+^{12}C and ^{16}O+^{16}O) manifested a bizarre trend of the excitation function close to 90°, with some recurrent broad structures resembling a "crowd of elephants" connected one another by the familiar "tail-trunk" link. Such "elephant scattering" was a mystery during the 70s, considering also that, during the 60s, the optical model potentials used to describe the scattering of such light systems were quite shallow. The large mole of accurate elastic scattering data collected during the 70s pointed out the need for using much more *deep* optical potential to describe the data. Such potentials can give rise to complex refraction phenomena, as rainbows and Airy structure, fully analog to the rainbows and supernumerary structures seen when the light is refracted by drops of water; this interpretation, able to explain the "elephant scattering" discussed above, represented a success of the nuclear reaction theory obtained in the 90s (see, e.g., [104, 105]), and

beautifully demonstrated, one more time, the strong interconnections between nuclear physics and other physics branches.

At the end of the 60s (see, e.g., Ref. [106]) and especially during the 70s (with the large series of works on this subject, both theoretical [107] and experimental [108], at the University of Maryland), it was introduced a new important experimental probe to unveil clustering in nuclei. The analysis of missing energy and triple differential cross sections of $(p, p\alpha)$ *knock-out* reactions at high bombarding energies (of the order, or larger than, 100 MeV) allowed to estimate the α-particle spectroscopic factors, S_α, that were compared both with model predictions and with experimental determinations coming from coeval α transfer studies. The results of α knock-out reactions on light p-shell nuclei of Ref. [108] were quite surprising: the experimental S_α values were in good agreement with shell model calculations and, on average, no evidence was found for additional α particle-like correlations. In a subsequent work, focusing on selected isotopes from ^{12}C to ^{66}Zn [109], S_α values well larger than the shell model predictions were observed for the self-conjugate nuclei ^{12}C,^{16}O,^{20}Ne. In the same period were also performed at Saclay new experiments of quasi-free electron scattering of the type $(e, e'd)$ and $(e, e'\alpha)$ on ^{6}Li to investigate its degree of clusterization [110]; the obtained results were similar to the ones found with knock-out reactions induced by light ions. To testify how this field of nuclear cluster physics is still a lively research line, we would mention a very recent example of α knock-out reactions used to probe the interplay between α clustering and neutron skin effect in medium-mass nuclei (stable Tin isotopic chain), see Ref. [111]. Further, it is worth noting that several knock-out experiments, induced by radioactive ion beams in inverse kinematics, are currently under investigations at several radioactive ion beams factory in the world (see, e.g., [112]).

The 70s were fruitful years also concerning the accurate study of three-body reactions and the occurrence of *quasi-free* scattering and reactions mechanisms in light ion collisions. Some pioneering works on this aspect were performed by Yugoslavian (Rudjer Boskovic Institute) and American collaborations (see, e.g., [113–115]). Soon after such seminal works, quasi-free mechanisms were applied to the study of clustering in light nuclei; for example, ^{5}He-α clusterization in ^{9}Be was investigated at the Tohoku University [116] with the quasi-free ^{5}He+^{3}He$\rightarrow \alpha + \alpha$ reaction, and the momentum distribution between the two clusters was determined. A large campaign of quasi-free reactions was also performed in the same years at the Catania University (see, e.g., [117–119]) and several details on the relative motion of clusters inside light nuclei were deduced. In the same period, it was also suggested that pre-equilibrium emission of α particles could be fruitfully used to study the pre-formation of the clusters in medium-mass nuclei (see, e.g., [120]).

60s and 70s are, in general, considered as the *golden era* of nuclear spectroscopy, and several details on the properties of rotational bands built on α cluster states, vibrational excitations and their interplay with single-particle states were investigated in that period. It is important to underline that this abundance of high-quality data was triggered also by two important technical progresses: the widespread use of high-resolution solid-state detectors with associated low-noise and stable analog front-end electronics [121], and the development of the new *split-pole* [122, 123] and *Q3D*

design [124] magnetic spectrometers to perform very high-resolution studies of nuclear spectroscopy in a broad range of the nuclide chart.

At the beginning of the 80s, a new and important branch of nuclear cluster physics started, with the discovery by Rose and Jones at Oxford of the cluster radioactivity in ^{223}Ra (1984), immediately confirmed by Aleksandrov et al. at the Kurchatov Institute [125], and subsequently deepened by Gales et al. at the Orsay Institute with the SOLENO spectrometer [126]. The emission of heavy clusters, as ^{14}C and other isotopes of carbon and neon from actinide nuclei was already theoretically predicted by Sandulescu, Poenaru and Greiner [127] and configured a new scenario linking the α radioactivity and the fission decay modes of an heavy nucleus. The observed branching ratio, $BR(^{14}C/\alpha) \approx 8 \times 10^{-10}$, was extremely small, but not far from theoretical predictions obtained with several nuclear structure models [128]. After this breakthrough discovery, several other studies with much more complex detection systems were performed. They were able to fight against a huge background of α particles and also to assure the isotopic identification of the emitted clusters [128]. For an overview on this very interesting part of cluster physics and its connections with nuclear structure of heavy ions, the reader is referred to [129, 130].

In the same period (from the end of 70s to the 80s), the phenomenology of dinuclear molecules was deepened by various experimental groups on several trajectories. At Stony Brook and Brookhaven, Cormier and collaborators performed new measurements of single and *double* inelastic scattering (to the 4.44 MeV, 2^+ state) in ^{12}C+^{12}C collisions from 15 to 45 MeV [131]. The integrated cross sections show broad oscillations typical of the insurgence of molecular states, associated with resonances having very large spin values. Several studies of elastic and inelastic scattering of asymmetric systems, as ^{12}C+^{16}O [132], and of scattering and reaction cross sections even for heavier systems (as ^{28}Si+^{28}Si, [133]) allowed to have a broader view of the molecular resonance phenomenon (see [134] for an overview). From the theoretical point of view, all the results on nuclear molecules were re-organized and clarified also thanks to the developments of the *Orbiting Cluster Model* by Nikola Cindro and Dinko Pocanic, and of the *Band Crossing Model* by Abe, Kondo and Matsuse. As indicated by the experimental data, the *Orbiting Cluster Model* predicted the $\ell = 0$ band-head of the molecular band at energies close to $B_{clust} + U_C$, where B_{clust} is the binding energy of the projectile+target in the composite system and U_C is the Coulomb barrier. Furthermore, all the resonance data are expected to stay in a quite narrow zone around a line representing a typical rotational band. This model predicted also *for which systems* the molecular resonances could be present or not. This important point was related to the value assumed by the *damping width* $\Gamma_\downarrow$ for the various colliding systems, and the predictions of this model were subsequently confirmed by experimental data. In the *Band Crossing Model*, it was predicted the existence of different molecular bands, where the underlying di-nuclear structure can show the presence of *unexcited* or *excited* nuclei. Such molecular bands can cross at certain angular momentum values J_{cross}, and in correspondence of such values an enhancement of the cross section is expected, in agreement with experimental findings of single and double inelastic scattering data [131, 135].

The 80s were a truly fruitful period also for the investigations concerning clustering with heavy-ion collisions, mainly performed with LINAC and cyclotrons. In 1984, an

experimental work at the HMI in Berlin determined the onset velocity at which the incomplete fusion mechanism starts to occur and determined the mass-asymmetry dependence of the onset of incomplete fusion phenomena between medium-mass nuclei [136]. It is worth noting that the massive transfer process at the basis of incomplete fusion can be favored by the cluster structure of the reaction partners (see, e.g., [137–140] and Sect. 7.1 for recent applications). On the side of direct reactions between heavy ions, the spin dependence of angular correlations between charged particles emitted in the binary decay of a given excited states was theoretically investigated, in a fully quantum mechanical framework, by the Oxford group [141]; a semi-classical method for similar analysis was previously reported by Da Silveira some years before [142].

During the 80s and 90s, nuclear reactions in the Fermi energy domain (i.e., at bombarding energies of $\approx$ 20 to 150 MeV/nucleon) were explored in details. Several theoretical models developed two decades before (see, e.g., [143, 144]) predicted the occurrence of clustering (mainly α clustering, because of its saturation properties) in *dilute* nuclear matter, at $\approx 1/5$ of the saturation density; these exotic density conditions can be reached by heavy-ion collisions at Fermi energies. The technological development of sophisticated multi-detector arrays made possible to explore such rich phenomenology starting from the 80s (see, e.g., [145]), while second-generation arrays developed during the 90s allowed even more complex analysis—thanks to improved particle identifications, better angular and energy resolution and almost complete solid angle coverage (see [146] for an overview). At the end of 80s, the possible occurrence of cluster structures in light hyper-nuclei (both Λ- or Σ-fed) attracted the interest of several theoretical groups (see, for example, the pioneering works of [147, 148]). This fruitful research line continued up to nowadays—also thanks to the development of new facilities for the production of new hyper-nuclei; in Refs. [149, 150], it is possible to find an overview of hyper-nuclear structure data.

In the last half century, we assisted in a huge development of theoretical works on nuclear clustering. The increasingly large performances of electronic calculus allowed the development of sophisticated models able to treat, in a microscopical way, the structure of light nuclei and the emergence of clusters. A simplified timeline of such developments is given in the first row of Fig. 3; more details on some models and methods that are currently used in cluster physics will be given in the following section. Among them, we should mention the huge contribution given by Molecular Dynamics models [151–154] both to the static and the dynamical description of nuclei. AMD and FMD models, for example, beautifully predict the occurrence of clustering in beryllium, carbon, and oxygen isotopes and allow the inspection of density matter distributions and the estimate of electromagnetic transition rates; some recent examples are discussed in Sects. 7–14 of this paper.

The last decade of the 20th century testified an *explosion* of topics related to clustering in nuclei, and we will give here a short summary on some of such discoveries.

In 1990, a revolutionary work [155], performed at the Kurchatov Institute in Moscow (Artemov, Goldberg, Wolski and collaborators), was published in the Yadernaia Fizika journal. It reported a novel technique for the analysis of α cluster states via elastic scattering of a heavy beam X (accelerated by a cyclotron) in inverse kinematics, i.e., colliding on a ^{4}He gas target filling a scattering chamber insulated from the

vacuum lines of the beam. A silicon detector was placed at the end of the gas region to register the spectrum of particles arriving at 0°. Ref. [155] *verbatim* indicated that "the gas which fills the chamber serves simultaneously as a target, a moderator for the primary beam of heavy ions, and an absorber which shield the detector from the direct beam". The interplay between the inverse kinematics and the different stopping powers of the beam particles and of the α particles in the ^{4}He gas would result in an α spectrum at 0° that is immediately linked to the scattering vertex distribution along the slowing-down itinerary of the beam in the gas and, consequently, to the shape of the excitation function of the $\alpha + X$ elastic scattering at 180°. This method would avoid the very long procedure of data taking of resonant elastic scattering excitation functions with direct kinematics experiments (i.e., hundreds of beam energy changes to cover, in fine steps of few keV or tens of keV, several MeV of excitation functions), and also the serious technical problem of measurement of scattering on gaseous targets (e.g., ^{16}O and ^{20}Ne, particularly important for cluster physics). Moreover, differently from direct kinematics studies, excellent energy resolution could be reached even using cyclotron beams (as originally made in Ref. [155] with the Kurchatov cyclotron, using ^{12}C and ^{15}N at 28 and 45 MeV, respectively). The huge advantages of the method proposed in Ref. [155], soon indicated in the literature as the *Thick Target Inverse Kinematic* (TTIK) method, are of vital importance for application with radioactive beams, and were at the basis of *hundreds* of modern investigations with stable and unstable beams that led to a profound revision of the spectroscopy of light nuclei during the last 30 years.

In the same year, a novel procedure for the analysis of data coming from three-body reactions was developed at the Catania University (Lattuada, Romano, Vinciguerra and collaborators) [156]. In this type of experiments, it was common to detect and identify just *two* of the three bodies in the exit channel and invoke conservation laws to determine the energy E_3 and properties (A_3, Z_3) of the third (undetected) particle. Anyway, there were serious problems in reconstructing the event dynamics when some of the constraints went out of control, e.g., when *contaminants* in the target were present. The new procedure allowed to determine unambiguously the mass number of the third body A_3 in the exit channel by studying a correlation between kinematic variables (energy, masses and momenta of the beam and of the two detected particles). The graphical application of this procedure led to a bi-dimensional correlation plot of experimental data, originally called *EP plot* by the authors, but now better known as *Catania plot*. From the analysis of the slopes of the loci formed by the data, it is possible to determine the value of A_3; this is often a precious information for the study of sequential processes involving the emission of clusters (see, e.g., [157] for one of the first application of the procedure).

The beginning of the 90s led also to the widespread use of silicon micro-strip detectors, already developed in the 80s for high-energy physics [158], also in nuclear physics experiments. The very good energy resolution, coupled with the excellent granularity given by the high segmentation, allowed to perform particle–particle coincidence measurements also in decay experiments with very narrow kinematic emission cones. Some very important examples of this type of studies were the search for direct decay of the Hoyle state, performed in 1994 by Freer and collaborators at the UPenn tandem

[159], and the search for a six-α chain state in ^{24}Mg (see [160] and the following literature on this subject).

During the 90s, further studies on heavy-ion di-nuclear resonances were performed principally at Oak Ridge and Strasbourg using high-coverage arrays for particle-gamma coincidences and high-energy ^{24}Mg, ^{28}Si beams delivered by super-Tandem accelerators.[6] Surprisingly, quite narrow resonances ($\approx$ 0.15 to 0.2 MeV) were found at very high excitation energies of the compound systems ($\approx$ 60 to 70 MeV); such resonances showed very large angular momenta ($\approx$ 34 to 42 $\hbar$). The analysis of the *spin alignment* of fragments pointed out the presence of very deformed equilibrium configurations of the pole–pole type in the ^{24}Mg+^{24}Mg (prolate–prolate) system [161], and of equator–equator type in ^{28}Si+^{28}Si (oblate–oblate) [162] system. This rich phenomenology was well described by the Uegaki and Abe di-nuclear molecular model calculations [163, 164]; in this framework, the possible occurrence of peculiar normal modes around a stable, but very deformed, configuration (as, e.g., the famous *butterfly* motion) explained the occurrence of several dinuclear resonances with the same J value.

In 1996, a fundamental work by von Oertzen [165] discussed the possible existence of dimeric structures in neutron-rich isotopes of beryllium. The occurrence of nuclear structure phenomena very similar to the molecular co-valence bonding theory was supported by two-center shell model (TCSM) calculations.[7] In particular, the TCSM allowed to determine the *correlation diagram* in perfect analogy with physical chemistry theory of covalent bonding in homo-nuclear diatomic molecules [168], considering the orbitals in the limiting cases of *united nucleus* and *separated nucleus* and calculating the corresponding molecular orbital characteristics as a function of the inter-cluster distance $r_{\alpha\alpha}$ [165]. In this frame, it was possible to fully understand the structure of the ground and the first excited states in ^{9}Be. For example, at $r_{\alpha\alpha} \approx 1$ to 4 fm, the filling of molecular orbitals predicts the valence neutron to be in a state with projection of angular momentum $K = 3/2$, exchange properties $p = g$ (g=*gerade*,u=*ungerade* as in physical chemistry) and parity $\pi = -$: this would correspond to a π-bonding for the *ground state* of ^{9}Be. At larger $r_{\alpha\alpha}$ values, the molecular orbital sequence is changed, and the valence neutrons should be in a $K = 1/2, p = u, \pi = +$ state, i.e., in a σ-bonding orbital; this peculiar type of bond would favor the formation of an almost stable nuclear dimer with a pronounced α cluster structure. This type of studies was subsequently extended also to the case of trimeric structure in isotopes of carbon [169, 170]. Considering the findings on the nuclear structure of neutron-rich isotopes of Be, C, O, and Ne on the light of the molecular model, von Oertzen proposed in 1999 an *extension* of the Ikeda diagram at the Rab Conference on Clustering: covalently bound nuclear molecular states would occur at energies close to the threshold for the decay into α (or heavier self-conjugate

[6] The ORNL tandem accelerator arrived to a maximum terminal voltage of 25 MV. The highest nominal terminal voltage, 35 MV, was reached by the Strasbourg VIVITRON super-Tandem machine, unfortunately now decommissioned.

[7] The *two-center shell model* was introduced in the 70s to describe the details of nuclear fission of heavy isotopes; its original version, with symmetric centers, is discussed in Ref. [166], while the extension to asymmetric centers is reported in Ref. [167].

nuclei) and neutrons. A pictorial view of this extension of the Ikeda diagram is given on the right side of Fig. 2.

The experimental discovery of Bose–Einstein condensation of rubidium atoms (1995) triggered several important questions also in the nuclear cluster community. Inside nuclei, bosonic α clusters can be produced as bound states of fermions, and the Bose character of the clusters is in competition with the fermionic properties of protons and neutrons. It is then possible to hypothesize the occurrence of phenomena of α condensation in self-conjugate nuclei. Several theoretical works faced this question at the end of 90s; for example, a new theoretical approach was proposed in Ref. [171] by introducing a new type of α-cluster wave function (THSR, from Tohsaki, Horiuchi, Schuck, Ropke) predicting the occurrence of condensed α structure in self-conjugate nuclei close to the Nα disintegration threshold. Once again, the Hoyle state of ^{12}C became the "prime suspect" to unveil the presence of such an exotic phenomenon of Bose–Einstein condensation in nuclear physics; some very recent results of this research work are discussed in Sect. 12.3. Other important theoretical developments of the end of the century were linked to the use of algebraic models to describe the structure of light nuclei (see, e.g., [172–174]); some recent developments are discussed in Sect. 3.5.

The last decade of the century was a period very fruitful to study cluster formation and emission mechanisms in heavy-ion collisions (see, e.g., [175–178]), and the occurrence of clusterization at low baryon densities [179–181], also thanks to the widespread development of new-generation multi-detection systems. Interesting results on nuclear spectroscopy came also from invariant mass studies of decaying resonances formed in heavy-ion collisions (see, e.g., [182, 183]), and from the detailed analysis of competition between fusion and other reaction mechanisms in light nuclei (see, e.g., [184–187]).

We brought our historical notes to the doorway of the 20th century; the first quarter of the 21st century should be considered, with full rights, *contemporary* to our epoch and for this reason less suitable for an historical overview. Indeed, several works of such period are cited in the following sections to discuss the current knowledge of clustering in nuclei.

We hope that the historians of nuclear physics, and all the senior colleagues that contributed in first person to the development of clustering in nuclear physics, would forgive us for the present narration, surely *incomplete*, a bit *romanticized* and perhaps *biased* because of personal contingencies. The main aim of this review is to show, especially to young students and researchers, the immense work made in the last 80 years toward the understanding of the structure of light nuclei, and the beautiful connections with several other research fields (not only inside the realm of Physics but also of Mathematics and Chemistry) that arose during such fantastic years.

3 Overview of current models of nuclear clustering

After having described some of the main historical steps connected to research on nuclear clustering, in this section, we will shortly describe the principles of some theoretical models (microscopical or macroscopical) that have been recently used in

nuclear physics to describe the clustered nature of (essentially) medium-light nuclei. A simplified timeline of the development of some nuclear models involved in studies on nuclear clustering is reported in Fig. 3.

3.1 Microscopic models: RGM, GCM and OCM

Microscopic cluster models [58, 188] focus mainly on the detailed description of the inter-cluster motion in light nuclei, with a detailed implementation of the Pauli exclusion principle among clusters. The ancestor of this class of models was the Resonating Group Method (RGM), first introduced by Wheeler in 1937 [34]; it was fruitfully implemented in the early 1960s to describe several structures of light nuclei by profiting from the increasingly large availability of electronic calculus resources. The RGM strongly influenced the evolution of other cluster models in the second half of the 20th century, as well as the development of the Generator Coordinate Method (GCM) [189] and the Orthogonality Condition Method (OCM) [190]. RGM and GCM are fully microscopic models while OCM could be seen as a semi-microscopic tool, since the observed *Pauli blocking* effects are not fully built from a microscopic ground.

Within the RGM framework, the structure of light nuclei is described by a superposition of all possible types of nucleon groupings. It is considered that nucleons can devote part of their time in different configurations called *groups*; for example, they can be arranged into α-particles or into other groupings (deuteron-like, diproton-like, etc). The method of resonating group structure is therefore in striking contrast with the concept of mean-field which is typical of the Hartree–Fock scheme. The wave function built with the RGM model is made of a properly antisymmetrized combination of partial wave functions, which correspond to any possible type of grouping. The RGM wave function takes advantage of the saturation of nuclear binding: in fact, the largest part of the binding energy of the whole nucleus lies in the internal binding of each group.

Considering a system of m protons and n neutrons, the total wave function Ψ can be written as the sum of several components, of which each term represents a particular grouping (configuration) of the whole number N of particles. Such a term is the product of wave functions Φ, which represents the motion of particles within each group. They are also multiplied by particular functions of the positions and spin variables (the total angular momentum m_S of a group) $F(X, m_S)$. The F^i functions are unknown and they belong to different configurations. For instance, for the ^{6}Li nucleus, F^1 might represent the relative motion of a α-particle and a deuteron, while F^2 could represent a configuration of ^{5}He plus proton, etc. Considering the anti-symmetrization, the general form of the nuclear wave function becomes:

$$\Psi \propto \sum_i F^i[\vec{X}_i(I), m_{S_i}(I); \vec{X}_i(II) m_{S_i}(II)]\Phi_i(I)\Phi_i(II) \tag{1}$$

where the sum runs over all configurations of possible groupings of (for simplicity) two clusters, indexed by i. Φ_i indicates the wave functions of each of the two clusters I and II. The coefficients F^i depend only on the inter-cluster coordinates $\vec{X}_i(I) - \vec{X}_i(II)$,

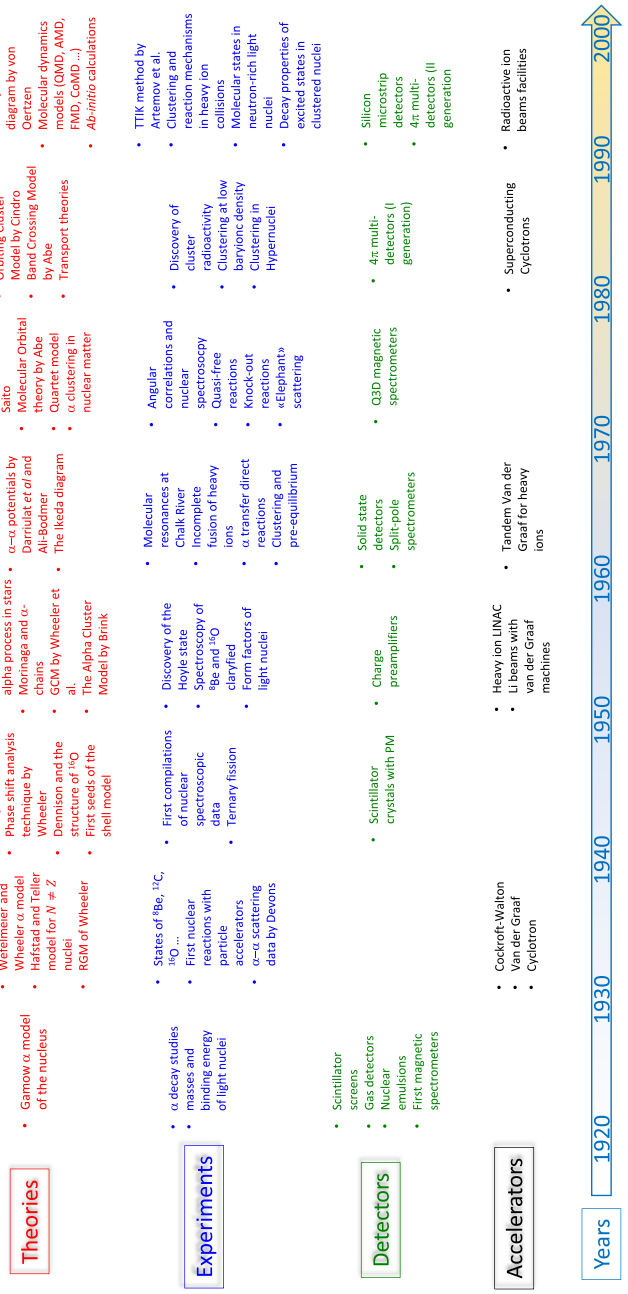

Fig. 3 A simplified timeline reporting *some* of the evolution steps concerning the cluster model of the atomic nucleus in the period 1920–2000. To be schematic, we separated the steps concerning theoretical methods, experimental discoveries, detection and associated equipment evolution, and developments of acceleration techniques. The reader is referred to the text for a more comprehensive historical view

allowing for a reduction of the corresponding degrees of freedom. They can be derived by solving a given set of integral-differential equations involving these coordinates as variables; the expression of these equations is rather complicated and, for this reason, the potential applicability of the model is typically limited mainly to small nuclear systems.

The RGM has been also applied to the description of nuclear reactions and scattering processes involving light nuclei; in particular, for example, it is able to reproduce nicely the trend of experimental astrophysical S-factor[8] of the ^{3}He$(\alpha, \gamma)^7$Be reaction at astrophysical energies [191].

The limitations seen with the RGM model can be overcome using GCM calculations. In this model, the F^i functions, describing the relative motion of clusters, are expanded over a set of projected Gaussian functions, centered at different points R_n of the physical space that are called *generator coordinates*. In this context, the wave-function of Eq. (1) can be re-formulated as:

$$\Psi^{JM\pi} \propto \sum_{\ell S} \sum_{n} f_{\ell S}^{J\pi}(R_n) \Phi_{\ell S}^{JM\pi}(R_n) \tag{2}$$

where $J\pi$ represent spin and parity of the system, and M the projection of the total spin on a quantization axis. The first sum is extended over all values of channel spins S and angular momenta ℓ, while the second one runs over all generator coordinates. The $f_{\ell S}^{J\pi}(R_n)$ functions take the name of *generator functions*. Their calculation is quite systematic when changing system, and can therefore be applied with large versatility to systems much more complicated than the ones treatable within the RGM model.

The OCM method, first introduced by Saito [190], was developed to take into account in an effective way the occurrence of the Pauli exclusion principle in the (complicated) kernels of integral equation of RGM model. In particular, Saito introduced a series of *forbidden states* (FS) to deal with; the inter-cluster wave-function must be *orthogonal* to the FS, which give rise to null states if an exact antisymmetrization procedure is performed. In this way, the interaction between clusters takes place only in the Hilbert space orthogonal to the FS space. It was discussed in [190] that the short-range inner repulsion in the α–α system was very well described by the orthogonality condition as an effective manifestation of the Pauli principle. In more recent times, the OCM has been profitably applied also to describe the behavior of systems made by more-than-two clusters (that would be quite difficult to be treated with the RGM); as an example, Horiuchi [192] applied OCM for the cluster description of the 7.65 and 10.3 MeV excited states in ^{12}C.

[8] The S-factor represents a useful method to display the behavior of a reaction cross section at deep sub-Coulomb energies. It is defined by the relation: $S(E) = \frac{1}{E} e^{2\pi\eta(E)} \sigma(E)$, where $\sigma(E)$ is the reaction cross section and $e^{2\pi\eta(E)}$ is the inverse of the s-wave penetrability factor. It is commonly adopted in Nuclear Astrophysics, where reactions are measured at very low incident energies. The presence of the $\frac{1}{E} e^{2\pi\eta(E)}$ factors qualitatively accounts for penetration of the Coulomb barrier in the entrance channel, removing quite effectively the exponential fall of the cross section for decreasing energies.

3.2 The quartet model

The main aim of the *quartet model* was the description of excited states of self-conjugate nuclei that cannot be easily described by means of the shell model. The assumption made in the quartet model is the existence of quartets. A *quartet* is a strong interacting structure made of 2 protons and 2 neutrons occupying a fourfold degenerate single-particle state [100]. At the basis of the model, there is also another simple empirical consideration: the separation energy of a nucleon in a self-conjugate nucleus is much larger than the one of an α-particle. For example, while the neutron emission threshold in ^{16}O is 15.7 MeV, the α emission threshold is only 7.2 MeV. This evidence indicates that the less bound nucleon interacts strongly with the other three which make up the emitted α-particle and much more weakly with the other nucleons of the nucleus. More in detail, in ^{16}O, a neutron of the $p_{1/2}$ orbital has about 5 MeV of interaction energy with the ^{12}C core and about 10 MeV interaction with the remaining nucleons of the $p_{1/2}$ orbit.

In the quartet model, excited states of self-conjugate nuclei are obtained by means of particle–hole excitations of quartet structures, characterized by strong internal binding energies and weak interaction between each other. For self-conjugate systems from ^{12}C to ^{52}Fe, quartets are restricted to the $(0p)$, $(0d,1s)$, and $(0f,1p)$ shells of a spherical harmonic oscillator. The interaction energy between two quartets across the $0p$ and $(0d,1s)$ and across the $(0d,1s)$ and $(0f,1p)$ shells can be determined by the position of the first 0^+ excited state of ^{16}O and ^{40}Ca (that are known from the literature to have a large α-structure [100]) respectively, while the interaction between the $(0p)$ and $(0f,1p)$ shell is supposed to be small due to the extremely small radial overlap of the relative wave functions. In this model, quartet–hole interactions are supposed to be constant, regardless of the A of the given self-conjugate nucleus and the number of excited quartets. Assuming an α particle as the core, one can indicate as $[xyz]$ a generic configuration of quartets arranged in the above-mentioned shells in the following way: x quartets stay in the $N = 1$ major shell, y quartets stay in the $N = 2$ major shell and z quartets stay in the $N = 3$ major shell. These configurations are typically indicated compactly as Q^x_p, $Q^y_{(sd)}$ and $Q^z_{(pf)}$. Restricting the calculation, for simplicity, to the first two orbits, $N = 1, 2$, one finds:

$$\begin{aligned} E^\star(Q^x_p Q^y_{(sd)}) =& E_0(4x+4, 2x+2) + E_0(4y+16, 2y+8) \\ & - E_0[4(x+y)+4, 2(x+y)+2] - E_0(16,8) + (3-x)yV_{p,(sd)} \end{aligned} \tag{3}$$

In Eq. (3), $E_0(A, Z)$ is the interaction energy of a nucleus with A nucleons and Z protons, while $V_{p,(sd)}$ is the interaction between y $N = 2$ quartets and $(3 - x)$ $N = 1$ holes. The latter quantity is determined experimentally by setting the one-quartet one-hole excitation energy equal to 6.05 MeV, i.e., the excitation energy of the $J^\pi = 0^+$ state in ^{16}O. We report in Table 2 the scheme of ^{20}Ne excited states which can be predicted using the quartet model; signals of the presence of [212] and [203] configurations were experimentally reported in α transfer reactions [101] and compound nucleus reactions [193], respectively.

Table 2 Some ^{20}Ne configurations predicted by the quartet model [100]

^{20}Ne $[xyz]$	$E^{\star}$(MeV)
[299]	0.0
[212]	5.1
[299]	8.8
[203]	$13.3 + V$
[129]	17.0
[152]	$17.4 + 2V$
[120]	$20.7 + 2V$
[111]	$24.2 + 4V$
[102]	$26.3 + 6V$

Both two shells and three shells $[xyz]$ configurations are shown. V represents the interaction between the $(0p)$ and $(0f,1p)$ shell, here left unspecified

Much more accurate predictions concerning the spectroscopy of light-to-medium nuclei have been recently obtained using a fully microscopical quartet model [194], which has been extended to include quartets with arbitrary values of isospin and angular momentum [195]. In this new framework, quartetting can be understood as a manifestation of four-body correlations not dissimilar to the pair formation mechanism between couples of nucleons. Excellent descriptions of the low energy part of level schemes of self-conjugate and non-self-conjugate nuclei have been reported [195].

3.3 Molecular Dynamics approaches

Molecular Dynamics (MD) approaches are microscopical many-body models extensively used to provide direct connections to the observable physical states of a nucleus (see, e.g., [154, 196, 197]). Such models have been used profitably both to describe the structure of nuclei in static conditions and also to describe the dynamical evolution of nuclear collision between light-to-heavy ions [151]. These models are based on the resolution of the Schrödinger equation using single-particle wave functions as Gaussian wave packets of the form:

$$\varphi_i = \phi_{\vec{X}_i} \chi_i \tau_i \tag{4}$$

where $\phi_{\vec{X}_i}$ represents the spatial part of the wave-function of the i-th nucleon:

$$\phi_{\vec{X}_i}(\vec{r}_j) \propto e^{-v\left(\vec{r}_j - \frac{\vec{X}_i}{\sqrt{v}}\right)^2} \tag{5}$$

X_i and v are the centroid and width of a wave packet, while χ_i and τ_i are, respectively, the intrinsic spin function and the isospin function.

Between the various models of the MD family, the *Antisymmetrized Molecular Dynamics* (AMD) model has been proven, in the years, to be particularly suitable

for the description of clustering phenomena in light nuclei. The AMD model was developed by Kanada-En'yo et al. [196–198], and it has been used quite extensively in the description of nuclear systems beyond the $N = Z$ line and to investigate structures which are not easily obtained with shell model calculations. This model is able to reproduce a big variety of nuclear properties, such as excitation energy, radii, magnetic moments and electromagnetic transition probabilities [153]. The AMD wave functions of a nucleus are described by an antisymmetrized product (by means of Slater determinant) of single-particle molecular dynamics functions of the type described in Eq. (4):

$$\Phi_{AMD}(\mathbf{Z}) = \frac{1}{\sqrt{A!}}\mathscr{A}\{\varphi_1, \varphi_2, \ldots, \varphi_A\} \tag{6}$$

The AMD wave function is parameterized by a set of complex parameters $\mathbf{Z} \equiv \{X_{ni}, \xi_i\}$ with $n = 1, 2, 3$ indexing the spatial coordinates X and $i = 1, \ldots, A$. The positions X_i of the centers of gravity of the Gaussians and the intrinsic spin orientations ξ_i are treated independently as variational parameters. The optimum wave function is determined from an optimization procedure that minimize the energy expectation value $\mathscr{E} \equiv \langle\Phi|H|\Phi\rangle/\langle\Phi|\Phi\rangle$. Calculations performed with the AMD model are able to reproduce both mean-field states and cluster states; this is one of the striking features of model, allowing to describe, in a consistent way, the coexistence of shell and cluster states in light nuclei [9].

Another interesting approach for the study of the structure of light nuclei is represented by the *Fermionic Molecular Dynamics* (FMD) model. The FMD wave function is of the same type of the AMD, with the major difference regarding the *width* parameter; while it is a common value for all nucleons in the case of AMD, in the case of FMD they can be independently tuned for each nucleon. In nuclear structure studies, the flexibility in the treatment of the width parameters of the FMD is particularly powerful, for example, to unveil the neutron-halo structure of neutron-rich nuclei [152].

3.4 The deformed harmonic oscillator (DHO)

Beyond the connection between clustering phenomena and binding energy distributions, another important point connected with α clustering is due to the occurrence of *symmetries* in the structure of light nuclei. They can in fact play an important role in the collective excitation of light nuclei, driving the formation of clusters through their influence on the mean-field [199]. The connections between mean-field and the cluster degrees of freedom have been investigated by means of the *deformed harmonic oscillator* model of nuclei.

The harmonic oscillator (HO) is one of the possible central potentials typically used in the nuclear shell model; it is especially adopted for the description of light nuclei. In this framework, nucleons are supposed to move in an harmonic oscillator potential, leading to energy levels of the form:

$$E = \hbar\omega(n + 3/2) \tag{7}$$

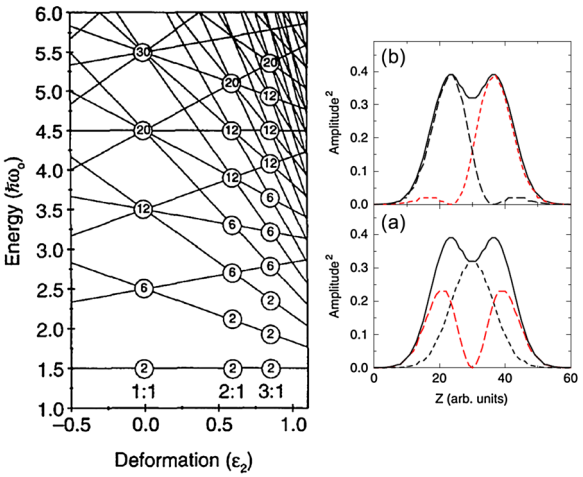

Fig. 4 (Left panel) Energy levels of the deformed harmonic oscillator as a function of the quadrupole deformation ϵ_2. Degeneracies of the levels are indicated in the correspondence of each crossing point. Shell structure appears for spherical configurations and 2:1 and 3:1 deformed configurations. From [200]. (Right panel) **b** HO wave functions of the form given in 10 shown as dashed lines. The solid line represents the overall ^{8}Be density $|\varphi_{0,0}|^2 + |\varphi_{0,1}|^2$. **a** The density corresponding to the HO configurations for ^{8}Be (solid line). Dashed lines show the two separate contributions $|\varphi_{0,0}|^2$ and $|\varphi_{0,1}|^2$. From [199]. Reprinted from Refs. [199, 200] under permission

where n is the number of oscillator quanta. A deformation in the potential, for example a stretching along the z-axis, lowers the oscillation frequency along the direction of the deformation, and increases the oscillation frequency in the orthogonal directions. The *degeneracy* of Eq. (7) is then removed and the new values of energy become:

$$E = \hbar\omega_\perp n_\perp + \hbar\omega_z n_z + \frac{3}{2}\hbar\omega_0 \tag{8}$$

where ω_z is the oscillation frequency along the deformation axis, $\omega_\perp$ the one for oscillations perpendicular to the z-axis and $\omega_0 = (2\omega_\perp + \omega_z)$. The so-called *quadrupole deformation* ϵ_2 is linked to the anisotropy of the oscillator, and can be expressed as:

$$\epsilon_2 = (\omega_\perp - \omega_z)/\omega_0 \tag{9}$$

Here, the total number of oscillator quanta is the sum of those on the parallel and perpendicular axes: $(n_z + n_\perp)$. Energy levels of the deformed HO are shown in the left panel of Fig. 4 [200]. Crossings of levels in the picture indicate energy values characterized by high degeneracy. Gaps similar to the ones seen in the shell model appear also in this case in correspondence of those energy values for which the degeneracy is maximized. As clearly visible from the picture, degeneracies and shell gaps occurring at $\epsilon_2 = 0$ (spherical nucleus) disappear as the potential is deformed, but reappear for deformations $(\omega_\perp : \omega_z)$ of 2:1 or 3:1. This occurs when the ratio of the oscillatory frequencies describing the three-dimensional deformed potential, ω_x, ω_y, ω_z, are integers. By examining the sequence of degeneracies, we can see that the

values (2, 6, 12, 20, ...) are repeated twice at a deformation 2:1 and three times for a deformation of 3:1, etc.

An application of the deformed HO to the case of ^{8}Be is rather straightforward. Being 2:1 the corresponding deformation, the levels which are labeled with degeneracy 2 are given by the quantum numbers $[n_\perp, n_z] = [0, 0]$ and $[0, 1]$. These levels can be occupied by pairs of protons and neutrons coupled to a zero-spin state. The density distributions are then given by the square of the wave functions $\varphi_{0,0}$ and $\varphi_{0,1}$, which correspond to the two distinct levels. The global ^{8}Be density is given by the sum $|\varphi_{0,0}|^2 + |\varphi_{0,1}|^2$. This is plotted in the right panel of Fig. 4b as a function of the z coordinate [200]. The feature which emerges is that the density is double-humped corresponding to the arrangement of protons and neutrons into two α-particles. The cluster wave functions can be written using the basis of linearly independent states φ_i:

$$\phi_{\alpha(\pm)} = \frac{1}{\sqrt{2}}(\varphi_{(0,0)} \pm \varphi_{(0,1)}) \tag{10}$$

which corresponds to projecting out the point symmetry of the two clusters. The overlap of an isolated α-particle, $\phi_\alpha = \frac{1}{\pi} e^{(-\omega^2 r^2/2)}$ is found to be $> 90\%$ [200]. The square of the two wave functions is shown in the right panel of Fig. 4a) (dashed lines) together with the overall ^{8}Be density.

What is evident is that the symmetries found in the degeneration of the states of deformed HO are reflected even in the density distribution, and they give rise to new magic numbers, often indicated as *deformed magic numbers*. They have been used in the literature in order to search for some peculiar cluster partitions [199]. In Ref. [201] it is demonstrated that these numbers can be expressed as the sums of spherical magic numbers. The results of this work are summarized in table 3, where each deformation is put in correspondence with the associated cluster structure. For a 2:1 deformation, for example, *super-deformed* structures should be found in ^{8}Be $(\alpha + \alpha)$, ^{20}Ne (^{16}O $+ \alpha$), ^{32}S (^{16}O $+$ ^{16}O), etc., while, in correspondence of a 3:1 structure, hyper-deformations are predicted in ^{12}C $(\alpha + \alpha + \alpha)$, ^{24}Mg $(\alpha +$ ^{16}O $+ \alpha)$, etc.

3.5 Algebraic models of clustering

Another very important family of nuclear models aimed at describing clustering in light nuclei makes full use of *algebraic* methods. One of the first models of this type (*vibron* model) was developed in Ref. [202] for the description of quasi-molecular spectra of dipolar nature; the $U(4)$ group theory is used to describe the two-cluster relative motion. This approach was subsequently combined with interacting boson or fermion approaches to describe also the spectroscopy of heavier nuclei. More recently, a semi-microscopic algebraic approach described the internal cluster degrees of freedoms in terms of the $SU(3)$ shell model, while the relative motion was described within the vibron model approach [203]. With this approach, a good description of the level scheme and the partial width of several excited states of ^{16,18}O and ^{24}Mg was reported [203].

Table 3 Decomposition of deformed magic numbers in terms of spherical magic numbers, at deformations of 2:1 and 3:1, from [201]

Deformed magic numbers	Spherical magic numbers	Cluster configuration
$\omega_\perp : \omega_z = 2:1$		
4	$2+2$	$\alpha+\alpha$
10	$8+2$	$^{16}\mathrm{O}+\alpha$
16	$8+8$	$^{16}\mathrm{O}+^{16}\mathrm{O}$
28	$20+8$	$^{40}\mathrm{Ca}+^{16}\mathrm{O}$
40	$20+20$	$^{40}\mathrm{Ca}+^{40}\mathrm{Ca}$
$\omega_\perp : \omega_z = 3:1$		
6	$2+2+2$	$\alpha+\alpha+\alpha$
12	$2+8+2$	$\alpha+^{16}\mathrm{O}+\alpha$
18	$8+2+8$	$^{16}\mathrm{O}+\alpha+^{16}\mathrm{O}$
24	$8+8+8$	$^{16}\mathrm{O}+^{16}\mathrm{O}+^{16}\mathrm{O}$
36	$8+20+8$	$^{16}\mathrm{O}+^{40}\mathrm{Ca}+^{16}\mathrm{O}$

The associated cluster structure is indicated on the right column for each deformed magic number

In more recent times, Bijker and Iachello introduced a novel way to interpret the regularities found in the level scheme of light self-conjugate nuclei as ^{12}C and ^{16}O. The description of cluster states in such nuclei could be in fact profitably performed in terms of representations of unitary algebras $U(\nu+1)$, being ν the number of space degrees of freedom. Within this approach, noticeable successes have been obtained in the description of the ^{12}C structure using the properties of the D_{3h} group point symmetry within the $U(7)$ model: good reproductions experimental data concerning excitation energy and spin-parities of almost all the known (cluster) states below $\approx$ 15 to 20 MeV, reduced electromagnetic transition strengths $B(E\ell)$ and form factors measured in electron scattering were obtained (see, e.g., [205]). A reasonable reproduction of ^{16}O levels was also obtained with this model by assuming a tetrahedral symmetry T_d [206]. Very recently, this approach was extended also to non-self-conjugate nuclei using double-group point symmetries (see also Sect. 12.4).

4 Astrophysical relevance of clustering

Clustering phenomena can play a key role in the nuclear astrophysics domain, where different scenarios of stellar nucleosynthesis and stellar evolution can be affected by the properties of nuclear states involved in the reactions [207, 208]. A key example of such effects is linked to the structure of carbon. ^{12}C is one of the major constituents of biological life, and, therefore, understanding its origins represents a key point for scientists [209]. The current theory of nucleosynthesis links the origin of ^{12}C to the so-called 3α process [53, 210]. This process occurs in stars during the helium-burning phase of stellar evolution and proceeds essentially via the initial fusion of two α-particles followed by the subsequent radiative capture of a third α to the ground

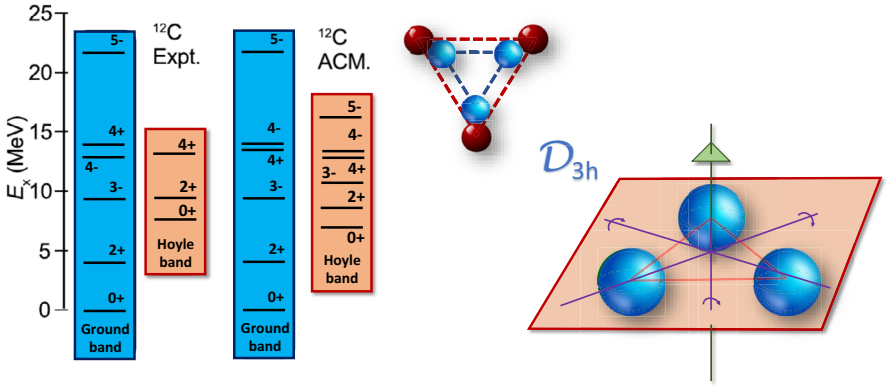

Fig. 5 (Left) ACM predictions for the ^{12}C ground state band (blue) and Hoyle state band (red), compared with recent results on ^{12}C spectroscopy. The triangular symmetry of both the ground state and Hoyle state is sketched pictorially at the center of the panel (adapted from Ref. [204]). (Right) Symmetries predicted for the D_{3h} point group. For further details, see [168]

state of ^{12}C. The reaction rate of this process would be strongly inhibited by its unstable intermediate stage, where a ^{8}Be is formed. The extremely short lifetime of the unbound ^{8}Be (of the order of 10^{-16} s) would act indeed as a sort of *bottleneck* for the whole process. A non-resonant two-step process, therefore, would have difficulties in explaining the observed abundances of carbon (and consequently of the heavier elements) in the universe. To overcome such a problem, in 1953 Fred Hoyle made the hypothesis that the 3α fusion could be a resonant process, proceeding via a peculiar state of ^{12}C placed close to the corresponding $^{8}\text{Be} + \alpha$ decay threshold [211, 212], as schematically shown in Fig. 6. This state, according to the Hoyle hypothesis, should be characterized by having $J^{\pi} = 0^{+}$, in such a way that the centrifugal barrier of the α-capture vanishes (s-wave capture) and the second step of the process maximizes the probability of producing ^{12}C. The fusion probability is further increased if the leading structure of the Hoyle state would be highly clustered, having a pronounced $^{8}\text{Be} + \alpha$ or 3α configuration (Fig. 5).

The existence of this state was confirmed a few years later (see also Sect. 2 for historical notes); during the 60s and 70s several studies were made on its energy position, which was found to lie at 7.654 MeV, only 285 keV above the α decay threshold, as shown in Fig. 6. Since three-body collisions are strongly inhibited in the temperature range where the helium burning occurs, one can conclude that the 3α process is essentially a two-step process made of:

$$^{4}\text{He} + {}^{4}\text{He} \longrightarrow {}^{8}\text{Be} \tag{11}$$

$$^{4}\text{He} + {}^{8}\text{Be} \longrightarrow {}^{12}\text{C} + \gamma \tag{12}$$

where the second step is maximized by the fact that the 92 keV of energy required to make such a fusion is remarkably close to the *Gamow window* for red giant stars [207], which is centered, as an example, at around 85 keV (60 keV width) for a typical temperature of 10^{8} K. The amount of ^{12}C that is so formed can be calculated from the

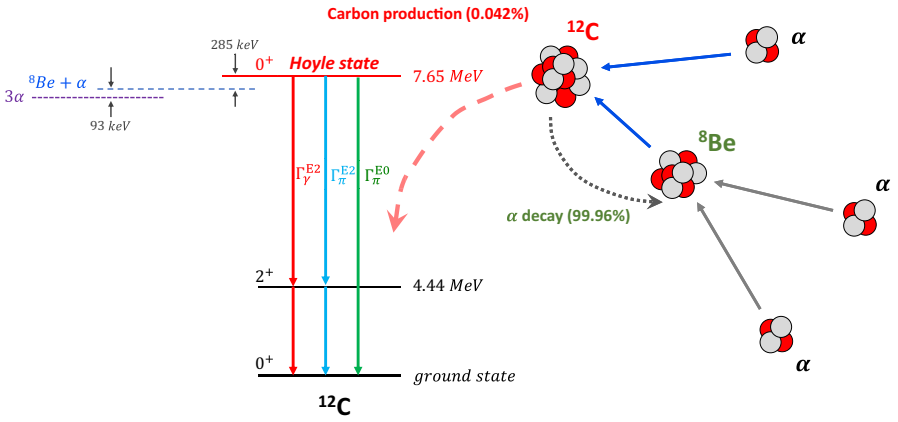

Fig. 6 Schematic view of the triple α process in stars and of the states of ^{12}C involved in the process. The possible electromagnetic transitions from the Hoyle state to the ground and first excited states in ^{12}C are indicated in different colors

competition between α-decay of the Hoyle state (which is regulated by the Γ_α partial width [207]) and radiative ones ($\Gamma_{\rm rad} = \Gamma_\gamma + \Gamma_{e^+e^-}$) for the two possible radiative transitions, e.g., gamma emission through the cascade toward the 2^+_1 state and pair production, which lead to the ground state of ^{12}C (see Fig. 6). The corresponding reaction rate is then given by:

$$< \sigma v >= \hbar^2 \left(\frac{2\pi}{\mu k_B T} \right)^{3/2} \frac{\Gamma_\alpha \Gamma_{\rm rad}}{\Gamma} e^{-\frac{E_R}{k_B T}} \tag{13}$$

being E_R the energy of the Hoyle resonance, k_B the Boltzmann constant, μ the reduced mass of the α+^{8}Be system and Γ the total level width. The latter is known to be almost coincident to the α decay width, i.e., $\Gamma = \Gamma_\alpha + \Gamma_{\rm rad} \approx \Gamma_\alpha$. This fact gives rise to a dynamical equilibrium ^{4}He+^{8}Be $\leftrightarrows^{12}$C* only perturbed by the very small leakage to the ^{12}C ground state given by the radiative decays. At stellar temperatures of $T \approx 10^8$ to 10^9 K, this process is thus dominated by the fusion through the ^{8}Be ground state; the reaction rate would then depend on the so-called *sequential decay* (SD) width of the Hoyle state, which corresponds to α-decays leading the residual 2α system in the 92 keV ^{8}Be level. However, in astrophysical scenarios that burn helium at lower temperatures, for instance, helium-accreting white dwarfs or neutron stars with small accretion rate, the reaction rate of the 3α process can involve a different decay mode of the Hoyle state: the non-resonant, or *direct*, α decay (DD) [213–215], where the two α particles bypass the formation of the ^{8}Be ground state. Recent theoretical calculations show that, at temperatures below 0.07 GK, the reaction rate of the direct process is largely enhanced with respect to the one calculated by assuming only the sequential scenario [216]; as an example, for temperatures around 0.02 GK such enhancement could arrive to 7–20 orders of magnitude [213, 217–220].

The knowledge of $\Gamma_{\rm rad}$ and Γ_π, entering in a direct way in the reaction rate calculation, was the subject of a campaign of experiments made during the 60s and 70s of the

20th century; a detailed report of the different experimental techniques used to derive the $\Gamma_{\rm rad}$ of the Hoyle state is given in [207]. On the other hand, in very recent times, the $\Gamma_{\rm rad}$ value was subject to new measurements that questioned the commonly accepted values reported in the literature by a factor 1.5; also the Γ_π was recently remeasured, but values in closer agreement with the literature ones have been reported. More extended discussions on such measurements, which would have a sizable impact on the 3α reaction rate, are reported in Sect. 12.3.

Naturally, similar investigations could be performed, *mutatis mutandis*, also for highly lying excited states in ^{12}C, which could play a role in nucleosynthesis environments at energies well larger than the ones involved in red giants. One of such examples is represented by the $\Gamma_{\rm rad}$ measurement for the 9.64 MeV 3^- state, which is incredibly challenging due to the predicted ultra-low values of the expected branching ratio, $\Gamma_{\rm rad} < 10^{-7}$. In Sect. 12.3 we will discuss some recent findings on this aspect.

Another key nucleus in astrophysics is ^{16}O, which is involved in helium-burning astrophysical scenarios through the ^{12}C$(\alpha,\gamma)^{16}$O reaction, following the triple-α process. These processes determine the relative abundances of C and O left by the He-burning. This has a crucial impact on the advanced phases of stellar evolution. As an example, if the carbon-to-oxygen ratio is larger, the cooling timescale of C–O white dwarfs becomes longer [221], while the amount of ^{56}Ni ejected by type Ia Supernovae becomes higher [222]. Concerning core-collapse Supernovae, the C/O ratio left after He-burning affects the chemical composition of the ejected material [223].

Nuclear astrophysics requires detailed knowledge of the ^{12}C$(\alpha,\gamma)^{16}$O reaction cross section over an energy region close to the α-separation energy S_{α_0}, the so-called *Gamow window*. Unfortunately, direct experiments to probe the cross section for this reaction are made extremely challenging by the amplitude of the Coulomb barrier between ^{12}C and α, which makes it about 5 orders of magnitude below the sensitivity achieved by state-of-the-art experiments [224]. Nuclear reaction theories are thus crucial to provide valuable *extrapolations* suitable for nuclear astrophysics. In ^{16}O there are four particle-bound excited states at $E_x = 6.05$ (0^+), 6.13 (3^-), 6.92 (2^+), and 7.12 (1^-) MeV, which are energetically close to S_{α_0} (7.16 MeV). While the two odd parity states are reasonably described by shell model calculations, the positive parity states are considered to be clustered states (as discussed also in the historical part, Sect. 2). Their description is crucial to understand the corresponding reaction mechanism, as the resonant capture (including the sub-threshold states) is expected to dominate the reaction rate of the ^{12}C$(\alpha,\gamma)^{16}$O radiative capture reaction [224]. To this end, a number of cluster models have been used. The clustered nature of ^{16}O affects in particular the strength of the $E2$ ground state transition from the $E_x = 6.92$ MeV 2^+ state, characterized by a pronounced cluster nature [225], and the strength of the $E1$ ground state transition, significantly enhanced by the contribution of the $E_x = 7.12$ MeV 1^- sub-threshold state and its interference with the resonance due to the $E_x = 9.59$ MeV cluster state. The role of the ^{16}O clusterization on this reaction was in particular studied with the resonating group method (see Sect. 3.1 for an overview of the method). In particular, single-channel and multi-channel RGM calculations with suitable effective interactions have been used to calculate the strength of the ^{12}C$(\alpha,\gamma)^{16}$O cascade transitions [226–229]. The possible existence of clustered configurations in ^{16}O was recently demonstrated in Ref. [230], using a modified shell

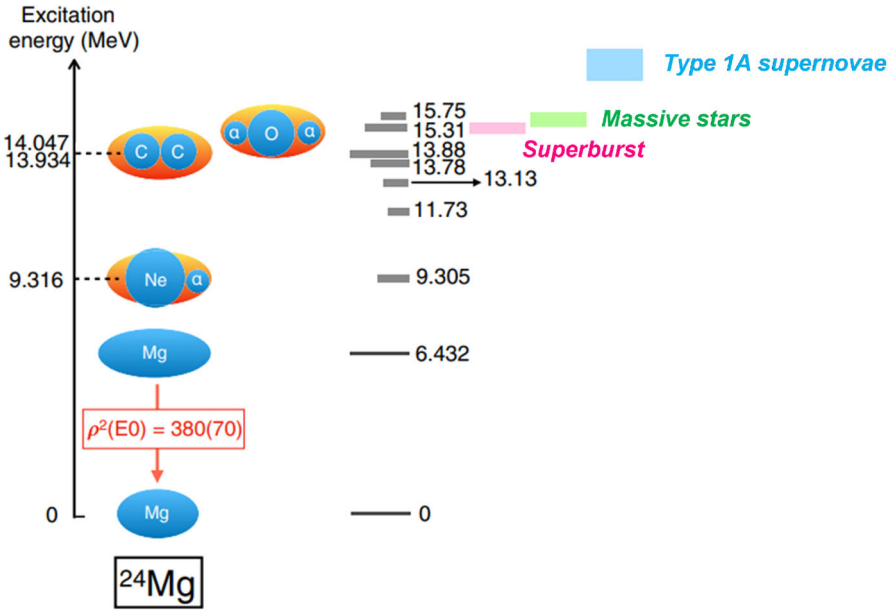

Fig. 7 Selected 0^+ states in ^{24}Mg that are close to some cluster disintegration thresholds. In particular, two recently discovered 0^+ states at 15.31 and 15.75 MeV could be characterized by a pronounced cluster structure and could have a sizeable impact on the rate determination of ^{12}C+^{12}C fusion reactions in superburst and massive stars scenarios. Reprinted from Ref. [87] under permission

model approach in the harmonic oscillator basis with a cluster-nucleon configuration interaction model. These calculations predict large α spectroscopic factors for natural parity states, in particular for the energy range near the α-threshold $6.0 < E_x < 8.5$ MeV, of fundamental importance to determine the reaction rate in astrophysical sites. In Sect. 14.2, we will discuss recent findings reported in the literature on this aspect.

^{12}C and ^{16}O are not the only nuclei for which the clustering structure plays a role in astrophysics scenarios. There are several other cases where clustering plays a role. For example, cluster states in the self-conjugate ^{20}Ne nucleus could have an influence on the rate determination of astrophysically important ^{19}F(p,α_0)^{16}O and ^{19}F(p,α_π)^{16}O reactions [231]. A strong role played by cluster structures has been recently proposed to explain the existence of two new candidates 0^+ states in ^{24}Mg at energies just above the ^{12}C+^{12}C cluster decomposition threshold, as shown in Fig. 7. Also in this case, the contamination of small fractions of p+^{23}Na and α+^{20}Ne components for such two states could have paramount importance in the resonant description of the ^{12}C+^{12}C fusion reaction, of huge relevance to the nucleosynthesis of super-busts or type-1a supernovae [87].

5 Clusters and nuclear molecules

Apart from self-conjugate nuclei, clustering phenomena occur also in the case of neutron-rich or neutron-deficient isotopes of beryllium, carbon, oxygen, neon, etc.

For example, in the case of neutron-rich nuclei, clustering features are strongly influenced by the presence of extra neutrons. The first attempt to theoretically describe clustering phenomena in non-α-conjugate systems was made by Hafstad and Teller [32] considering a series of neutron-rich isotopes with only one extra-neutron plus the corresponding self-conjugate nucleus: ^{5}He, ^{9}Be, ^{13}C and ^{17}O. They observed how the binding energies of these $4n + 1$ nuclei depend not only on the α–α interaction, but also on the role of the extra-neutron, thus reflecting the additional degrees of freedom brought by it to the whole system. In this way, while the binding energy of ^{5}He was reflecting the α–n interaction, the ^{9}Be ($\alpha + n + \alpha$) was recognized to have a contribution to the Hamiltonian coming from an *exchange* interaction. The basic description of neutron-rich nuclei given in this pioneering work was that of clustered systems in which *covalent exchange neutrons* are shared between α-cores, resulting in an increase of the stability of the structure. This behavior presents a quite clear analogy with physical chemistry concepts, and for this reason the extra neutrons take the name of *covalent particles*, while the corresponding nuclear configuration is indicated as a *nuclear cluster molecule* [7, 199]. Naturally, it is important to stress that in the case of nuclei with an extra-neutron outside of the α-centers, the analogy to molecules is useful but must be handled with some caution. Indeed, the Born–Oppenheimer method [232] treats the covalent electrons as rapidly moving particles with a mass much smaller than the ones of the atoms. This approximation is excellent for molecules, where the mass ratio of the nucleus to the electron is of the order of $\frac{m_n}{m_e} \approx 10^4$, but less valid, at first sight, in the nuclear field, where the mass of the valence nucleon is of the same order of magnitude of the α-centers [233]. Nevertheless, Fonseca, Revai and Matveenko in 1979 demonstrated that, in three-body model calculations involving two heavy particles and a lighter one (e.g., α+n+α in ^{9}Be), interacting through short-range s-wave potentials, the Born–Oppenheimer method leads to good results for the binding energies and wave functions even when the mass ratio $\frac{m_H}{m_L}$ between the heavy and light particle is not too large, $\frac{m_H}{m_L} \gtrsim 1$.

The variety of cluster structures that can be obtained by considering light neutron-rich nuclei in the framework of the cluster model is shown qualitatively in the so-called *modified Ikeda diagram*, see Fig. 2, right side. This diagram is analogous to the Ikeda one for self-conjugate nuclei (Fig. 2) but was extended to the case of systems with extra neutrons. The evolution of clustering phenomena is here described as a function of the *neutron-richness*; there is also an indication of the decay thresholds where these molecular structures should appear.

Carbon and beryllium isotopes are remarkable examples of molecular cluster structures, since they represent the simplest nuclear molecules constituted, respectively, by two-center (*dimeric*) and three-center (*trimeric*) configurations [169, 234]. The stabilizing effect played by extra neutrons can be quite well understood by looking at the case of ^{9}Be. While ^{8}Be is unbound against α-decay, ^{9}Be is stable. Given the highly clustered nature of ^{8}Be, one can assume a $\alpha + n + \alpha$ structure for an appropriate description of ^{9}Be. Electron scattering experiments on ^{9}Be indicated a high deformation of this nucleus, in possible agreement with a dimeric structure [235, 236]. ^{10}Be is a further interesting case since it can be described in terms of a nuclear *dimer* with a

couple of valence neutrons [170]. In this case, also the pairing forces between valence neutrons can play a role in the stability of the whole super-deformed nucleus.

To describe the structure of light nuclei with extra (or deficient) neutrons, the AMD model represents an excellent tool to disentangle single-particle and molecular-like aspects, which often coexist. For example, a theoretical study of low-lying excited states of the ^{10}Be isotope was performed by Kanada-En'yo et al. [237] by means of variational calculations After parity and total angular momentum Projection (VAP) in the framework of AMD. In this model, excited levels are organized in rotational bands with band-heads $K = 0_1^+$, 2_2^+, 0_2^+, and 1_1^-. For each case, they analyze both proton and neutron density distributions, and they report quite deformed shapes, typical of the $2\alpha + 2n$ clustering structure. From an analysis of the single-particle wave functions of valence neutrons, the 0_1^+ as well as the 2^+ and 4^+ members of the ground band is found to be in the negative-parity orbitals; in terms of the bonding theory, they are characterized to be π bonds [168, 232]. In this configuration, valence neutrons are orthogonal to the α-centers axis which, consequently, have a less pronounced separation. On the other hand, clustering phenomena are even more evident in the 1^- band and, especially, in the 0_2^+ band (built, respectively, on the 5.96 MeV 1^- and the 6.18 MeV 0^+ states). The latter is characterized by significant components of positive parity orbits, which, in a physical chemistry fashion, are analogous to the σ orbit. In this case, valence neutrons are localized in the region between clusters, leading to a larger distance between the α centers and a much more developed cluster nature. These findings are in agreement with the ones of von Oertzen [170], obtained with his dimer model of beryllium isotopes. Other calculations have been performed using a microscopic $\alpha+\alpha+n+n$ model based on the molecular orbit (MO) approach [243]. Low-lying states of ^{10}Be were predicted using several configurations of valence neutrons built as combinations of three basic orbitals, originating from the low-lying $3/2^-$, $1/2^+$ and $1/2^-$ states in ^{9}Be. The ^{10}Be ground state together with the 0_3^+ state appear to be characterized by the π orbit of the valence neutrons; they do not exhibit a particularly pronounced cluster separation. The second 0^+ state, being characterized by a σ orbit, shows a large inter-cluster distance, in agreement with AMD calculations [237]. The present experimental knowledge of ^{10}Be cluster states and rotational bands is still not completely clear [238, 239]; recent experimental and theoretical progresses on this subject will be discussed in Sect. 10.4.

The above discussion on beryllium isotopes can be extended also to the case of multi-center molecules, or nuclear polymers [170]. Carbon isotopes represent the simplest cases, since they are constituted by 3 α-centers [7, 199]. Along the carbon isotopic chain, particularly remarkable examples are present among both *proton-rich* and *neutron-rich* isotopes. For example, concerning the proton-rich ^{11}C, Kanada and collaborators proposed a systematic study of its negative-parity states within the AMD framework [240]. In this work, they were able to reproduce the $3/2_3^-$ state at an excitation energy of 8.10 MeV; furthermore, its structure seems to correspond to the Hoyle state in ^{12}C, being considered as a gas-like state with a pronounced 2α $+^3$He configuration, where the two α-clusters and the ^{3}He are weakly interacting and spatially extended. On the other hand, a $5/2_2^-$ state is found quite at the same excitation energy, but without cluster properties. A comparison with the spectroscopy of *mirror nucleus* ^{11}B has revealed a correspondence between states of these two nuclei; for

example, the above-discussed $3/2_3^-$ state of ^{11}C is linked to the 8.56 MeV mirror state in ^{11}B, characterized by having a diluted-gas structure [241, 242]. Cluster states of ^{11}C have been also organized into rotational bands, and these results are discussed in [243, 244].

The first neutron-rich carbon isotope is the ^{13}C. As in the case of ^{11}C, its cluster configurations is strongly connected to the one of ^{12}C [169]. One of the first systematic studies, by Milin and von Oertzen [170], focused on the existence of *parity doublets*, i.e., couples of rotational bands with opposite parity and the same structure. These bands reflect the intrinsic asymmetry of the underlying structure ($^9\mathrm{Be} + \alpha$ or $\alpha + \alpha + \alpha + \mathrm{n}$). Starting from the known spectroscopy at that time, they suggested the occurrence of a $K^\pi = 3/2^-$ molecular band built on the 9.897 MeV state and a $K^\pi = 3/2^+$ molecular band having the 11.080 MeV as band-head. Several of the states belonging to these bands were found to be populated in reactions involving α-transfer, and this could be a signal of their pronounced α-cluster nature. The properties of these states have also been characterized on the basis of a MO model. From an analysis of the moment of inertia, they suggest a linear chain arrangement of the three α-particles bound by a covalent neutron. States corresponding to the $^9\mathrm{Be}(1/2^+, 1.68$ MeV$) + \alpha$ structure are predicted as well and they have been linked by the authors to possible triangular configurations. A doublet of $J^\pi = 1/2^\pm$ experimentally observed states lying, respectively, at 10.996 MeV and 8.86 MeV could be candidates for this structure. Finally, they suggested that the distinction between linear and triangular fashions in the ^{13}C cluster arrangement could be connected to the occurrence of σ and π-orbitals for the ground and first excited states of ^{9}Be, in which the valence neutron occupies two orthogonal configurations.

^{13}C low-lying states have been also object of microscopic 3α–n calculations, as reported in Refs. [245–248]. High energy ^{13}C rotational bands, based on its 3α cluster structure, were predicted by Furutachi and collaborators [246] using a $3\alpha + n$ cluster model based on the GCM wave function. They suggested the existence of two rotational bands built on $3/2_2^-$ (11.4 MeV) and $3/2_3^-$ (14.5 MeV) band-heads states around the threshold energy, being both characterized by large moment of inertia and a pronounced cluster configuration. Another important subject was the presence of $1/2^\pm$ states in ^{13}C with a pronounced 3α nature. They could be characterized by a structure made by coupling a valence neutron to the Hoyle state in ^{12}C. AMD calculations pointed out that the $1/2_3^-$ ($E_x \approx 15.0$ MeV) has a strong $3\alpha + n$ structure, giving rise to a linear chain band ($K^\pi = 1/2^-$) with a large deformation [247]. Another possible Hoyle-analog state is found, by means of $3\alpha + n$ OCM calculations [248], at an excitation energy of about 14.9 MeV. This state is described by a gas-like configuration with an extremely large radius (4.3fm), and it has a dominant (≈ 0.6) $^{12}\mathrm{C}(0_2^+) \otimes \mathrm{n}(\mathrm{s}_{1/2})$ spectroscopic factor.

Also ^{14}C has been recently proposed to be characterized by a strong molecular-like nature, which could even give rise to a linear chain-like structure. AMD model calculations by Suhara and Kanada-En'yo [249] suggested the existence of a positive-parity prolate band (ending with a 4^+ state) with a 0^+ band-head just a few MeV above the ^{10}Be+α threshold. They calculated also the dimensionless α particle widths of the members of such band, being of the order of 10–20%. The linear chain structure is stabilized by its orthogonality to low-lying states; such low energy cluster states

are triaxially deformed, and are built starting from bases with bending configurations. Density distributions derived from AMD wave functions pointed out the occurrence of a configuration of ^{14}C where two α particles and two neutrons are closely placed, resembling a ^{10}Be molecular state, while the second α particle is more distant from this structure. Qualitatively, this behavior suggested an easy population of molecular-like cluster states in ^{14}C via ^{10}Be+α resonant elastic scattering and triggered an intense campaign of experiments (see Sect. 12.5).

Unfortunately, few calculations are available for the odd heavy isotopes of carbon, as ^{15,17,19} C. For example, in Ref. [250] the structure of the ground and low energy excited states of such isotopes is treated within the GCM approach, by considering the even isotope + neutron configuration and allowing for the possibility of core excitations. Interestingly, the authors pointed out a reduction of the spin–orbit force, leading to a smaller energy distance between split levels. A small neutron halo structure was also suggested for the ^{15}C ground state [251].

A more extended literature has been recently produced on the theoretical prediction of cluster structures in ^{16}C. Its possible molecular configurations are constituted by a symmetric three-center structure of the type $3\alpha + 4n$, with the possibility of showing also a stable linear-chain configuration: its stability against the bending motion was pointed out by MO calculations [252]. More recently, AMD theoretical calculations [253] suggested the existence of two different types of trimeric structures: one with the α-clusters forming an isosceles triangular configuration and the other having a linear-chain fashion. The latter is particularly stable—thanks to the role of the valence neutrons. Concerning the triangular configuration, valence neutrons are found to occupy the *sd* shell, while the linear-chain configurations are qualitatively understood in terms of $3/2^-_\pi$ and $1/2^-_\sigma$ molecular orbits, as predicted by the molecular orbital model [252]. Such states were classified in Ref. [253] in triangular-like and linear-like rotational bands, with band-heads, respectively, at 8.0 MeV and 15.5 MeV. Recent experimental results on such important aspects will be discussed in Sect. 12.6.

Obviously, also heavier nuclides can give rise to strong molecular-like configurations driven by clustering. Some examples are given by neutron-rich oxygen and neon isotopes [7]. Indeed, signatures of alpha clustering have been identified in ^{18}O via α+^{14}C decay after inelastic scattering analysis or with transfer reactions [254, 255]: apart from the existence of rotational bands characterized by large moment of inertia and parity doubling, due to the breaking of the intrinsic reflection symmetry [256–258], some states in ^{18}O have reduced partial widths for the α+^{14}C cluster configuration that are close to the single particle limit [259]. Detailed analysis on the structure and properties of ^{18}O positive parity states characterized by complex many-particle-many-holes configurations (e.g., 4p-2h or 6p-4h, that can be linked to the occurrence of α+clustering in ^{18}O) have been discussed, e.g., in Refs. [260, 261]. Similar considerations can be drawn for Neon and Magnesium isotopes; as an example, several theoretical works discussed the occurrence of α clustering in ^{22}Ne, both with microscopic algebraic methods [262] or with an extended two-cluster model using GCM [263].

6 An overview of the main techniques for the study of clustering

The research on the *spectroscopy* of light nuclei is one of the key aspects to understand clustering. Such studies are related to the knowledge of fundamental properties of the largest possible number of states of a nucleus. The main properties investigated in spectroscopic studies are E_x, J, T, π, Γ, C^2S, where E_x is the excitation energy of the state, J is the total angular momentum, T is the isospin, π is the parity of the corresponding wave-function, which is connected to its spatial symmetry, the symbol Γ indicates the width (total or partial) of the state and C^2S are the so-called *spectroscopic factors*. The latter are the square modules of the *spectroscopic amplitudes*, which are formally connected, as we will discuss in the following, to the projection of the nuclear wave-function onto each possible nuclear configuration. Together with these quantities, also *electromagnetic moments* (mainly magnetic dipole and electric quadrupole and octupole moments) of nuclear states are of extreme importance in nuclear physics, but since they are mainly investigated with hyper-fine structure experiments, or with analysis involving correlation studies of emitted γ-quanta, their detailed discussion goes beyond the framework of this report, which is mainly focused on the spectroscopy of states by means of charged particles or neutron detection. Another very important property, which can indicate the degree of collectivity of a given state, is linked to the reduced transition probability $B(E2)$ for electric quadrupole transitions between two nuclear states. In the presence of α-clustering phenomena, such values are typically well larger than the shell model predictions (see, e.g., [264] for a recent application to α clustering effects in heavy nuclei).

The spectroscopic properties listed above can be studied by means of different types of experiments; basically, they could involve nucleus-nucleus collisions at low and intermediate energies or, especially for heavier nuclei, the study of the decay processes of naturally occurring or artificially synthesized radio-isotopes. In this work, we will discuss essentially the first category of experiments.

Nuclear reactions between light ions can be subdivided into two main categories: *compound nucleus reactions*, i.e., reactions that can involve the *formation* of a resonant state as an intermediate stage, and the so-called *direct reactions*, typically involving the *production* of an excited state as a final product of the collision. In the last case, the properties of the *produced* state can be investigated by detecting the corresponding decay products (particle–particle and multi-particle *correlations*).

In the next paragraphs, we will discuss some aspects of both the reaction mechanisms and on the main analysis techniques applied to deduce experimental information on the spectroscopy of nuclear states.

6.1 *Formation* experiments: Compound nucleus reactions

High-precision experiments involving the formation of a compound nucleus represent a powerful way to probe clustering in nuclei.[9] Let us consider a projectile nucleus

[9] The scheme of compound nucleus reaction was introduced by Niels Bohr in 1936. According to the Bohr idea, a low-energy incident particle can be fully *absorbed* by the target nucleus, and after several internal collisions, it will share its momentum with the other nucleons of the target. The kinetic energy and the

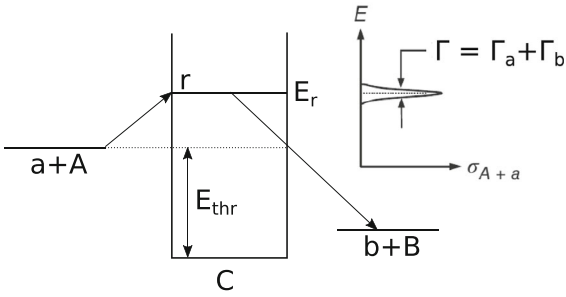

Fig. 8 Schematic view of a compound nucleus reactions populating a resonant state at an energy E_r. The state is formed by $a + A$ collision and decays in the $b + B$ channel. A schematic view of the occurrence of an *isolated* resonance in the A(a,b)B reaction cross section is shown on the right side of the panel

a impinging on a target nucleus A at low bombarding energy: we can observe the *formation* of a compound system C at a given excitation energy. This meta-stable system can subsequently decay in any of the *open*[10] channels.

We can now assume, for simplicity, that the formation of the compound nucleus C populates an *isolated* resonance of the many-body system, and that there are only two open channels, a and b (the latter corresponds to the emission of an *ejectile* nucleus b and a *residual* nucleus B, as sketched in the Fig. 8). The theory of nuclear reactions [33, 208] points out an important aspect: the *cross section* σ must depend on the properties of the excited state of the compound nucleus through the logarithmic derivative f_l of the radial wave-function $u_l(r)$ at the nuclear boundary $r = R$. The solution of the Schrödinger equation outside of the nuclear surface leads to the expression of the radial wave function; it assumes the form (see Refs. [208, 233, 267] for a complete derivation):

$$\begin{aligned} u_l(r) &= A u_l^+(r) + B u_l^-(r) \\ &= A e^{-i\delta_l}[G_l(r) + i F_l(r)] + B e^{-i\delta_l}[G_l(r) - i F_l(r)], \quad r > R \end{aligned} \tag{14}$$

where u_l^+ and u_l^- represent respectively the asymptotic limits of incoming and outgoing spherical wave at large distances from the reaction vertex. The quantity δ_l is the Coulomb *phase shift*. In the case of $l = 0$ neutrons, several simplifications occur: $F_l = kr j_l(kr)$ and $G_l = kr\eta_l(kr)$, being $j_l(kr)$ and $\eta_l(kr)$ respectively the spherical Bessel and Neumann functions. In the more complex case of a charged particle with a given orbital angular momentum ℓ, they correspond, respectively, to the *regular* and *irregular* Coulomb wave functions. In this context are particularly important the *real* quantities S_l and P_l, which are called respectively *shift factor* and *penetration factor*.

binding energy of the incoming particle will be converted into excitation energy of the system formed by the merging of target + projectile, the so-called *compound nucleus* [265, 266].

[10] *Open* means that this channel fulfills the conservation laws that characterize strong forces: energy, angular momentum, parity, charge, isospin, baryon number.

They are fully determined by the boundary conditions of f_l outside the nucleus:

$$\begin{aligned} f_l &= R\left(\frac{1}{u_l^+(r)}\frac{du_l^+(r)}{dr}\right)_{r=R} \\ &= R\left[\frac{G_l(dG_l/dr)+F_l(dF_l/dr)+iG_l(dF_l/dr)-iF_l(dG_l/dr)}{F_l^2+G_l^2}\right]_{r=R} \\ &\equiv S_l + iP_l \end{aligned} \tag{15}$$

being:

$$\begin{aligned} S_l &= R\left[\frac{F_l(dF_l/dr)+G_l(dG_l/dr)}{F_l^2+G_l^2}\right]_{r=R} \\ P_l &= R\left(\frac{k}{F_l^2+G_l^2}\right)_{r=R} \end{aligned} \tag{16}$$

These quantities depend on the wave-number k in the center of mass system, the channel radius R and the orbital angular momentum l; the Coulomb functions for charged particles depends also on the Sommerfeld parameter η [33]. Let us consider $l = 0$ neutrons for simplicity; in this case, being $F_0 = sin(kr)$ and $G_0 = cos(kr)$ [268], we will obtain $P_0 = kr$ and $S_0 = 0$, indicating the vanishing of the shift factor in absence of a barrier. The reaction cross section close to an isolated resonance can be derived in terms of P_l and S_l (see, e.g., [33]), leading to the well-known *Breit–Wigner* formula:

$$\sigma = (2l+1)\frac{\pi}{k^2}\frac{\Gamma_a\Gamma_b}{(E-E_r)^2+\Gamma_r^2/4} \tag{17}$$

where Γ_a and Γ_b are the so-called *partial widths* for, respectively, the entrance channel and the exit channel of the reaction. In particular, they are equal to

$$\begin{aligned} \Gamma_a &\equiv -\frac{2[P_l(E)]_a}{(\partial f_l/\partial E)_{E_r^0}} = 2P_l^a(E)\gamma_a^2 \\ \Gamma_b &= 2P_l^b(E)\gamma_b^2 \end{aligned} \tag{18}$$

In the equations above, $P_l^a(E)$ and $P_l^b(E)$ are, respectively, the penetrability factors for the entrance and the exit channels. The penetrability factor appears in the definition of the partial widths because a particle has to penetrate the barrier to give rise to the reaction. γ_a^2 and γ_b^2 are the so-called *reduced widths*, and they are easily obtained via Eq. (18) by inversion. The cross section depends on the properties of the *interior* of the compound nucleus through these numbers. Moreover, they are connected to the above-mentioned spectroscopic factors C^2S, as we will see later.

The total width of the resonance would correspond, approximately, to the width of the observed Lorentzian-like function characterizing the cross section close to an

isolated resonance. It is proportional to the inverse of the resonance lifetime, and corresponds to the sum of each partial width:

$$\Gamma_r = \Gamma_a + \Gamma_b \tag{19}$$

E_r is the *observed* resonance energy, a very important property of a resonant state. It is defined as:

$$E_r = E_r^0 - S_l(E)\gamma_a^2 \tag{20}$$

This equation indicates that the observed resonance energy E_r, appearing in the formulation of the cross section for an isolated resonance, is shifted with respect to the *formal* energy E_r^0 of a quantity $-S_l(E)\gamma_a^2$. This feature is genuinely due to the presence of a barrier in the entrance channel.

To understand the link between the nuclear reaction quantities discussed here and the nuclear structure of a state, we can consider a semi-classic example (see, e.g, [266]). Let us consider an excited state of ^{11}Be, whose wave function Ψ_1 corresponds to the ground state of ^{10}Be with a further neutron in the $2s_{1/2}$ orbit, i.e.,

$$\Psi_1(^{11}\mathrm{Be}) = \Psi(^{10}\mathrm{Be}_{\mathrm{gs}}) \otimes \Psi(2s_{1/2}) \tag{21}$$

Being ^{10}Be an even–even nucleus, its ground state is 0^+ and thus the state of Eq. (21) would have $J^\pi = 1/2^+$. This represents a highly excited state of ^{11}Be with an unbound neutron (the last bound neutron state would stay in the $1p_{1/2}$ orbital, according to shell model predictions), which can be released in a nucleon-emitting process like:

$$^{11}\mathrm{Be}^* \longrightarrow {}^{10}\mathrm{Be}_{\mathrm{gs}} + \mathrm{n}(2\mathrm{s}_{1/2}) \tag{22}$$

If we indicate with v_i the velocity of the neutron *inside* the ^{11}Be nucleus and with R the radius of the nucleus, the extra neutron will reach the nuclear surface in a time of the order of R/v_i. When hitting the surface, it will feel a change in the potential which can reflect it again inside the nucleus. It is possible to demonstrate (on the basis of a simple wave mechanics calculation, see e.g. [266]) that, on average and in first approximation, it will be reflected a number of times equal to $v_i/4v_e$, where v_e is the velocity with which the outgoing neutron is eventually emitted [266]. The average time required for a neutron to be emitted is thus:

$$\tau_0 \approx \frac{R}{v_i}\frac{v_i}{4v_e} = \frac{R}{4v_e} \tag{23}$$

Considerations based on a more accurate description of the transmission coefficients lead to a slightly different expression:

$$\tau_0 \approx \frac{R}{3v_e} \rightarrow \Gamma_0 \approx 3\frac{\hbar v_e}{R} \tag{24}$$

If we indicate with μ the reduced mass of the binary channel decomposition that we are considering, and taking into account that v_e is the relative velocity of the decay partners, we have $\mu v_e = \hbar k$, being k the *external* wavenumber, related to the unbound particles. After immediate substitutions, we have:

$$\Gamma_0 \approx 3\frac{\hbar v_e}{R} = \frac{3\hbar^2 k}{\mu R} = \frac{3\hbar^2 kR}{\mu R^2} = 2 \cdot kR \cdot \frac{3}{2}\frac{\hbar^2}{\mu R^2} \tag{25}$$

But for s-wave neutrons, the penetrability is simply $P_0 = kR$, as said before; if we consider the definition of Eq. (18), we can consider the so-called *single-particle limit* or *Wigner limit* as the following value for the reduced partial width:

$$\gamma_0^2 = \frac{3}{2}\frac{\hbar^2}{\mu R^2} \tag{26}$$

It is possible to derive the Wigner limit also in a fully quantum mechanical picture, for a given shape of the potential; to do this beautiful exercise of quantum scattering theory, the reader is referred to [267].

If we now consider all the possible configurations of the type of Eq. (21) leading to a $J^\pi = 1/2^+$ state, we can write the expansion:

$$\begin{aligned}\Psi_i(^{11}\mathrm{Be}^*) = c_{i1}\Psi(^{10}\mathrm{Be}_{\mathrm{gs}}) \otimes \Psi(2s_{1/2}) + c_{i2}\Psi(^{10}\mathrm{Be}_{1^-}) \otimes \Psi(1p_{1/2}) \\ + c_{i3}\Psi(^{10}\mathrm{Be}_{2^+}) \otimes \Psi(1d_{5/2}) + \ldots\end{aligned} \tag{27}$$

This represents a wave-function expansion of a generic $1/2^+$ state i of ^{11}Be in the ^{10}Be + n configurations. In a dynamical view, we can consider that the nucleus will spend a given quantity of time in each of them. The decay partial width of the state i via neutron emission in a given configuration k will be therefore linked to the partial lifetime and the partial widths by:

$$\Gamma_{i,k} = \hbar\lambda_{0k}|c_{ik}|^2 \tag{28}$$

Here, λ_{0k} represents the decay rate of the k-th configuration (see Eq. 23) and the factors c_{ik}^2, which are the square of the amplitudes c_{ik}, are equivalent to the fraction of time spent by the nucleus in the k-th configuration. For a given configuration we define:

$$\theta_{i,k}^2 = |c_{ik}|^2 \tag{29}$$

which corresponds to the *dimensionless* reduced partial widths, i.e., the ratio of the above-discussed decay partial widths to the ones at the Wigner limit $\theta_{ik}^2 = \frac{\gamma_{ik}^2}{\gamma_{0,ik}^2}$. From the nature of the factors c_{ik} defined in Eq. (27), we can derive the *sum rule*:

$$\sum_i \theta_i^2 = 1 \tag{30}$$

Therefore, for a generic state i decaying via neutron emission, $\theta_i^2 \leq 1$. If the structure of the i-th state is fully dominated by a particular single-particle configuration, like, in our example, ^{10}Be + n, it will have $\theta_i^2 = 1$: in this case, the decay partial width is said to be *at the Wigner limit*. The investigation of the partial width of a nuclear state, made by analyzing the experimental data on reaction cross sections, is therefore very useful to probe the occurrence of a peculiar configuration in the nuclear structure of a state. This is clearly the case of clustering phenomena, for which we can expect that the partial widths linked to the α emission (or, for heavier nuclei, of other cluster decomposition, as ^{8}Be or ^{12}C emission) are characterized by having a significant fraction (typically larger than 10%) of the Wigner limit.

The above subjects not only apply to the case of $l = 0$ $X+n$ configurations but can be easily generalized to all the possible channels. Its extension to the more complex case of emission of charged particles in an arbitrary l wave can be derived in the following way (see Ref. [208, 266] for more details). We will make the hypothesis that the compound nucleus populates the resonance r and that there is only one open channel c. The corresponding wave function of this meta-stable state, which contributes to the emission in the channel c is expressed by a linear combination of radial single-particle wave functions u_{rk}^c, each of them contributing to a particular configuration of the compound system in the decomposition c[11]:

$$\Psi_r(\vec{R}) = \left[\sum_k c_{rk} u_{rk}^c(R)\right] \frac{Y_{lm}(\theta, \varphi)}{R} \tag{31}$$

The partial width Γ_c of the resonant state can be determined as the probability flux of the particle through the only open channel c. This number can be calculated by integrating the quantum-mechanical current [267, 269], through a sphere of radius R, in the whole solid angle:

$$\Gamma_r^c = \hbar \int_{4\pi} R^2 j \mathrm{d}\Omega = \hbar \int_{4\pi} R^2 \frac{\hbar}{2i\mu} \left(\Psi_r^\star \frac{\partial \Psi_r}{\partial r} - \frac{\partial \Psi_r^\star}{\partial r} \Psi_r\right) \mathrm{d}\Omega \tag{32}$$

After some algebric re-arrangement (see Ref. [208]) we find:

$$\Gamma_r^c = 2\frac{\hbar^2}{\mu R} P_l^c(E) C^2 S \varphi_{ck}^2 \tag{33}$$

being:

$$C^2 S = c_{rk}^2 \tag{34}$$

$$\varphi_{ck}^2 = \frac{R}{2} |u_{rk}^c(R)|^2 \tag{35}$$

[11] Typically, a channel (decomposition c) involves the presence of the two particles b and Y. Each *particular configuration of a given decomposition* is found by solving the Schrödinger equation for a Hamiltonian describing the motion of particle b within the well generated by $b + Y$ in the single-particle approximation. This equation leads to several (discrete) solutions that will represent a *particular configuration* of the decomposition c ($\equiv b + Y$).

The C^2S quantities are called *spectroscopic factors*,[12] which are the square of the *spectroscopic amplitudes* used in the linear combination of Eq. (31), while the φ^2_{ck} quantities are the decay rate in the channel c from each configuration k.

The spectroscopic factor, which is intimately linked with the structure of a state, is a measure of the probability that a compound state r, with a cluster configuration c, can be described by the single-particle configuration k. From the Eq. (33), we can write the partial width of the decay of a state in a particular channel as a product of three factors: (i) the probability that the nucleons will arrange themselves in the configuration corresponding to the final state (C^2S), the probability that the single particle will be present at the boundary ($\propto |u^c_{rk}(R)|^2$),[13] and the probability to penetrate centrifugal and Coulomb barrier by the particle ($P^c_l(E)$).

6.2 R-matrix theory

In the compound nucleus scenario, the *R-matrix* theory is often used to extract spectroscopic properties of nuclear states like E_x, J, π, γ^2_c from the experimental data of excitation functions and angular distribution of nuclear reaction cross sections; it is, therefore, a very useful tool to investigate clustering phenomena light nuclei. A detailed treatment of R-matrix theory can be found in Ref. [267, 271]; we will give just a sketch in the following.

This method was introduced by Wigner and subsequently refined by Wigner and Eisenbud [272, 273] during the 30's. The observables of nuclear reactions are described in terms of several parameters: the radius a of a *nuclear sphere*, the energy levels, and the reduced widths. They are typically left as free parameters in best-fit procedures of experimental data. No assumptions are indeed made concerning the shape of the wave functions inside the nuclear *sphere*, and only their properties at the surface of the nuclear sphere are used. These properties are expressed in terms of the logarithmic derivatives of the wave functions at the boundaries, which form the matrix element of the R-matrix. The theory is therefore very general since it is free of any detail characterizing the potential energy function inside the nucleus, except the assumption regarding the formation of a compound nucleus. The R-matrix theory allows extending the previously discussed Breit–Wigner formula of the cross section to a more general formulation which includes an arbitrary number of channels and an arbitrary number of resonances, taking into account the interference effects between resonances. The R-matrix relates the value of the wave function in the internal region to its derivative at each in-going channel. It is defined, for an arbitrary number of channels c, c', as:

$$\mathfrak{R}_{c,c'} \equiv \sum_r \frac{\gamma_{rc'}\gamma_{rc}}{E_r - E} \tag{36}$$

[12] C^2 represents the square of a Clebsch–Gordan coefficient taking into account the *isospin* of the entrance and exit reaction channels, while S is the actual spectroscopic factor. However, in the literature often the whole product C^2S is indicated as *spectroscopic factor*

[13] This quantity, usually set to unity in simplified calculations [270], can be more precisely estimated by solving the Schrödinger equation for a Wood–Saxon potential. See [208] for details.

The definition (36) connects the elements of the R-matrix explicitly to the energy, since γ_{rc} and E_r are energy-independent parameters. The poles of the R-matrix occur at each value E_r of energy and each of the elements $\mathfrak{R}_{c,c'}$ represents a real number. The position of the poles is furthermore independent on the channels c and c'. In the framework of R-matrix, a channel is identified by the quantum numbers $\{\alpha(I_1 I_2)sl, JM\}$, where $\alpha(I_1 I_2)$ represent a specific state of excitation α of a specific pair of nuclei 1 and 2, having spins I_1 and I_2, $\vec{s} = \vec{I_1} + \vec{I_2}$ is the channel spin, l is the orbital angular momentum of their relative motion and $\vec{J}$ and M are the total spin and its component along a quantization axis. For the entrance channel consisting of a projectile and a target nucleus, one can set $\vec{I_1} = \vec{j_p}$ and $\vec{I_2} = \vec{j_t}$, consequently:

$$\vec{J} = \vec{l} + \vec{j_p} + \vec{j_t} \tag{37}$$

Because of the degeneracy of these values, there are $(2l+1)(2j_p+1)(2j_t+1)$ different sets of spin orientations with the same probability. The cross section has therefore to be multiplied for the statistical factor:

$$g(J) = \frac{2J+1}{(2l+1)(2j_p+1)(2j_t+1)} \tag{38}$$

The cross section, as well as the phase shifts, can be derived from the R-matrix using the boundary conditions and the energy independent parameters γ_{rc}. As an example, in the case of an isolated resonance and an arbitrary number of channels, one can derive the so-called *generalized one-level Breit–Wigner formula* for a generic reaction leading from the α channel to the α':

$$\sigma(\alpha, \alpha') = \frac{\pi}{k^2} \frac{2J+1}{(2j_p+1)(2j_t+1)} \frac{\left(\sum_{ls} \Gamma_{rc}\right)\left(\sum_{l's'} \Gamma_{rc'}\right)}{(E - E_r - \Delta_r)^2 + \Gamma_r^2/4} \tag{39}$$

where $\Gamma_{rc} = 2P_c(E)\gamma_{rc}^2$ are the partial widths, $\Gamma_r(E) = \sum_c \Gamma_{rc}(E)$ is the total width of the resonance r and $\Delta_r(E) = \sum_c \Delta_{rc}(E)$ is the total level shift. The latter is the superposition of partial level shifts, which appeared in the formulation of the single-channel Breit–Wigner of paragraph 6.1: $\Delta_{rc}(E) = -[S_c(E) - S_c(E_r)]\gamma_{rc}^2$. Both penetration and shift factors are referred to the *interaction radius*. Normally it is chosen to be as small as possible so that the quantities of the resonance theory contain primarily information on the nuclear interaction. For this reason, it is commonly taken equal to the smallest separation distance of the nuclear pair for the reaction to occur, i.e., the *channel radius* $R = r_0(A_t^{1/3} + A_p^{1/3})$, with a radius parameter lying in the range $r_0 = 1.0$–1.5 fm. A simplification of Eq. (39) was introduced by Thomas in 1951, observing that since the shift factor $S_c(E)$ depends only weakly on the energy, it could have been expanded in the following way:

$$E - E_r - \Delta_r \approx (E - E_r)\left[1 - \left(\frac{\mathrm{d}\Delta_r}{\mathrm{d}E}\right)_{E_r}\right] \tag{40}$$

Using the result of Eq. (40), the commonly used formulation of Eq. (39), which reproduces the $\alpha \rightarrow \alpha'$ cross section for an isolated resonance r, becomes:

$$\sigma(\alpha, \alpha') = \frac{\pi}{k^2} \frac{2J+1}{(2j_p+1)(2j_t+1)} \frac{\left(\sum_{ls} \Gamma^o_{rc}\right)\left(\sum_{l's'} \Gamma^o_{rc'}\right)}{(E-E_r)^2 + \Gamma_r^2/4} \tag{41}$$

where the *formal widths* Γ_{rc} have been replaced by the *observed widths* Γ^o_{rc}:

$$\Gamma^o_{rc} \equiv \frac{\Gamma_{rc}}{1-(\mathrm{d}\Delta_r/\mathrm{d}E)_{E_r}} = \frac{\Gamma_{rc}}{1+\left(\sum_{c''} \gamma^2_{rc''} \frac{dS_{c''}}{dE}\right)_{E_r}} \tag{42}$$

which applies also to the reduced widths. The difference between formal and observed width is much more important as the reduced width of the state becomes large.

Operatively, it is possible to use multi-channel multi-level R-matrix formulations like [274, 275] to find the set of parameters E_x, J, π, γ_c^2 which reproduces the experimental trend of the cross section for each channel and each process considered. In particular, the approach of [275] has the sizable advantage of using, as starting parameters in the fit search, the observable values and not the formal ones, strongly simplifying the R-matrix analysis of data. Since clustering phenomena are related to states having pronounced (i.e., close to the Wigner limit) partial widths for α-emission (Γ_α), the study of compound nucleus reaction channels which involve the emission of an α-particle, like *resonant elastic scattering* (RES) (α,α), *resonant inelastic scattering* (α, α'), (p, α) and (d, α) reactions, is of great help to determine the Γ_α partial width of a given excited state from best-fit procedures.

6.3 Direct reactions and correlations

In addition to the compound nucleus reaction mechanism, which typically occurs at low energies, also the so-called *direct reactions* are very important to study clustering. This mechanism becomes increasingly important as the bombarding energies increase, even if evidences for direct reaction mechanisms at very sub-barrier energies have been reported in the literature, especially in the presence of a pronounced cluster structure of the reaction partners [276, 277].

Particularly relevant for this aim are *transfer reactions* and *breakup reactions*. All these reactions have in common a quite short interaction time, being of the order of 10^{-22} s, i.e., the typical time scale of a nucleon, moving with average kinetic energy $(3/5E_F)$ inside a nucleus, to traverse the nuclear diameter of the target. This time is much shorter than the typical time needed for a complete momentum sharing in the compound nucleus, $\approx 10^{-16}$ s. Another important feature of direct reactions is that they retain memory of the momentum carried by the incident particle. In direct reactions there are few (or just one) nucleonic collisions and, consequently, strong asymmetries of angular distributions are observed. Except for specific cases with strong particle-exchange effects, the direction of the emitted particles in direct reactions is typically peaked at forward angles.

A simple classification of transfer reactions subdivides them into *pick-up* and *stripping* reactions. In both cases, we observe a transfer of one or a few nucleons between reaction partners. Pick-up reactions are characterized by the transfer of nucleons from the target to the projectile, while in stripping reactions it is the opposite. The perturbation of the nuclear field of the target is minimal and, for this reason, there is a strong tendency for the residual nucleus to be left in a state of low excitation.

A very important characteristic of direct reactions is the link between the angular momentum transferred in the reaction and the angular distribution of ejectiles. Normally, an angular distribution of a transfer reaction results from a superposition of waves emanating from all parts of the nuclear surface. This generates an interference effect which leads to particular diffraction-like patterns. These effects, and the perturbations on the incoming and outgoing waves due to the Coulomb and nuclear potential in the entrance and exit channels, are taken into account by means of the Distorted Wave Born Approximation (DWBA) or using Coupled Channel (CC) approaches [278, 279], by treating the incident and emitted particles as moving under the influence of an optical model potential. DWBA and CC calculations can predict the angular distribution of a transfer reaction, provided that carefully tuned optical potential and bound state descriptions are introduced as ingredients in the calculations. Under the assumption that the transferred nucleons enter one of the orbits without disturbing the nucleus, the angular distribution of the cross section $\sigma(\theta)$ can be written as follows:

$$\sigma(\theta) = C^2S \cdot \sigma_{DWBA,CC}(\theta) \tag{43}$$

where C^2S is the so-called *spectroscopic factor*. This value is linked to the scalar product of the wave-function of the populated nuclear state onto the wave-function of the cluster decomposition studied with the transfer reaction. As an example, we can consider the ^{12}C$(d,p)^{13}$C one-neutron transfer reaction. If one indicates with l_t and j_t, respectively, the orbital angular momentum of the transferred neutron and its total angular momentum, the configuration of the nucleus upon its entry is:

$$^{12}\mathrm{C}_{\mathrm{gs}} + \mathrm{n}(l_t,\, j_t) \tag{44}$$

The ground state of ^{12}C has $J^\pi = 0^+$; if, for example, we assume $l_t = 1$ and $j_t = 3/2$, the state formed in ^{13}C would have $J^\pi = 3/2^-$. In general, the state can be described as a mixing of all the possible configurations of the type given in Eq. (44), weighted by the corresponding spectroscopic amplitude. The probability to form a given $3/2^-$ state of ^{13}C will be therefore proportional to the time fraction spent in each of the configurations. In this frame, the wave function for a given $3/2^-$ state i will be:

$$\Psi_{3/2}(i) = \theta_1 \Psi[^{12}\mathrm{C}_{\mathrm{gs}}] \otimes \Psi(p_{3/2}) + \cdots \tag{45}$$

If a particular $\theta_j^2 = 1$, only one term of the expansion contributes to the state i. This would be in ideal agreement with the hypotheses used in deriving σ_{DWBA} and then $C^2S = 1$. In general, this is not true, and $C^2S = \theta_j^2$; C^2S are therefore the spectroscopic factors related to each configuration. C^2S can be directly obtained by comparing experimental data of one-nucleon transfer angular distributions to DWBA

or CC calculations, even for states which are below threshold and for which it is not possible to define decay partial widths.

The above considerations can also be applied to multi-nucleon transfer processes. In particular, given the pronounced cluster structure of light nuclei, α-particle transfer reactions are a very useful tool to investigate clustering features of nuclear states [280]. In this framework, reactions as (^{6}Li,d), (^{7}Li,t) and (^{12}C,^{8}Be) at energies of some times the Coulomb barrier have been used during the last decades to obtain the spectroscopic α factors S_α for nuclei in the p- and sd- shells [74], which are frequently very different from shell model predictions.

Other direct reactions very useful to probe clustering are the *knock-out* ones. They are reactions typically induced by high-energy proton beams, which, during the collision, would directly remove an α particle from the target nucleus. Also in this case it is possible to have access to the S_α values (for example, via the analysis of triple differential cross sections) for a large variety of nuclei of light-to-medium masses (see, e.g., Refs. [281, 282]).

Breakup reactions are another type of direct reactions often adopted to study α clustering in light nuclei above the emission threshold. They lead to a change of the nature of a nucleus via the interaction with another nucleus (e.g., by inelastic scattering or particle transfer) above the particle decay threshold, followed by its rupture into two (or more) charged particles. There are some advantages, in terms of kinematics, in the study of *projectile* breakup reaction. In this case, in fact, breakup fragments are forward-focused, because of the boost given by the projectile, and they can have enough energy to overcome detection and/or identification thresholds of experimental apparatuses.

We can make a further distinction of break-up processes into *sequential* and *direct* breakup. In the latter, the projectile nucleus suddenly disintegrates because of electrodynamics or density gradient effects occurring during its interaction with the target [283]. In this case, breakup fragments do not bring detailed information on the spectroscopy of excited state of the emitting nucleus. At variance, sequential breakup reactions are two-step process in which the nucleus is initially excited by means of the interaction with the target, and then it sequentially breaks-up into two (or more) particles to de-excite the parent nucleus. The spectroscopy of the excited state leading to the decay of the nucleus can be studied by measuring masses and momenta of the outgoing particles.

As an example, we assume a sequential breakup reaction of the type $X + Y \rightarrow X^\star + Y \rightarrow \sum_i x_{i=1}^N + Y$, where the N breakup fragments x_i of masses m_i are emitted by the intermediate excited state $X^\star$. The four-momentum of the i-th fragment will be:

$$q_i \equiv (x_i^0; x_i^1, x_i^2, x_i^3) = (E_i, p_i^x, p_i^y, p_i^z) \tag{46}$$

where we assumed $c = 1$. The total four-momentum will be given by $q = \sum_{i=1}^N q_i$, and the calculation of its (invariant) square leads to the expression:

$$\mathcal{M} = \sqrt{q^\mu q_\mu} = \sqrt{q^0 q^0 - q^1 q^1 - q^2 q^2 - q^3 q^3} \tag{47}$$

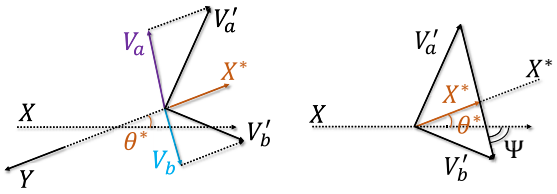

Fig. 9 Kinematics of vectors typically used to perform angular correlation studies in sequential break-up experiments. Primed quantities are expressed for the laboratory frame, while the non-primed ones are expressed in the zero-momentum frame. Adapted from Refs. [141, 284, 285]

where $\mathcal{M}$ is the *invariant mass* of the decaying excited state. The excitation energy of $X^\star$ is therefore given by the difference between its invariant mass and the mass of the ground state X:

$$E_x = \mathcal{M} - m(X) \tag{48}$$

Equation (48) allows to determine the energy position of excited states populated in a breakup reaction. This method to study the spectroscopy of nuclear states is one of the several *multi-particle correlation* techniques often used in nuclear physics, and it is particularly useful to probe cluster configurations in excited nuclei, since they have pronounced decay widths for the emission of constituent clusters.

In this framework, it is also possible to obtain further spectroscopic information on the nuclear structure of the emitting nucleus, like the spin J. For simplicity, we will consider the case of a binary decay of a state $X^\star$ into two spinless particles. In this case, the reaction can be indicated as $X + Y \rightarrow X^\star + Y \rightarrow a + b + Y$, where a and b are the correlated breakup fragments. The process is sketched in the left panel of Fig. 9, where the velocity vectors of all the particles emitted in the final states are drawn. In the "center of mass" of the reaction (*zero-momentum* frame), $X^\star$ and Y are emitted in opposite directions; the same occurs for the fragments a and b in their emission center of mass frame (the reference frame where $X^\star$ is at rest). We indicated in the figure the quantities used to determine the spin of the decaying state. The first is the angle formed by the direction of $X^\star$ in the reaction center of mass and the incoming beam direction, which is usually indicated as $\theta^\star$. Another important quantity is illustrated in the right side of Fig. 9. It is indicated as Ψ and it represents the angle formed by the relative velocity vector $\vec{v_{rel}} = \vec{v_b}' - \vec{v_a}'$ of the two fragments in the laboratory frame with the beam axis. By assuming that the emission of a and b proceeds from the decay of $X^\star$, from semi-classical considerations [141, 284] the double differential cross section $\frac{d^2\sigma}{\mathrm{d}\Omega^*_\theta \mathrm{d}\Omega_\Psi}$ would depend on $\theta^\star$ and Ψ as:

$$\frac{d^2\sigma}{\mathrm{d}\Omega_{\theta^*}\mathrm{d}\Omega_\Psi} \propto |P_\ell(cos(\Psi + \alpha\theta^*))|^2 \tag{49}$$

where P_ℓ is the ℓ-order Legendre polynomial and ℓ is the angular momentum of the two emitted particles. The so-called phase shift α is defined as $\alpha = \ell_f/J$, i.e., it

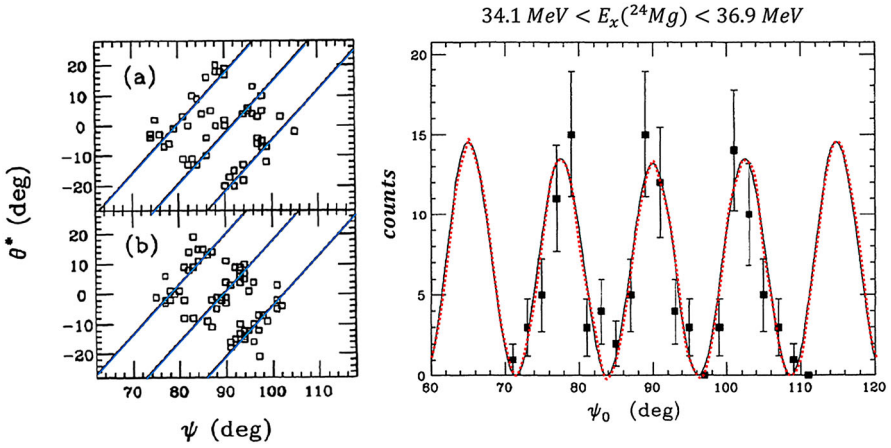

Fig. 10 (left) $\psi - \theta^*$ scatter plots obtained in the study of correlations between the particles emitted in the ^{16}O+^{12}C $\rightarrow$ ^{24}Mg*+^{4}He $\rightarrow$ ^{12}C+^{12}C+^{4}He reaction at 113 MeV bombarding energy. (**a**, **b**) Panels refer to two slightly different excitation energy windows in ^{24}Mg. (right) Projections of $\psi - \theta^*$ scatter plots on the direction orthogonal to the ridges of the data (blue lines of left panel). The red dashed line indicated the contribution expected from $J = 14$ states. Reprinted from Ref. [157] under permission

would represent the ratio of the final state *grazing* angular momentum to the spin of the resonance J. Equation (49) gives rise to *ridges* in the double differential cross section, as shown in Fig. 10. If we project the data in a direction orthogonal to the ridges, the obtained picture is the one shown in the same figure (left panel), where the periodicity reflects the ℓ-order Legendre polynomial. In such a way, it is possible to estimate ℓ and, for zero channel-spin cases, directly the J of the resonance $J = \ell$. A commonly used method to obtain firm estimates of ℓ is based on collecting experimental data at θ^* values close to zero, in order to minimize the effect due to the phase shift term $\alpha\theta^*$ [77].

In the case of multi-particle decay (i.e., with emission of more than two fragments) of an unbound state, it is possible to use multi-particle correlation techniques to inspect the decay path of the state. An important example, both in the nuclear and sub-nuclear fields, is represented by the decay of a resonance in three equal-mass particles. In such a case, as for the Hoyle state in ^{12}C, one can expect direct decays of the type $X^\star \rightarrow y_1 + y_2 + y_3$ or sequential decays, where a two-step process occurs: $X^\star \rightarrow y_1 + Y^\star \rightarrow y_1 + y_2 + y_3$. In this context, symmetric Dalitz plot can be inspected to visualize geometrically the different decay patterns and to extract their amplitudes. These plots were introduced in particle physics by Dalitz and Fabri [286, 287] but they have been largely used for multi-particle decay studies of nuclei (see, e.g., [160, 288]).

A symmetric Dalitz plot is built using the kinetic energy $E_{i,j,k}$ of the three particles in the rest reference frame of the parent nucleus $X^\star$. We can then define the Dalitz plot coordinates as:

$$\varepsilon_{i,j,k} = E_{i,j,k}/(E_i + E_j + E_k) \tag{50}$$

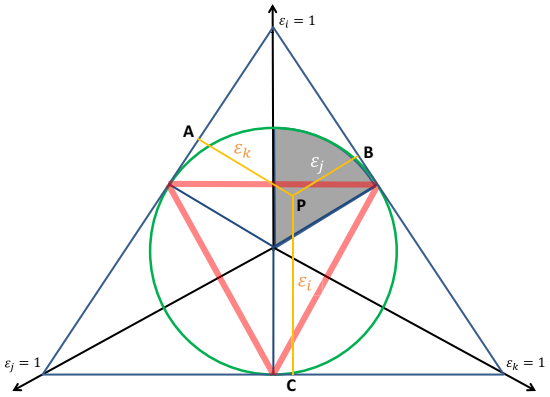

Fig. 11 A scheme of a symmetric Dalitz plot used to describe the decay into three particles of equal mass. $\varepsilon_i, \varepsilon_j, \varepsilon_k$ are the normalized decay energies described in the text. The green circle represent the boundary due to the (non-relativistic) momentum conservation; in relativistic applications, the circle is deformed into a shield-like locus. The red lines indicated qualitatively the expected loci for a pure sequential decay pattern of the Hoyle state of ^{12}C in α+^{8}Be $\rightarrow 3\alpha$

which are often indicated as *normalized decay energies*. The possibility of representing such coordinates into an equilateral triangle follows from the so-called *Viviani*'s theorem: for a generic point P inside the triangle, the sum of its distances from each side of the triangle is a constant. In this way experimental points, corresponding to $(\varepsilon_i, \varepsilon_j, \varepsilon_k)$ energy coordinates, are localized inside the triangle in Fig. 11. Furthermore, the (non-relativistic) momentum conservation in the decay would give a constraint that confines the data into a *circle*. In the case of direct decays driven by *phase space* considerations, the energy can be shared with any of the possible combinations $\varepsilon_{i,j,k}$, and the whole circle is populated, with a filling modulation that strongly reflects the spin of the emitting state. For the case of sequential decays, instead, the energies of the decay must fulfill much more restrictive constraints, leading typically to the population of straight bands within the circle. A typical choice made for simplicity in showing data consists in selecting $\varepsilon_i > \varepsilon_j > \varepsilon_k$; by doing this, the data collapse into one sector of the circle inside the triangle of Fig. 11. In the figure, horizontal bands typically occurring in the presence of sequential decays are qualitatively represented for the emblematic case of the Hoyle state sequential decay. The use of the Dalitz plot has been of paramount importance in the study of the decay pattern of the Hoyle state (see Fig. 12 for a typical example), for which several conflicting theories and experimental findings have been reported in the literature. Recent theoretical and experimental findings on such aspects will be discussed in large detail in the Sect. 12.3.

7 Recent progresses on clusters in light nuclei

In this section and in the following ones, we briefly describe some recent findings on the cluster structure of selected light nuclei (from Helium to Neon isotopes) and their impact on the knowledge of nuclear theories and on several aspects of nuclear astrophysics. The findings discussed here will mainly concern some selected publications

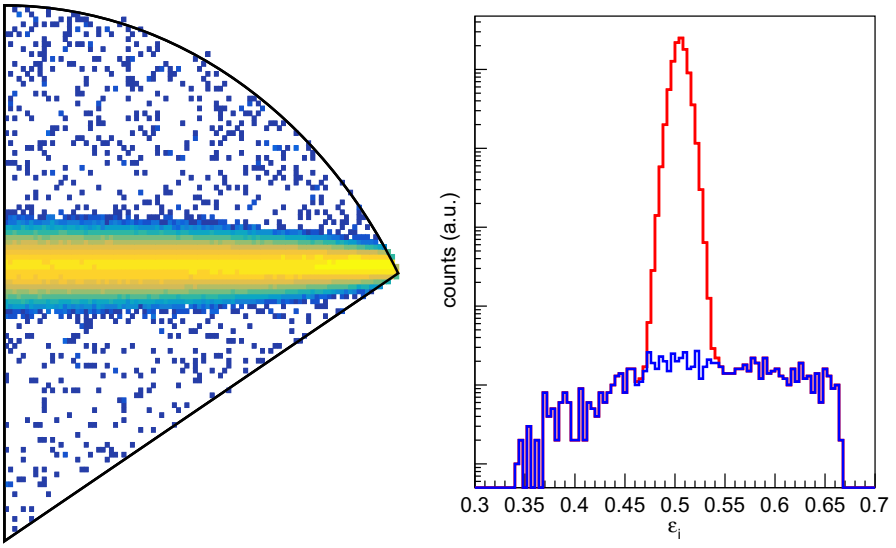

Fig. 12 (Left) A qualitative example of the expected population of a symmetric Dalitz plot in the case of a 3α decay of ^{12}C in the Hoyle state with sequential (assuming 99.9% branching) and direct (0.1%, phase space-driven) patterns. Values of energy and angular resolution of the simulated particles are chosen similarly to the ones commonly seen in multi-detection systems used in this type of experiments. (Right) The radial projection of events represented in the Dalitz plot. The expected direct (phase space) contributions are shown in blue

of the last 5 years (2017–2022). For the sake of clarity, we discuss such results by grouping them for a given element or, when a large body of data is available, for a given isotope or a group of isotopes.

7.1 Some general references

A recent critical review of results concerning the general properties of light exotic isotopes of helium, lithium, and beryllium is given in Ref. [289]. Clustering effects are also discussed in the review about bound states and continuum properties at the interface between theoretical and experimental nuclear physics in [290].

Charge form factors of several self-conjugate nuclei have been theoretically calculated with the crystal-like approach of the *alpha*-cluster model with dispersion in Ref. [291], by assuming different geometrical configurations of the clusters, and compared with experimental results. The energy density functional theory was applied in the context of the optical model to describe the elastic scattering of α particles on self-conjugate nuclei in Ref. [292].

Refs. [293, 294] theoretically investigated cluster formation and properties in nuclear matter, while a panoramic view on the reaction mechanisms induced by weakly bound Li and Be isotopes is given in Ref. [295]. Clustering effects in the ground states of self- and non-self-conjugate nuclei can be inspected also using Hanbury–Brown–Twiss correlation analysis [296] and by analyzing the harmonic components of particle

flows emitted in ultra-relativistic collisions involving a clustered projectile and a heavy target [297]. Calculations on ^{7,9}Be, ^{12}C and ^{16}O ultra-relativistic collisions on lead have been reported in Ref. [298]: elliptic flows are sensitive to clusterization in Beryllium isotopes, while triangular flows are sensitive to the clusterization in ^{12}C and ^{16}O. Signal of production of self-conjugate nuclei both in the ground state and in states close to the $N\alpha$ disintegration threshold have been found also in fragmentation events of relativistic projectiles [299]. Bose–Einstein condensation in strongly interacting matter is discussed in [300], while clusterization effects of the four-nucleon system at kinetic freeze-out conditions in relativistic heavy-ion collisions were investigated using path-integral Monte Carlo techniques in Ref. [301].

Cluster motion in the ground state and radial excitations of self-conjugate nuclei as ^{8}Be, ^{12}C and ^{16}O were analyzed with a microscopic $N\alpha$ approach in Ref. [302]. Ref. [303] discussed the possibility to observe a collective motion of α-clusters with respect to a heavy core in nuclei above ^{100}Sn and the interplay between giant dipole resonance phenomena and α oscillations.

A comprehensive study of the structural properties of 0^+ excited states in several $N = Z$ nuclei was performed in the framework of the *quartet* model in Ref. [304]; in this model, a *quartet* indicates generally a correlated structure of two protons and two neutrons coupled to zero total isospin. The possibility of describing excited states of self-conjugate nuclei by considering excited quartets is discussed in [305].

The question of localization of nucleons in connection with the formation of clusters in light-to-medium self-conjugate nuclei and in nuclear matter was extensively discussed in Ref. [306] by means of nuclear energy density functional theory. In this context, the boundaries of transition from coexisting cluster and mean-field states to a Fermi liquid state were found to involve nuclei having mass numbers $A \approx 20$ to 30. The study of spatial structure in self-conjugate and non-self-conjugate light nuclei was also performed in the framework of the Feynman path integral method in Ref. [307]. Among the various results, the use of the hyper-spherical function method allowed to determine the structure of the ground and Hoyle states in ^{12}C, showing respectively a regular triangular α cluster structure and a oscillation between a triangular α structure and a compact dinuclear structure of the ^{8}Be+α type.

A review work on the interplay between few-body effects and mean-field properties of light nuclei, in connection with clustering, is given in Ref. [308]. Connections between hyper- and mega-deformations and cluster molecular states have been theoretically discussed with the cranked relativistic mean-field model in Ref. [309]. The impact of the variational basis used to describe resonances in three-body systems in the context of the alpha cluster mode of the nucleus is critically reviewed in [310], with applications to the energy position and radii of ^{12}C and ^{24}Mg states.

As discussed in Sect. 3.4, clustering properties of light nuclei can be understood by considering the symmetries occurring in the quantum-mechanical deformed harmonic oscillator. A very recent overview of this aspect, involving both prolate and oblate deformations, is given in [311]; it is also demonstrated that molecular-like exchange of protons and neutrons is indeed encoded into the mean-field description of the nucleus. In another work, [312], predictions from the oblate side of the deformed harmonic oscillator model point out the possible α cluster nature of oblate states in ^{12}C and the ^{16}O+3α cluster nature of oblate states in ^{28}Si. As nicely pointed out in Ref. [313],

group symmetries of the algebraic cluster model (ACM) would lead to selection rules in α transfer reactions, for example, involving ^{12}C and ^{16}O nuclei. As shown in [313], the use of Young tableaux expresses in a simple and pictorial way the occurrence of such selection rules. In Refs. [314, 315], the question of symmetries governing the structures of ^{12}C and ^{16}O nuclei was investigated with the Semi-microscopic Algebraic Cluster Model (SACM), and the important role played by the Pauli Exclusion Principle on predictions of low-lying excited states in both these nuclei was discussed in great detail.

An interesting re-investigation on the magnetic dipole moments in excited states of self-conjugate nuclei up to chromium was reported in Ref. [316]. The gyromagnetic factors of excited states obtained from experimental data are $g \approx +0.5$, a value in close agreement (within statistical uncertainties) to simple quantum mechanical predictions for macroscopic α cluster model. This peculiar finding was interpreted in the framework of collective excitations of α-clusters, giving support to the hypothesis of the occurrence of α clusterization for excited states of self-conjugate nuclei. The impact of extra neutrons on the structure of neutron-rich isotopes of self-conjugate nuclei, and the interplay between shell closures and α clusterization, was also inferred from the analysis of gyromagnetic factors of excited states of $N = Z + 1$, $N = Z + 2$ nuclei.

Clustering considerations in ^{11}Be led the authors of [317] to speculate on the existence of *Rydberg-like* nuclear molecules, made by two 0^+ nuclei and two neutrons in covalent sharing between them. From the calculations, their existence is not completely ruled out, and they could be observed in laboratory experiments, for example, as by-products of nuclear fragmentation reactions.

Concerning the role played by the α clustering in driving different reaction mechanisms in heavy-ion collisions, we underline the surprising result of [318] in studying the ^{17}O+^{12}C fusion excitation function: a broad oscillation is seen in the data, apparently not dissimilar to the ones present in the ^{16}O+^{12}C self-conjugate system and linked to the occurrence of molecular-like resonances.

At bombarding energies well larger than the Coulomb barrier, the investigation of effects due to the Q_α value of the projectile in heavy-ion collisions was performed in Refs. [138, 140, 319], where projectile with lower Q_α values seem more inclined to give rise to incomplete fusion phenomena. The role of nuclear stopping in the formation of clusters in C+C collisions at 95 MeV/nucleon was investigated by comparing molecular dynamics calculations with experimental data in Ref. [320, 321].

7.2 Some observations

From all the previous works, it emerges the need to deepen the concepts and the effects due to the symmetrical arrangements that α clusters can manifest in light nuclei, with particular emphasis on the search for the connections between various up-to-date cluster models based on different theoretical grounds (e.g. algebraic models compared with molecular dynamics ones) but leading to similar predictions. It would be also important to consider in more detail the effects played on the cluster structures by the exclusion principle on the various models discussed here, and to improve the

theoretical research on clusterization algorithms inside transport models for heavy-ion reactions at large energies. The last point, in particular, could have some interesting repercussions also in other physics contexts (e.g. applied physics or cosmic-ray studies) because of its impact on accurate predictions of absolute cross sections in the intermediate to relativistic energy domains. From the experimental point of view, we believe that the suggestion for the occurrence of selection rules in α-transfer reactions due to group symmetry considerations [313] would deserve some further experimental deepening; improvements in the determination of quadrupole electric and dipole magnetic momenta of excited states of self-conjugate nuclei and their neutron-rich isotopes would also be useful to further benchmark cluster model predictions, according to the recent work of [316]. The surprising findings of [318] of broad resonances in a non-self-conjugate reaction system would urge for the measurements of fusion cross sections all along the oxygen isotopic chain, both stable and unstable; it could be also useful to populate the same fused system, ^{29}Si, with a different entrance channel, in order to have an independent benchmark of the reported results.

8 Clustering in helium isotopes

The description of neutron-rich He isotopes can represent an important bridge between few-body theories of the nucleus and clustering models. A consistent description of the energy position and widths of the ground state and the first excited states of the isotopic chain $^{5-10}$He has been recently reported in Ref. [322], using the single-particle Berggren basis and by numerically solving the many-body problem via the Gamow density-matrix renormalization group (G-DMRG) method for open quantum systems. Such calculations could serve also as a guideline for the determination of the position and properties of the poorly known ^{9,10}He states; for example, a parity inversion is predicted for low-lying states in ^{9}He.

A detailed study of the structure of states of ^{7}He at low excitation energies was performed also in Ref. [323] using an ab initio calculation with the Daejeon16 potential; in particular, the solution of the multi-channel problem allowed to determine the partial decay widths toward different neutron decay channels. Indirect measurements with the Trojan Horse Method of the cross section of the unbound ^{5}He nucleus reaction on a ^{3}He target at astrophysical energies have been recently reported in Ref. [324].

Results of a new break-up experiment, where ^{8}He projectiles at 15 MeV/nucleon impinged on C and Pb targets, were reported in Ref. [325]. The main aim was to study the decomposition of ^{8}He into the ^{6}He+n+n channel. The break-up of ^{8}He on carbon targets was found to be essentially *sequential* in nature, passing through the ground state of ^{7}He; this finding turns out to be consistent with neutrons emitted with a time delay of about 1400 fm/c, in agreement with the lifetime of ^{7}He. At variance, the nature of break-up events induced on a lead target was found to be more direct.

9 Clustering in Lithium isotopes

Lithium isotopes have been frequently used as clustered projectiles to induce incomplete fusion reactions on heavy targets. For example, in Refs. [326, 327], reactions induced by ^{7}Li on ^{93}Nb were studied at energies near the Coulomb barrier. A careful selection of kinematical conditions in the analysis of reaction products allowed to highlight events purely due to triton stripping processes and to study their important role in the enhancement of α-particle emission in reactions induced by weakly bound nuclei. Triton cluster transfer has also been found to be the main reaction responsible for the suppression of complete fusion, and enhancement of incomplete fusion mechanisms, in ^{7}Li+^{209}Bi reactions at near-barrier energies [328]. A possible explanation of the large α yield seen in several reactions induced by ^{6}Li was also offered in Ref. [329] by considering the dominance of non-elastic break-up events (treated with the Ichimura–Austern–Vincent approach [330]) on the elastic break-up components (treated with the continuum-discretized coupled channel model). The cluster structure of ^{6}Li has been profitably used to perform several Trojan–Horse experiments; a recent comparison between results obtained using ^{6}Li or ^{3}He Trojan Horse projectiles is discussed in Ref. [331].

The population of isoscalar resonances in ^{6}Li has been studied with ^{6}Li+^{15}N collisions at $E_{cm} = 23.1$ MeV [332]. In another experiment, the detailed comparison of elastic scattering cross sections at backward angles in ^{6}Li+^{10}B and ^{7}Li+^{10}B collisions at the same incident energy (51 MeV of ^{10}B in inverse kinematics) revealed sizeable differences; the possible origin of such effect could be ascribed to the coupling with breakup, while the elastic transfer mechanism and the reorientation effects in ^{7}Li are found to be negligible [333]. DWBA calculations performed with the use of Sao Paulo potential to describe ^{6}He+^{6,7}Li reactions at near-barrier energies pointed out the important role of overall breakup effects to describe the inclusive emission of α particles [334].

Other studies concerning the analysis of reaction mechanisms induced by lithium isotopes on medium-to-heavy mass targets (as elastic and inelastic scattering, breakup, stripping reactions, and one-nucleon transfer) have been discussed by several authors (see, e.g. [335–339]), putting in evidence the pronounced role of the dominant $\alpha+d$ and $\alpha+t$ cluster configurations in ^{6}Li and ^{7}Li, respectively. A non-negligible contribution coming from the direct break-up of ^{7}Li beam into p+^{6}He has also been recently observed in ^{7}Li+^{112}Sn collisions [340], pointing out the importance of p+^{6}He cluster configuration.

An interesting analysis of ^{8}Li+^{209}Bi reaction at near barrier energies [341] allowed to deepen the origin of the suppression of complete fusion (of the order of 30%) in collisions induced by light weakly bound stable or nearly stable nuclei. In the past, this effect was associated with the presence of low break-up thresholds into charged clusters. The observation of fusion suppression in the neutron-rich radioactive nucleus ^{8}Li is therefore puzzling: the lowest breakup threshold is seen for the ^{7}Li+n channel (2.03 MeV), but this channel cannot contribute to fusion suppression because ^{7}Li retains all the projectile charge. A detailed correlation analysis of cluster fragments indicates that break-up events are too slow to explain the observed fusion suppression. The observation of a large cross section for unaccompanied α particles would suggest

the major role in fusion suppression played by charge clustering effects in the projectile (facilitating partial charge capture), rather than the position of the particle decay threshold.

The cluster structure of stable and radioactive Lithium isotopes *eo ipso* has also been the subject of intense activities. In Ref. [342] the structure of states in ^{6}He and ^{6}Li was investigated with a new real-time evolution method (REM approach), which is able to generate the ergodic ensemble of the basis wave functions. The halo properties of the two isobars are reasonably well described, even if the calculated binding energies of 0^+ states are slightly shifted with respect to experimental values and the r.m.s. radii are overestimated.

Isoscalar and isovector ^{6}Li states at small excitation energies have been studied in Ref. [343] by solving two single-channel Lippmann–Schwinger equations in the framework of an effective two-body clusterization method where the deuteron can be found in its ground ($^3S_1$) or virtual ($^1S_0$) state. The energy position of the first three isoscalar states (1^+, 3^+, 2^+) is reproduced with extreme precision, while larger shifts are seen for the isovector states (especially for the 0^+). The theoretically obtained level scheme allows to reasonably reproduce experimental data of excitation function and angular distributions for the d+ ^{4}He elastic scattering up to $\approx$ 10 MeV bombarding energy. A method to separate isoscalar and isovector dipole excitation in ^{6}Li from heavy-ion collision data at medium energies (100–400 A.MeV) has been discussed in [344].

In a different approach [345], the ground state properties of ^{6}Li have been calculated by solving Faddeev equations in the momentum space and using the CD-Bonn force and the Bang potential to describe, respectively, the neutron–proton and the nucleon α interaction. The solution obtained using separable interactions agrees exactly with solutions based on non-separable forces. Energies of the ground and excited states of ^{6}Li were also recently calculated with the variational quantum eigensolver (VQE) algorithm using a superconducting quantum chip [346]; the deviations are of the order of a few percent with respect to exact diagonalization procedures. The study of the three-body problem p+n+α with a wide variety of nucleon–nucleon and alpha–nucleon interactions led to a common description of the structure of the ground state of ^{6}Li in agreement with the few boy universality principles of quantum mechanics [347]; in this framework, ^{6}Li could be seen as two-nucleon halo nucleus. Several spectroscopic properties of ^{6}Li states and electromagnetic transition strengths were investigated with an ab initio no-core full-configuration (NCFC) approach in Ref. [348].

The dipole excitation of ^{6}Li was re-investigated experimentally at the newSUBARU facility from the neutron threshold up to 60 MeV. The occurrence of a low (peaked at $\approx$ 12 MeV, LEGDR) and a high (peaked at $\approx$ 31 MeV, HEGDR) energy component was confirmed [349]. While the LEGDR was associated with the ordinary $1\hbar\omega$ $1p-1h$ excitation in ^{6}Li, the HEGDR was associated with an α cluster excitation in ^{6}Li, confirming an old suggestion made in Ref. [350]. This study triggered new theoretical calculations to deepen the interpretation of experimental observations: they were discussed in Refs. [351, 352] by using, respectively, a six-body microscopical calculation and an extended version of the QMD model.

Concerning ^{7}Li, an exclusive break-up experiment (in the α+t channel) performed by coupling a magnetic spectrometer with a silicon detector pointed out the dominance

of non-resonant effects in the break-up cross section, while the coupling with the second excited state at 4.652 MeV is needed to describe the elastic scattering cross section [353]. The structure properties of the ground state and the first excited states of the mirror couple ^{7}Li and ^{7}Be have been studied microscopically by the algebraic version of the RGM. They have been used to determine the S-factors and branching ratios of the astrophysical important reactions ^{3}H(α,γ)^{7}Li and ^{3}He(α,γ)^{7}Be and compared with experimental data [354].

^{7}Li unbound states have been studied with the no-core shell model with continuum (NCSMC) method, using chiral nucleon–nucleon interactions as the only input [355]. Very interestingly, it is predicted an s-wave resonance in the ^{6}He+p channel at very low energy above the reaction threshold, which could be relevant in the astrophysical context. Inelastic scattering of fast neutrons on ^{6,7}Li targets was theoretically studied in Ref. [356] by solving the Faddeev equations to describe the problem of neutron interaction with the two clusters forming the ground state of target nuclei. Clustering effects in the neutron-rich ^{9}Li isotope have been studied in [357] via energy and angular correlations analysis of ^{9}Li+Pb breakup data at 32.7 MeV/nucleon. In particular, it was studied the decomposition channel into the two neutron-rich clusters ^{6}He+t with the help of CDCC. Two resonant states decaying into such channel were found at 9.8 MeV and 12.8 MeV, with suggested J^{π} assignments respectively $3/2^{-}$ and $7/2^{-}$. These results support the prediction of the GCM for ^{9}Li.

The ^{11}Li three-cluster structure (^{11}Li+n+n) was studied with the hyper-spherical formalism associated with the GCM in Ref. [358], considering also the possibility of core excitation. Despite the numerical difficulties due to the very large number of Slater determinants needed to describe the ^{9}Li core, a reasonable description of the neutron and matter radii is obtained, while the proton radius is slightly smaller than the experimental one. A comparison with the ^{9}Li proton radius suggests a possible effect of the neutron halo of ^{11}Li on the structure of the ^{9}Li core. Finally, the possible occurrence of Cooper pairs in ^{11}Li is discussed in [359].

9.1 Some observations

The Li isotopic chain constitutes, to our opinion, a strange case in the study of clustering in light nuclei: while there are no doubts about the strong presence of clustering in the well-studied ^{6,7}Li isotopes, the same cannot be said for the other, neutron-rich, unstable isotopes. It is worth noting the fact that hints on the existence of a pronounced cluster structure in ^{8}Li indirectly comes from a recent complete fusion experiment [341]. This finding would suggest performing new experiments also on the nuclear structure side; a possibility could be represented by the study of ^{6}He+d scattering and reactions with novel active target detectors to understand the nature of very broad states above $\approx$ 9 MeV. Similar proposals might involve the study of the ^{9}Li cluster structure with the doubly radioactive collision ^{6}He+t: the resonant elastic scattering could give interesting spectroscopic information in a region where practically no data are still present. Also electron scattering experiments on radioactive Li beams could be very useful to have a clearer experimental view of matter distributions in such

isotopes, while (p,pd) and (p,pt) knock-out experiments in inverse kinematics could help to unveil the possible presence of exotic ^{6}He+d,t clustering structures.

10 Clustering in Beryllium isotopes

The structure of the neutron-rich beryllium isotopes ^{9}Be, ^{10}Be, ^{12}Be was theoretically investigated with the real-time evolution method (REM) in Ref. [360]: the density distributions clearly suggest the occurrence of molecular structures in ^{10}Be. The reproduction of levels in ^{9}Be, ^{10}Be is in qualitative agreement with experimental data, apart from some inversion in the position of opposite parity levels. An analysis of intrinsic momentum distributions expected in the isotopic chain ^{8,9,10}Be was reported in Ref. [361]. The momentum distribution of α–α system shows clustering signatures even in the intrinsic frame of momentum space, in a fashion complementary to the observations in the coordinate space, because of strong anti-symmetrization effects.

The spectroscopy of bound and resonance states of the $^{9}_{\Lambda}$Be hypernucleus was investigated in the framework of a $2\alpha + \Lambda$ microscopic model in Ref. [362], with particular attention to the influence due to the cluster polarization on the energy and widths of $^{9}_{\Lambda}$Be states and on phase shift trends in $^{5}_{\Lambda}$He+α scattering processes.

10.1 Clustering in ^{7}Be

A study of ^{7}Be break-up was performed in Ref. [363]. Excited ^{7}Be nuclei have been populated by transfer reactions induced by ^{6}Li on ^{112}Sn; the selected cluster break-up channel was ^{3}He+^{4}He. Coupled channel calculations successfully reproduced the angular distributions obtained in the exclusive measurements of direct break-up events and sequential break-up into the unbound states at 4.57 ($7/2^{-}$) and 7.63 MeV ($5/2^{-}$). The existence of a controversial $3/2^{+}$ state close to the ^{6}Li+p threshold was discussed in Ref. [364] by a re-analysis of the existing data; it was estimated also its possible impact on the ^{3}He(^{4}He,γ)^{7}Be reaction rate. Still on the astrophysical side, an extrapolation of S-factor for the ^{3}He(^{4}He,γ)^{7}Be reaction down to the solar energy region has also been recently determined with the next-to-leading-order (NLO) amplitude in an effective field theory (EFT) [365]; recent EFT calculations were reported also for the ^{3}He+^{4}He elastic scattering data [366].

Concerning the measurements of matter and charge radii of ^{7}Be, a new experiment of elastic scattering ^{7}Be+p in inverse kinematics and at small angles was performed at GSI [367]; the matter radius value, $R_m = 2.42(4)\,fm$, is larger than the ones previously reported in the literature and based on the analysis of the total interaction and reaction cross sections. The comparison of R_m with the charge radius pointed out the presence of a sizable proton skin ($\delta_n p = 0.23(10)\,fm$).

10.2 Clustering in ^{8}Be

An experiment of the ^{7}Li(p,γ)$\alpha\alpha$ reaction at 0.441 MeV allowed to improve the determination of the radiative widths of states in ^{8}Be, up to the 2^{+}_{3} state. The adopted

complete kinematics approach avoids experimental difficulties arising from direct gamma-ray detection [368]. A dedicated R-matrix analysis of the obtained excitation spectrum shows that the ground state dominates the spectrum below 2 MeV and has a non-negligible contribution in the whole energy range. This finding indicates that a simple integration of the excitation energy spectrum leads to an overestimation of the decay strength toward the first excited state. Furthermore, the R-matrix analysis pointed out the need to include a 2^+ background pole in the fit (indicating a non-resonant continuum contribution in the spectrum), and the possible presence of a broad 0^+ state at around 12 MeV [368].

Several theoretical works deepened the study of clustering in ^{8}Be. Tensor effects were included in the antisymmetrized quasi-cluster model of Ref. [369]; in particular, the tensor suppression gives a significant contribution to the short-range repulsion between two alpha-clusters in ^{8}Be. In another work, the combination of the Complex Scaling Method [370] within the framework of the non-localized cluster model [371] allowed to describe the binding energy of ^{8}Be and the properties (energy position and width) of the 2^+ and 4^+ resonant states. α–α scattering phase shifts and properties of ^{8}Be states were also investigated in the framework of the chiral effective field theory [372]; the calculations elucidate the role played by the two-pion-exchange effects and short-range terms in the interaction between the clusters.

A recent simultaneous R-matrix fit of ^{4}He+^{4}He elastic scattering differential cross sections and phase shifts, and of ^{4}He$(\alpha, \gamma)^8$Be radiative capture cross section (for the $4^+ \rightarrow 2^+$ transition) around the 4^+ resonance at $\simeq$ 11.4 MeV, redetermined some properties of the low-lying states in ^{8}Be [373]. In particular, the obtained Γ_α values for the ground state and the 4^+ state are lower than the commonly accepted values in the literature, while the reduced $E2$ transition strength ($21.96 \pm 3.86 e^2 fm^4$) is in agreement with the value obtained experimentally, and confirms the large deformation of ^{8}Be.

Ab initio calculations of cluster characteristics of ^{8}Be were discussed in [374], using a basis including No-Core Shell Model wave functions and translationally invariant wave functions of various cluster channels. An interesting finding is that the contribution of the non-clustered components of the basis to the total binding energy is still large, despite the typical cluster structure of ^{8}Be. The total binding energy of ^{8}Be and the properties of its excited states were also investigated via lattice calculations in Ref. [375].

10.3 Clustering in ^{9}Be

The weakly bound ^{9}Be nucleus has been recently used as a projectile to induce complete or incomplete fusion reactions, or to investigate the occurrence of break-up and α or neutron transfer events in collisions with medium-to-heavy ions [376–380].

The ^{9}Be properties (energy position and width of low-lying states) were theoretically explored with a three-cluster algebraic model in Ref. [381]. A reasonable description of experimental data is found, even if some inversion in the position of levels at higher energies is seen. A detailed analysis of the resonance properties of

$1/2^+$ states was also reported. The search for a state with properties analog to the Hoyle state suggested the narrow $5/2^-$ state at 2.43 MeV.

The recent development of the Cluster Shell Model (CSM), allowed to investigate single-particle levels in cluster potentials with Z_2, D_{3h}, T_d symmetries, as typically observed for ^{8}Be, ^{12}C and ^{16}O nuclei, respectively [382]. In particular, in Ref. [383], the $K^\pi = 3/2^-, 1/2^\pm$ rotational bands of ^{9}Be predicted by CSM are in very good agreement with experimental data and point out the occurrence of a molecular-like cluster configuration. The estimates of charge and matter radii, electromagnetic moments, and transition strengths are in nice agreement with experimental data, and point out the survival of the underlying 2α cluster configuration even by adding a further neutron.

From the experimental point of view, properties of excited states in ^{9}Be were studied by inelastic scattering of deuterons on ^{9}Be at 23 MeV bombarding energy [384]. The analysis of angular distributions with DWBA calculations allowed to determine the transferred angular momentum and on the J^π of ^{9}Be states up to 8 MeV. In this frame it was possible to deepen the open question of the unexpected J^π assignments made in Ref. [385] for the 2.78, 4.70, 5.59, 7.94 MeV states; the results of [384] are indeed in agreement with previously reported assignments given in Ref. [386]. The organization of ^{9}Be states into rotational bands is also discussed in [384]. An estimate of radii is also derived, and it is found that for the $K^\pi = 1/2^+$ and $K^\pi = 1/2^-$ bands, the r.m.s. radii are respectively 40% and 20% larger than the ground state band. Particular attention was devoted to understanding the structure of the broad 3.82 MeV $3/2^-$ state, which was described as a single-particle state coupled to an excited ^{8}Be core in the $J_{\text{core}} = 2$ state.

Several angular distributions obtained in ^{9}Be(d,x) reactions (being x=p,d,t,α) at 19.5 and 35 MeV were studied in Ref. [387] within the DWBA and Coupled Channels approach. The interaction potential of the entrance channel was calculated with the Double-Folding method using the α–α-n three-body wave function of ^{9}Be. Strong coupling effects were observed for the (d,p) and (d,t) one-nucleon transfer processes, while it was found that, due to the clustered nature of the projectile, in the ^{9}Be(d,α)^{7}Li reaction a dominant direct ^{5}He transfer mechanisms is present.

A recent measurement of ^{8}Li+p reactions leading to charged particle channels (as (p,p), (p,d) and (p,α) reactions) was performed at the RIBRAS facility in São Paulo [388], at center-of-mass energies $E_{cm} \approx 0.8$ to 1.8 MeV. A comprehensive R-matrix fit of several excitation functions obtained at various angles for the various studied channels allowed to fix better the partial decay widths Γ_p,Γ_d,Γ_α of states in ^{9}Be close to the proton decay threshold. The tentative J^π assignments for the 17.298, 17.493, and 18.650 MeV states reported in Ref. [386] were confirmed, and new $3/2^+$ and $7/2^-$ assignments were suggested for the 18.02 and 18.58 MeV states, for which no estimates were previously reported in the literature. For the 18.650 MeV state, the analysis suggests the presence of isospin mixing, differently from the pure $T = 3/2$ tentative assignment of [386]. From a theoretical point of view, the influence of a low energy $1/2^-$ resonance at 87 keV ($E_x = 16.975$MeV) in the ^{8}Li(p,γ)^{9}Be reaction rate was discussed in Ref. [389].

10.4 Clustering in ^{10}Be

The structure of ^{10}Be was the object of several recent theoretical works. In Ref. [390], it was predicted a strong connection between di-neutron correlations in ^{10}Be and the spin–orbit interaction, leading to sizable effects in the magnitude of the p+^{10}Be inelastic scattering cross section toward the second 2^+ state.

Inelastic scattering of protons and α on ^{10}Be can also be used to probe the isospin character of states belonging to ordinary and molecular-like bands in ^{10}Be. Calculations performed in Ref. [391] by combining AMD and a microscopic coupled channel approach suggested the p+^{10}Be inelastic scattering as a sensitive probe to unveil the neutron dominance in the second 2^+ state. An extended version of the AMD model was also used to understand the role of clustering and the transition current densities in low energy dipole mode and GDR excitation in ^{10}Be [392].

The study of high-energy states (> 10 MeV) in ^{10}Be was undertaken in Ref. [394] using a multi-channel algebraic scattering method (MCAS) to solve coupled sets of Lippmann-Schwinger equations for the α+^{6}He cluster system. The inclusion of high-energy states in ^{6}He in the calculations leads to the occurrence of high spin states in ^{10}Be at energies larger than 10 MeV.

The influence of different nucleon–nucleon potentials on the structure of bound and resonant states in ^{10}Be was investigated in Ref. [395] in the framework of a three-cluster microscopic model (describing the ^{10}Be with a α+α+^{2}n structure). This allowed to probe the effects due to ^{8}Be and ^{6}He cluster polarization on the structure of ^{10}Be; in particular, cluster polarization increases the attraction between the interacting clusters, leading to a lowering of energies for bound and resonance states and also to a reduction of the width of several resonance states.

From the experimental point of view, the spectroscopic factors for five bound states in ^{10}Be were obtained at ISOLDE via one-neutron transfer reactions (d,t) and (p,d) in inverse kinematics with the use of a radioactive beam of ^{11}Be [396]. Differential cross sections were analyzed within the DWBA framework, and the obtained spectroscopic factors were compared to values already reported in the literature. The sizable differences observed with the literature values could be ascribed to the presence of multi-step processes having a relatively major role at the low center of mass energies explored in the experiment.

The question of the existence of a possible high spin (6^+) member of the molecular band in ^{10}Be was investigated with a new experiment in Ref. [397]. ^{6}He+^{4}He scattering data close to 180° were obtained in inverse kinematic with a very complex array, made by ionization chamber and proportional counters, scintillators and silicon detectors, to face off a series of experimental difficulties due to the presence of background and to the similarity in energy loss of ^{6}He and ^{4}He particles. The data analysis points out difficulties in finding a 6^+ state at 13.5 MeV previously suggested in Ref. [398]; considering that such a state could decay toward the ^{6}He ground state or to the ^{6}He first excited state, the work [397] suggests an upper limit $\frac{\Gamma_\alpha}{\Gamma_\alpha'} < 0.017$, possibly in agreement with the small population of such state seen in [398].

10.5 Clustering in ^{11}Be

The static properties of ^{11}Be were studied in Ref. [399] using AMD+RGM calculations. The behavior of the molecular σ and π orbitals was reconstructed and the simulated level scheme closely reproduces the experimental data. The estimated spectroscopic factors for low energy states in ^{11}Be match well the experimental results. The wave function obtained for the valence neutron was furthermore used to reproduce several data (as spectra, triple differential cross sections, and momentum distributions) obtained from break-up experiments at intermediate energies. Multi-channel algebraic method calculations of Ref. [400] describe reasonably the excitation energy spectra of mirror ^{11}Be and ^{11}C nuclei, by considering respectively the presence of a valence neutron and a valence proton coupled with a mass 10 core. From the analysis, it emerges a strong role due to the coupling of the valence neutron with the 2^+_1 collective state of the ^{10}Be in describing the positive-parity ground state band in ^{11}Be.

Investigations on the collective rotations of the positive-parity deformed configurations of ^{11}Be were studied in [401] in the framework of a non-adiabatic coupled-channel formalism and the Berggren single-particle ensemble: the collective rotation for the ground band is stabilized because of the closure of the $\ell = 0$ neutron decay channel and of angular momentum alignment effects. In Ref. [402], spectroscopic factors of ^{11}Be reported in the literature were investigated in the framework of the Nilsson model, and useful formulas for spectroscopic factors, expressed in terms of the amplitudes of the deformed wave functions, were reported.

10.6 Clustering in ^{12}Be

^{12}Be plays a key role to disentangle clustering in neutron-rich light nuclei. Its strong α cluster structure dominates over the effects due to the $N = 8$ shell closure.

To investigate the cluster nature of ^{12}Be, recent calculations performed using a wave function of the Tohsaki–Horiuchi–Schuck–Röpke (THSR) type inside the distorted wave impulse approximation (DWIA) formalism for direct reactions, suggested the possibility of using data of triple-differential cross section of the ^{12}Be(p,pα)^{8}He knock-out reaction to disentangle the α-cluster amplitude at the nuclear surface of this beryllium isotope [403]. The behavior of the reduced width amplitudes, the spectroscopic factors, and the radii for the ground state and the second 0^+ state in ^{12}Be were theoretically discussed with the AMD and the REM approaches in Ref. [404].

From the experimental side, a series of measurements of the ^{11}Be(d,p)^{12}Be stripping reaction allowed to explore the structure of low-lying unbound states in ^{12}Be [405] and the occurrence of intruding phenomena linked with the breaking of $N = 8$ shell closure [406]. It was reported for the first time the existence of a resonance at 3.21 MeV, just above the one-neutron separation threshold. A DWBA analysis of angular distributions and a concurrent inspection of the decay widths allowed to perform a 0^- spin-parity assignment for this new state, which would correspond to a 1p-1h configuration.

A signal of the interplay between collectivity and magicity in ^{12}Be was obtained by an accurate measurement of the lifetime of its 2^+_1 state with the Doppler Shift Atten-

uation Method (DSAM) [407] with the GRETINA array. The corresponding reduced transition strength $B(E2) = 14.2e^2 fm^4$ is quite large despite the shell closure, and it is well larger than previously reported values; the comparison with model calculations clearly indicated a break-down of the $N = 8$ shell closure.

A detailed investigation of the ^{4}He(^{8}He,^{4}He)^{8}He and ^{4}He(^{8}He,^{6}He)^{6}He reactions with a gas target and two arrays of segmented silicon detectors is discussed in Ref. [408]. Angular distributions for both channels show a peculiar pattern indicating the presence of a broad (≈ 1 MeV) $J^\pi = 4^+$ state in the ^{12}Be compound nucleus at about 14.5 MeV excitation energy. Such resonance parameters are in agreement with two center cluster model predictions indicating the occurrence of exotic molecular-like configurations.

10.7 Some observations

Nearly all recent experiments discussed here agree on the strong presence of clusterization effects in the whole Be isotopic chain, in agreement with the general aspects already discussed in Sects. 2 and 5. The possibility to organize the level scheme of ^{8}Be and ^{9}Be—thanks to the symmetries due to their dumb-bell structure [382, 383] points out the need to strengthen the current available spectroscopic information on such isotopes from the experimental side. In doing such type of investigations, it could be useful to exploit also the advantages of complete kinematics methods suggested in [368]. It is worth noting the resolution of the controversy on the spin-parity assignment of low-lying states in ^{9}Be [384], which gives support to the bands ordering given in [383]; in this framework, it would be useful to experimentally fix the remaining uncertain assignments on $7/2^\pm$ states around 12 MeV. On the proton-rich side, the possible existence of a $3/2^+$ state ^{7}Be close to the p+^{6}Li threshold is still highly controversial and should be resolved with new experiments. Concerning the structure of ^{10}Be, the classification of states in terms of ordinary and molecular bands is now understood with a general consensus, although some important aspects still need to be clarified, *in primis* the existence of high spin (6^+, 8^+) members in the molecular band that have been theoretically predicted by algebraic SU(3) calculations. Considering the results of [397], it is urgent to perform new experiments to inspect the possible decay of the suggested 6^+ state at 13.5 MeV into the $^6He(2^+) + \alpha$ decay channel, which is expected to be dominant with respect to the decay into the $^6He_{gs} + \alpha$ channel. A possibility to perform such a complex experiment could come from coupling active targets with large-area neutron detectors. Dedicated experiments should also be performed to investigate the properties of suggested high-spin molecular-like states in ^{12}Be at energies above 14 MeV.

11 Clustering in Boron isotopes

Recent efforts have been made toward the theoretical study of boron isotopes with microscopical cluster models. Low-lying resonances in ^{9}B were investigated within the framework of the three-cluster model and the Modified Hasegawa–Nagata Potential

(MHNP), making use of hyper-spherical harmonics [381]. Within this framework, ^{9}B is described with a dominant α+α+p configuration, providing evidence for rotational bands that seem to agree with experimental data, and probing the nature of the first $1/2^{+}$ excited state, which is not yet fixed experimentally. An investigation of the first $1/2^{+}$ state in ^{9}B is also given in Ref. [409], using the formalism of the THSR wave-function, which describes cluster-correlated dynamics of valence nucleons. The new THSR calculations take into account the correlation of the extra-proton and α-clusters, and are able to reproduce low-lying excited states of ^{9}B observed experimentally.

Clustering in neutron-rich boron isotopes near the dripline has been predicted using the antisymmetrized quasi-cluster model (AQCM), which allows utilizing jj-coupling shell model wave functions as the clusters. The lowest shell model states of ^{17}B have been described as ^{8}He+^{9}Li cluster configurations [410].

The occurrence of a proton halo in ^{8}B was studied theoretically in Ref. [411] using an extended version of the THSR wave function, by assuming the ground state of ^{8}B as made by p+^{3}He+α clusters. Microscopic calculations of the optical potentials needed to describe elastic scattering and breakup reactions data of ^{8}B on several targets allow disentangling some details of its nature, including its proton halo coupled with the ^{7}Be core [412].

The structure of ^{10}B is involved in the ^{6}Li(α,γ)^{10}B reaction, which, together with the ^{10}B(α,d)^{12}C reaction, might offer an alternative path to the traditional triple-α process in first generation stars. In this framework, the investigation of the α-cluster nature of ^{10}B and ^{14}N is crucial as it could enhance the rate of this sequence of reactions. In Ref. [413], the authors perform a comprehensive R-matrix fit of a broad data set of ^{6}Li(α,γ)^{10}B reaction cross section data to investigate such a possibility. This work contributed to refining the width of the $E_{cm} = 1200$ keV 1_3^+ state in ^{10}B, which has an impact in astrophysics. ^{10}B was also the subject of experimental investigations at the HELIOS spectrometer, exploiting the ^{10}B(p,p')^{10}B* inelastic scattering in inverse kinematics [414]. Deriving data provided constraints for ab initio calculations using realistic nuclear forces. Another indication of the cluster structure of boron isotopes has been recently obtained using laser spectroscopy techniques to determine charge radii of ^{10,11}B [415]. The difference in the measured charge radii for ^{10}B and ^{11}B isotopes, $\langle r_c^2\rangle^{11} - \langle r_c^2\rangle^{10} = -0.49(12)$ fm^2, is qualitatively explained by a possible cluster structure of the boron nuclei and quantitatively used to benchmark new ab initio nuclear structure calculations using the no-core shell model and Green's function Monte Carlo approaches.

For the ^{11}B isotope, the spectroscopic amplitude for the α cluster configuration of the ground state was determined for the first time by analyzing the α-transfer reaction ^{7}Li(^{6}Li,d)^{11}B reaction with a magnetic spectrograph [416]; the α spectroscopic amplitudes for the $3S_0$ and $2D_2$ components of the ^{11}B ground state are respectively 0.64 ± 0.09 and 0.74 ± 0.09 for the uncoupled case. Other spectroscopic data for excited states of ^{11}B above the α threshold were recently discussed in Ref. [417] by analyzing with R-matrix fit the excitation functions of α+^{7}Li elastic and inelastic scattering and ^{7}Li(α,γ_0)^{11}B reaction data; large dimensionless reduced partial widths θ_α^2 values were reported for the 9.86 and 10.33 MeV states. The presence of clustered states near the α threshold can lead to an increase of the reaction rates for α-capture reactions on ^{7}Li that are involved in the nucleosynthesis in first-generation stars.

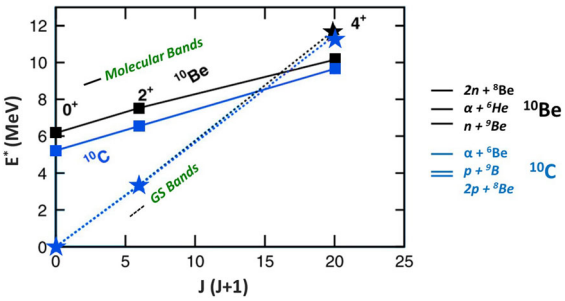

Fig. 13 Ground and molecular bands for the couple of mirror isotopes ^{10}Be and ^{10}C. On the right, the positions of relevant particle-decay thresholds are shown. Adapted from Ref. [393]

The ^{10}B+n system has been studied via the measurement of charged particles emitted from neutron-induced reactions in the energy regimes from 1 to 20 MeV at Los Alamos [418]. The spectroscopy of the ^{11}B compound system has been refined via a comprehensive R-matrix fit of new and previously published differential cross section data. A comparison is made to the molecular and cluster state candidates observed in these reactions.

A detailed analysis of differential cross-sectional angular distribution data, involving stable (^{11}B) and unstable (^{8,12}B) beams on a ^{9}Be target, is described in Ref. [338], exploiting secondary beams produced by the RIBRAS facility. The authors use an optical model with the Wood–Saxon form factor and the São Paulo potential to investigate the effect of the cluster configuration in the projectile inelastic excitation, breakup, and stripping reactions on the quasi-elastic angular distributions.

The investigation of possible α cluster structure in ^{13}B was recently performed at TRIUMF by studying the resonant elastic scattering ^{9}Li+^{4}He in inverse kinematics, using a gas target and an array of silicon telescopes [419]. The obtained excitation functions at some backward polar angles were reasonably reproduced by calculations from a simplified molecular rotational reaction model and also by optical model calculations. In particular, the agreement with the molecular rotational model predictions could qualitatively indicate the formation of cluster structure in ^{13}B.

11.1 Some observations

Among all the light elements considered here, boron isotopes are perhaps the ones for which the onset of possible cluster structures is less known, mainly because of missing experiments. For example, the position and width of the first $1/2^+$ excited state of ^{9}B, which should be the analog of the broad 1.68 MeV state in ^{9}Be, are still subject to large uncertainties, that need to be clarified. Similarly, some $T = 1/2$ isobaric analog states are still missing in the ^{9}B scheme, and this is currently a limit in the unveiling of $\alpha + p + \alpha$ cluster structures potentially present in ^{9}B and predicted by theoretical calculations discussed in the previous section; this point would stimulate new experiments. Further efforts are also required to inspect the onset of clustering in ^{12}B and ^{13}B; some results of ^{8,9}Li+^{4}He resonant elastic scattering data have been reported in the literature, but their interpretation is still qualitative and should be deepened.

12 Clustering in carbon isotopes

The three-α nature of cluster states in carbon isotopes made their study particularly interesting in nuclear physics. For example, in recent theoretical calculations performed with AMD [420], the spectroscopic factors of several low-lying states in even isotopes of carbon (^{12,14,16,18}C) and their neutron skin thickness were determined. Interestingly, an anti-correlation effect is seen: smaller neutron skin thicknesses are associated with larger S_α values. The study of matter distribution and the determination of matter radii for neutron-rich carbon isotopes (^{14,15,16,17}C) was the subject of several proton+C elastic scattering experiments performed at 700 A.MeV in inverse kinematics at GSI [421]. The obtained matter radii agree well with theoretical predictions of Ref. [422] and point out the presence of a neutron halo structure for ^{15}C and of sizable neutron skins for ^{16,17}C.

The occurrence of cluster structures in C isotopes for increasingly large neutron numbers was investigated with lattice Monte Carlo calculations based on chiral effective field theory [423]. From the analysis of proton and neutron density distributions and the geometry of cluster correlations, it was suggested that excited states analog to the Hoyle state could be found also in ^{14}C and ^{16}C.

12.1 Clustering in ^{10}C

A comprehensive study of 2p+2α correlations with the HIRA array [393] allowed to determine the decay branching ratios of several excited states in ^{10}C above the proton threshold into the p+^{9}B, 2p+^{8}Be, α+^{6}Be. The analysis of particle–particle correlation plots and of the reduced widths of states, coupled with consideration based on the mirror system ^{10}Be, led to the observation of rotational bands analog to the ^{10}Be case. In particular, the molecular band built on the second 0^+ state in ^{10}C (5.282 MeV) show a momentum of inertia nearly identical to the ^{10}Be molecular band, underlining a strong clusterization in such proton-rich nucleus, see Fig. 13. All the members of the molecular band in ^{10}C have a non-negligible branching toward the democratic two-proton decay channel, passing through the broad s-wave resonance of ^{9}B. Suggestions for a strong clusterization in ^{10}C come also from the continuum-discretized coupled channel analysis of elastic scattering data ^{10}C+^{58}Ni at energies close to the barrier reported in Ref. [424].

12.2 Clustering in ^{11}C

Two recent experimental works explored the structure of ^{11}C above the proton emission threshold by analyzing the ^{10}B(p,α)^{7}Be reaction at low energies (< 1.5 MeV). In Refs. [425, 426], the Trojan Horse Method was used to determine the reaction cross section down to astrophysical energies; the resulting data were interpreted with R-matrix fit and the obtained spectroscopy of unbound states is similar to previous results reported in the literature (see, e.g. [427, 428]). A direct experiment was also performed in Toronto and Notre Dame [429], improving the spectroscopy of states in the 8.7–10.7 MeV region of excitation energies in ^{11}C and including the presence of a $5/2^-$ state

at 9.38 MeV, with a large α_0 branching ratio. A recent work studied the breakup of ^{11}C beams at intermediate energies [430] and reconstructed the excited states in ^{11}C, confirming the existence of the $5/2^-$ state at 9.38 MeV; in agreement with a previous suggestion made in [431], they indicate that this state could be a member of the $K^\pi = 3/2^-$ band, characterized by a quite large moment of inertia. However, some uncertainties in the spectroscopy of ^{11}C still persist. In a comprehensive R-matrix analysis of new experimental data of several p+^{10}B reaction channels, reported in Ref. [432], only positive-parity states are needed to reproduce the ^{10}B(p,α)^{7}Be and ^{10}B(p,γ)^{11}C in the region from the proton threshold up to $\approx$ 11.5 MeV excitation energy. New experiments would help to clarify the situation.

The spectroscopy of higher energy excited states, in comparison with the analog states in ^{11}B, was explored with an inverse kinematics elastic scattering experiment in Ref. [433]. Spectroscopic factors of states close to the proton threshold were theoretically interpreted by using the shell model embedded in the continuum in Ref. [434].

12.3 Clustering in ^{12}C

Several recent theoretical works focused on the description of peculiar aspects of the structure of the ground or excited states in ^{12}C. The structure of the first five 0^+ states was theoretically interpreted with the Bloch-Brink α cluster model, coupled with the replica exchange Monte Carlo method to sample large Slater determinants [435]. The analysis of potential energy surfaces as a function of deformation allows to determine the characteristics of such states; for example, the second 0^+ state, built on a shallow minimum of the potential energy surface, has a gas-like structure, while the fifth 0^+ state would show a very pronounced triangular structure with large moment of inertia. The gas properties of the Hoyle state were also studied with the THSR wave function in Ref. [436]. States above the Hoyle state were also analyzed in the framework of the field-theoretical super-fluid cluster model in Ref. [437]: in this model, the 0^+_3 and 0^+_4 states are interpreted as Zeromode excitations, while the 2^+_2 and 4^+_1 states are seen as Bogoliubov-DeGennes vibrations of the Hoyle state. The structure of the negative-parity 3^-_1 and 4^-_1 states of ^{12}C was investigated with a container model in Ref. [438] and, differently from a rigid triangular assumption, a non-localized cluster motion in the two-dimensional container was clearly seen. The structure of positive-parity states at low energies has been investigated with no-core shell model calculations in Ref. [439]. In this model, the Hoyle state can be described through deformed prolate collective modes rather than vibrational modes, while it is the giant monopole 0^+ resonance, lying at higher energies, which resembles the oblate deformation of the ^{12}C ground state. A good reproduction of the spectroscopic properties of ^{12}C was also obtained in the framework of the energy density functional theory, as discussed in Ref. [440].

The nature of the first four 0^+ states in ^{12}C was inspected in Ref. [441] by studying the properties of corresponding states in the $^{13}_{\Lambda}$C hypernucleus with an extension of the THSR model. Following the Ikeda rule, all the excited states occur around the cor-

responding cluster-decay threshold. Furthermore, for the first time in a hypernucleus, it was predicted the existence of a linear-chain state for the $^{12}C(0_3^+)$ in $^{13}_{\Lambda}C$.

Several recently discovered high-energy states in ^{12}C match well the predictions of the Skyrme model, originally made in Ref. [442], and subsequently extended also to lower excitation in Ref. [443] by considering the ^{12}C as a deformable body. In this context, estimates for electromagnetic transition rates were also obtained and discussed in Ref. [444].

The high-energy isoscalar dipolar excitation of ^{12}C, and in particular the interplay between the cluster and toroidal natures of such excitations in ^{12}C, was studied with simulations with the AMD+GCM model in Ref. [445].

From the nuclear reaction side, an effective field theory with next-to-leading order approximation led to a prediction of the astrophysical factor S_{E1} for the radiative capture of α particles by ^{12}C of 59 ± 3 keV b at 300 keV (Gamow peak), a factor $\approx$ 30% smaller than previous estimates [446].

In Ref. [447], it was suggested to use linearly polarized monochromatic beams of γ rays (available in the next future, e.g., at the ELI-NP facility) to perform nuclear fluorescence experiments that would be in principle able to discriminate, without model dependencies, between the various proposed geometric cluster configurations for ^{12}C: the depolarization ratios that would be obtained experimentally should show a peculiar pattern for each type of point-symmetry considered in the nuclear molecule.

A big theoretical effort has been made also in the description of cluster effects in α+^{12}C inelastic scattering collisions, considering also that new data at intermediate energies were obtained recently at the Osaka University with the Grand Raiden spectrometer [448]. A detailed comparison of the angular distributions of the α+^{12}C inelastic scattering toward the yrast 2_1^+ state (4.44 MeV) and the 2_2^+ state at ≈ 10 MeV (member of the Hoyle band) shows a "shrinkage" effect of angular distribution that, in a diffractional fashion, could be attributed to an increased radius for the 2_2^+ state; microscopic calculations allow to estimate, from the data analysis, an enhancement of the nuclear radius $\Delta R \approx 0.6$ to 1.0 fm for the 2_2^+ [460].

A theoretical analysis of the nature of the ground and the Hoyle state was recently discussed in Ref. [449] using Monte Carlo Shell Model (MCSM) calculations in the framework of unsupervised statistical learning, with the MCSM basis vectors analyzed with dendrograms. A nice reproduction of quadrupole moments and transition strengths for the lowermost states of ^{12}C is reported. Interestingly, in this approach, the Hoyle state appear to be not fully dominated by a cluster structure, but still showing a residual quantum liquid behavior, with 2/3 vs 1/3 mixing factors.

On the experimental side, ^{12}C structure was the subject of several high-precision investigations aiming at understanding its cluster structure. Several investigations involved the study of rare processes in the decay of the Hoyle state. The direct decay into three α particles was the subject of two high-precision independent experiments [453, 454] that lowered the upper limit of the direct decay branching ratio to $\approx 0.04\%$ (95% CL), almost an order of magnitude smaller than previous estimates [456, 458]. A similar value was obtained in Ref. [451], by analyzing the decay of Hoyle state formed by the β decay of ^{12}N with a TPC; the use of β decay to populate the Hoyle state would lead to an almost medium-free decay environment. The very low value of the direct (especially concerning the equal energy decay pattern) to sequential branching ratio

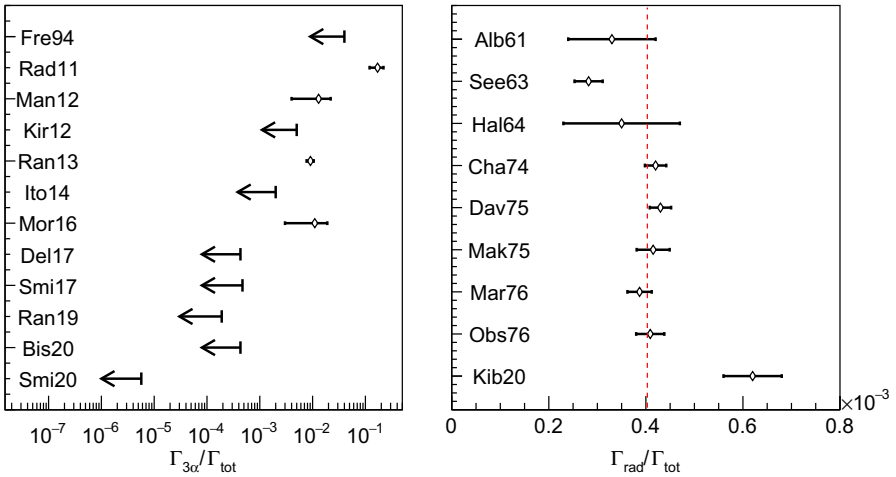

Fig. 14 Summary of the experiments probing the decay branching ratios of the Hoyle state in ^{12}C. (Left panel) Direct α-decay branching ratio $\Gamma_{3\alpha}/\Gamma_{tot}$ from [450] (Smi20), [451] (Bis20), [452] (Ran19), [453] (Smi17), [454] (Del17), [455] (Mor16), [456] (Ito14), [457] (Ran13), [458] (Kir12), [459] (Man12), [461] (Rad11), and [8] (Fre14). (Right panel) radiative partial width $\Gamma_{rad}/\Gamma_{tot}$ from [462] (Kib20), [463] (Obs76), [464] (Mar76), [465] (Mak75), [466] (Dav75), [467] (Cha74), [468] (Hal64), [469] (See63), and [470] (Alb61)

restricts the space for the possible description of the Hoyle state as a Bose–Einstein condensate [453]. These experiments triggered new theoretical works: in Ref. [471] the effect of Coulomb interaction between the three α particles is included in an R-matrix formalism to inspect the topological details of the sequential and direct decay patterns. In particular, it is found that even in a pure sequential decay, some strength outside the main ridge in the Dalitz plot should be observed. In Ref. [472] detailed one- and two-dimensional tunneling calculations were performed to obtain theoretical estimates for the direct *versus* sequential decay branching ratio, and the obtained value was more than one order of magnitude lower than the previously reported upper limits. A new high-precision inelastic scattering experiment had success in further lowering the direct decay branching ratios down to an upper limit of 0.019% (95% CL) [452]. The availability of high-quality gamma beams and a TPC detection system allowed to investigate the ^{12}C(γ,α)^{8}Be reaction [450]; and in particular to find an upper limit for the partial width of direct decay of the 2_2^+ state in ^{12}C, which is considered by several models to be a collective excitation of the Hoyle state. This value can be transformed, by calculating penetrability with the WKB approach, into the corresponding direct decay branching ratio for the Hoyle state itself, resulting in the very small upper limit of $\Gamma_{3\alpha}/\Gamma = 5.7 \times 10^{-6}$, barely possible to be reached with experiments searching for non-sequential events by directly looking to the Hoyle state decay (see Fig. 14 (left) for a general overview of the values reported in the literature). In a subsequent theoretical work following the same line [473], the effects of different starting 3α configurations on semi-classical penetrability calculations were considered in the estimate of direct decay branching ratios.

Apart from the direct decay width of the Hoyle state, other decay properties of this state were recently the subject of experimental investigations, in some cases with surprising results. For example, a new experiment of triple coincidence proton-$\gamma\gamma$ in p+^{12}C inelastic scattering collisions [462] led to a determination of the radiative branching ratio $\frac{\Gamma_{\rm rad}}{\Gamma} = 6.2(6) \times 10^{-4}$, a factor ≈ 1.5 times larger than the commonly accepted value derived from several experiments in the 60s and 70s. This value, coupled with a recent re-determination of the $E0$ branching ratio of the Hoyle state, reported in Ref. [474], and with the commonly accepted absolute partial width for the $E0$ decay (62.3 μeV, see [8]), lead to an absolute $\Gamma_{\rm rad}$ value that is 34% larger than the currently adopted value. Since this value directly enters into the triple α reaction rate calculations, the contribution of the triple α process should be consequently revised. In Fig. 14 (right) we plot all the determinations of the $\frac{\Gamma_{\rm rad}}{\Gamma}$ radiative branching ratios reported in the literature to now, illustrating the tension between data. A recent experimental investigation of the neutron-assisted triple alpha process was reported in Ref. [475], using a TPC to track the decay of the Hoyle state in n+^{12}C inelastic scattering and using the detailed balance theorem. The obtained enhancement factor of the triple α reaction rate was much smaller than predictions based on Hauser–Feshbach calculations [476].

In a recent paper [477], a non-zero value of the radiative branching ratio for the 3^- state of ^{12}C at 9.64 MeV was reported (1.3×10^{-6}); this finding would have a sizeable effect on the reaction rate for the triple α process in high temperature ($T > 2$GK) environments, such as supernova explosions. Non-vanishing values of branching ratios for radiative transitions in the 9.64 MeV state were reported also in Ref. [478] using complex multi-detection systems. It is worth noting that in the work of Ref. [477], a new estimate of the $\frac{\Gamma_{\rm rad}}{\Gamma}$ branching ratio for the Hoyle state was also reported ($4.3 \pm 0.8 \times 10^{-4}$); this value, even if affected by a relatively large uncertainty, is in agreement with the old estimates and in disagreement with the recent results of [462], contributing to increase the tension between data.

Another recent aspect of the structure of ^{12}C that was recently investigated concerned the possible existence of an Efimov-like state [479] at energy (7.458 MeV) slightly smaller than the Hoyle state one. This state would have a strong interest from the cluster point of view since its triple α structure should be stabilized by the interactions of the unbound α–α subsystem. A dedicated experiment performed with a time projection chamber to investigate the possible particle decay of such a state, coupled with previous data coming from γ analysis, excluded its existence with a large confidence level [480]. Another recent experiment, performed with a 4π multi-detector [481], lead to less sharp conclusions on the existence of an Efimov state in ^{12}C; anyway, if such a state would exist, the data seem to rule out its sequential decay in favor of a direct one.

Concerning the properties of other states in ^{12}C, a recent analysis of reorientation effects in a Coulomb excitation experiment allowed to measure the spectroscopic quadrupole moment of the 2^+_1, 4.44 MeV state ($Q_S = +0.071(25)$eb), confirming the oblate structure for this state [494]. On the higher energy side, new experiments of α+^{12}C inelastic scattering and ^{14}C(p,t) reactions, analyzing the ejectile spectra and the angular distributions of particle decay, unveiled the presence of an excess monopole

strength at $E_x \approx 9$ MeV [482] that was attributed to the occurrence of a breathing mode excitation of the Hoyle state. At still higher excitation energies, a revision of the partial decay widths of the 16.1 MeV 2^+ state in ^{12}C was discussed in Ref. [483], as a result of a re-measurement of the ^{11}B(p,α) reaction. A complete kinematics experiment on the ^{11}B(p,3α)γ reaction allowed a revision of the Γ_γ partial widths for excited states in ^{12}C above the α threshold and pointed out the possible existence of a natural parity state at $\approx$ 11.8 MeV [484]. The 3α decay of the unnatural parity state, 2^- at 16.62 MeV, of ^{12}C was revised in detail in Ref. [485] by a new experiment; contrarily to previous estimates reported in the literature, the relative orbital angular momentum of the decay into α+^{8}Be(2_1^+) was determined unambiguously to be dominantly $\ell = 1$, with an admixture of $\ell = 3$.

A recent proton-transfer experiment ^{11}B(^{3}He,d)^{12}C at 25 MeV studied the spectroscopic properties of several excited states in ^{12}C up to about 23 MeV excitation energy [486]. For the state at 20.98 MeV, the $J^\pi = 3^-$ and $T = 0$ assignments were suggested, while for the 22.4 Mev state ($J^\pi = 5^-$ according to [205], and belonging to the ground state band as predicted by the ACM) a possible alternative $J^\pi = 6^+$ assignment is derived from the DWBA analysis of the angular distribution, even if the presence of a couple of states with $J^\pi = 5^-$ and $J^\pi = 6^+$ in close vicinity cannot be excluded. Under this assumption, a state at around 22.4 MeV with $J^\pi = 6^+$ could fit well in the Hoyle band [486].

12.4 Clustering in ^{13}C

Several theoretical works attempted to describe the cluster structure of ^{13}C; this is a very important topic since this nucleus is the most simple candidate where a triple α underlying structure can be formed together with extra neutrons. In this frame, an extension of the symmetry considerations already made with the ACM was recently reported in Ref. [487]. Rotational and vibrational structures of ^{13}C was here investigated using the symmetries of the D'_{3h} double group representations. In particular, the ground band would be characterized by the $E_{1/2}^{(+)}$ representation, and would be made by three members, having $K^\pi = 1/2^-, 5/2^+, 7/2^+$ and the same moment of inertia. Similar considerations, *mutatis mutandis*, would holds for the first excited band, which can be understood with $E_{1/2}^{(-)}$ representation. The model predicts also a $E_{3/2}$ representation that would lead to bands characterized by parity doubling. Tuning a few parameters, a good reproduction of the level scheme of ^{13}C was achieved, suggesting a new and powerful way to classify the spectroscopy of this important isotope. A confirmation of the presence of a triangular α structure in the ground band of ^{13}C was obtained also using the REM method in [488], while some deviations from the triangular structure are seen for the other excited states (Fig. 15).

Another interesting analysis concerned the study of the structure of ^{13}C states with the AMD model [502], with the aim of identifying possible states that could be described as the coupling of an extra-neutron with a Hoyle-like structure. The detailed analysis of radii, spectroscopic amplitudes, and decay widths obtained in the calculations pointed out that the second $1/2^+$ state at 10.996 MeV could be the Hoyle-analog state in ^{13}C, with a prominent ^{12}C(0_2^+) $\otimes$ $s_{1/2}$ cluster structure.

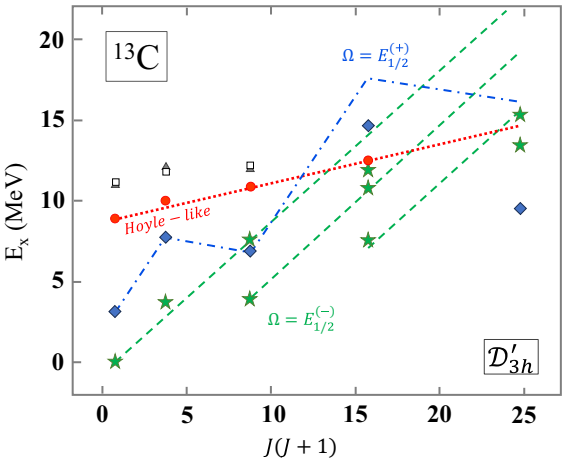

Fig. 15 Rotational bands of ^{13}C predicted by symmetry considerations in the D'_{3h} double group representations, as suggested in [487]. Green dashed lines: $\Omega = E^{(-)}_{1/2}$ bands. Blue dash-dotted line: one of the $\Omega = E^{(+)}_{1/2}$ bands. Red dotted line: Hoyle-like band. Experimental points are indicated in different colors. Adapted from Ref. [487]

From the experimental point of view, in Ref. [489] new results on α+^{9}Be resonant elastic and inelastic scattering experiments, obtained at the TTT3 tandem accelerator in Naples from direct kinematics collisions, were discussed together with previous results reported in the literature for the ^{9}Be(α,n)^{12}C reactions. A comprehensive R-matrix fit of data allowed to fix several ambiguities still present in the spectroscopy of ^{13}C states; the possible existence of two opposite parity $K = 3/2$ molecular-like bands, theoretically suggested in [256], was also discussed. It is worth noting that several states reported in the given level scheme could be allocated into several bands predicted in [487] from symmetry considerations. A better fixing of unbound excited state properties in ^{13}C could be obtained in future also using the resonant elastic and inelastic scattering data $^{12}C(n, n_1)$ recently reported in Ref. [490].

A new experiment of ^{13}C+^{9}Be elastic scattering at bombarding energies $\approx$ 16 to 19 MeV [491] measured angular distributions at very backward angles, a region where important elastic α-transfer amplitudes from the projectile can interfere with the ordinary elastic scattering processes. The analysis of elastic scattering angular distributions with the Coupled Reaction Channel method allowed to determine the spectroscopical amplitude, $SA = 0.569$, for the α+^{9}Be cluster structure of the ground state of ^{13}C.

12.5 Clustering in ^{14,15}C

^{14}C nucleus has a large interest since the couple of extra neutrons with respect to a simple 3α configuration can be subject of correlations that could have an influence on the formation of the molecular orbitals. From the theoretical point of view, the AMD model was used to pin down the decay properties of possible linear-chain states in ^{14}C above the α+^{14}C energy threshold (12.01 MeV), and two rotational bands with a pronounced linear-chain configurations were found [492]. The first band is characterized by neutrons forming a π-bond, and the energy position and decay widths

reported in the literature agree quite well with respect to predictions. The second band is characterized by neutrons forming a σ-bond and involves states of higher excitation energies. Interestingly, a peculiarity of this second band is a predicted sizeable branching ratio into the three-body decay ^{6}He+α+α, which could be therefore considered as a fingerprint of the formation of the σ-bond in a linear chain. A comparative analysis between linear chain states associated to σ-bond in the mirror nuclei ^{14}C and ^{14}O was performed with AMD model in Ref. [493]: the analysis of a Thomas–Ehrman-like shift effect, the peculiar differences in the Γ_α values and the presence of characteristic decay patterns can be considered as fingerprints of linear chain molecular structures. Another study, reported in Ref. [495], investigated with the AMD model the nature of several excited states in ^{14}C: in particular, it is found that the third 0^+ state can be interpreted as a vibrational mode of a triangular 3α configuration, with a sizeable monopole transition strength, while the 0^+_4 has a pronounced linear chain structure.

From the experimental point of view, after the work of Ref. [496], where the resonant elastic scattering of ^{10}Be on ^{4}He gas in inverse kinematics was investigated with a TPC chamber and two states with $J^\pi = 2^+$ and 4^+ above the α decay threshold were unambiguously identified, new subsequent experimental results were reported in Ref. [497] using a ^{10}Be beam impinging on a ^{4}He gas target. The R-matrix analysis of elastic scattering excitation functions and angular distributions leads to spectroscopical properties of ^{14}C excited states in the $\approx$ 14 to 19 MeV range that would strictly correspond to the ones predicted by AMD for the existence of linear chain states, giving strong support to this hypothesis.

^{14}C spectroscopy was also investigated by studying ^{9}Be+^{9}Be$\rightarrow$ ^{4}He+^{14}C* reactions at 45 MeV, sequentially followed by the ^{4}He+^{10}Be decay of the ^{14}C* nucleus [498]. Invariant mass spectroscopy analysis shows the occurrence of two states in ^{14}C at 22.5 and 23.5 MeV. In particular, the state at 22.5 MeV has considerable decay branching toward ^{10}Be states at excitation energies close to 6 MeV, in line with several predictions for the decay of a linear-chain state based on σ-bond in ^{14}C.

Concerning the ^{15}C nucleus, a theoretical study performed with the MCAS technique allowed to reasonably reproduce the energy positions and J^π of low energy states, and also several total width estimations are not far from the experimental results [499].

From the experimental point of view, two-neutron removal events were analyzed for ^{15,16}C isotopes [500] with much smaller uncertainties than previous experiments; in this way, the even-odd staggering of the two-neutron removal cross section, typically seen for the heavier isotopes of carbon (A = 16–20), was confirmed also for the lowermost part of the isotopic chain, in agreement with several theoretical calculations of two-neutron knock-out cross sections.

12.6 Clustering in ^{16,17}C

Recent theoretical investigations of ^{16}C focused their attention mainly on the existence of linear-chain structures. In particular, AMD calculations performed in Ref. [501] indicate that a positive-parity molecular band, built on the 0^+_6 state at 16.81 MeV, is made by states with a linear chain structure, leading to a very large moment of inertia

($\hbar^2/2I = 112$ keV). In this case, the valence neutrons occupy the molecular orbitals $(3/2^-_\pi)^2(1/2^-_\sigma)^2$, and the states of the band have large ^{4}He and ^{6}He reduced widths. Indeed, the occurrence of a large reduced width for the ^{4}He+^{12}Be(2^+_1) decay of states, together with the considerations already made on the moment of inertia, is suggested as a *smoking gun* proof of the existence of a linear-chain configuration in ^{16}C. In a subsequent work with the AMD model [503] the existence of an extremely deformed linear chain state at excitation energies above 30 MeV was discussed; it was pointed out that in this case the leading structure of states would have the valence neutrons in the molecular orbitals $(1/2^-_\sigma)^2(1/2^+_\sigma)^2$ and a huge moment of inertia ($\hbar^2/2I = 50$ keV). The stability of linear chain configurations for ^{16}C was investigated also with a 3D lattice cranking model in the frame of a covariant density functional theory [504]. It was reported that, at the lowermost angular velocities, the valence nucleons tend to be in the π molecular orbital, while by increasing the angular velocity, valence neutrons pass from the π molecular orbital to the σ one, and this would result into a stabilization of the 3α chain structure.

From the experimental point of view, a new experiment of inelastic scattering of a ^{16}C radioactive beam on a deuterium target at intermediate energies was performed at HIRFL-RIBLL in China [505, 506]. The sequential decay of excited states of ^{16}C into ^{4}He+^{12}Be and ^{6}He+^{10}Be was investigated in a complete kinematics experiment making use of highly segmented hodoscopes (for the detection of decay fragments) coupled to annular silicon detectors segmented in strips (for the detection of the recoiling deuterons). The energy and angular resolutions of the setup allowed to discriminate the different Q-value peaks of the triple coincidences d+^{4}He+^{12}Be and d+^{6}He+^{10}Be, allowing a clean selection of the decay pattern of a given state in ^{16}C. The analysis of angular correlations determined also the J^π of the 16.5 MeV state, 0^+, in agreement with AMD calculations that predict such a state as the band-head of a 3α linear chain band. The energy position of states at larger excitation energies (up to $\approx$ 29 MeV) are in reasonable agreement with AMD calculations, and also the AMD predictions on specific decay patterns due to the presence of the linear chain band are in agreement with the experimental data; these findings would give support to the existence of a chain structure with valence neutrons in the $(3/2^-_\pi)^2(1/2^-_\sigma)^2$ configuration. The observation of a highly excited state at 27.2 MeV, with a prominent decay branching into the ^{6}He+^{10}Be*($\approx$ 6 MeV) could be in agreement with AMD predictions on the existence of an exotic linear chain molecular band where valence neutrons occupy the $(1/2^-_\sigma)^2(1/2^+_\sigma)^2$ orbitals.

Concerning ^{17}C, the results of a new one-neutron transfer reaction in inverse kinematics were reported in Ref. [507], using the TIARA silicon array and some modules of the EXOGAM array. The spectroscopic factors obtained for the ground state and the first two excited states (at 217 and 335 keV) were compared with several theoretical predictions; in particular, the 217 keV $1/2^+$ state, having the valence neutron in the $\ell = 0$ configuration and very low separation energy, seems to be candidate to have a one-neutron halo structure.

12.7 Some observations

Carbon isotopes, and among them the very special case of ^{12}C, represent the *cornerstone* of clustering studies in light nuclei, with the huge scientific production reported in the previous section just in the last 5 years. Nevertheless, to our opinion, several open questions deserve urgent answers from the experimental side. For example, the tension between the $\Gamma_{\rm rad}$ values for the Hoyle state (see Fig. 14) needs to be resolved as soon as possible with high-precision and low-background experiments, not only because this quantity is involved in the understanding of the cluster structure in ^{12}C, but also because of its impact in the astrophysical domain: it enters directly into the reaction rate calculation (Eq. 13). Further, a better knowledge of the spectroscopy of high-lying states in ^{12}C would be important to validate the ACM predictions and the underlying D_{3h} symmetry. On the proton-rich side, the newly discovered ^{10}C molecular band gives support to the occurrence of clustering due to covalent protons and stimulates further investigations on the same ground of the ^{10}Be case. The situation is less clear for the ^{11}C case; in particular, the conflicting results obtained in recent experiments for the spectroscopy of states in the 9–10 MeV region prevent a clear understanding of the members of the suggested $K^\pi = 3/2^-$ molecular band, calling for new measurements. On the neutron-rich side, it could be interesting to re-organize all the spectroscopic information of high-lying states in ^{13}C available up to now into the family of bands suggested by the $D_{3h'}$ double-group representation. For the even isotopes ^{14,16}C, strong evidence supporting the occurrence of molecular structures with a linear α-chain was discussed in the previous section, and this finding would indicate once more how important is the role played by covalent bonding for the stability of very exotic shapes.

13 Clustering in Nitrogen isotopes

Some recent experimental data were reported also for the odd-Z nitrogen isotopic chain. Invariant mass methods have been recently exploited to investigate the two-proton decay from excited ^{11}N states [393]. In particular, the 3p+2α exit channel has been considered, alongside data from previously published invariant mass studies involving inelastic excitation, multinucleon knockout, and neutron pickup reactions. This analysis shows evidence for a molecular band in ^{11}N built on the second $3/2^-$ state, which decays by emitting two protons, whose members have been assigned up to $J^\pi = 9/2^-$ [393]. These states are found to match their likely analogs in the mirror nucleus ^{11}Be. Particle-decaying states in ^{11,12}N have also been investigated in Ref. [508] via invariant mass methods. Analogs of 4p+2α ^{12}O states were found in ^{12}N in the 2p+^{10}B and 2p+α+^{6}Li channels.

Proton-unbound levels in ^{12}N were investigated using the transfer reaction ^{14}N(p,t)^{12}N, providing decay particle spectra for the populated levels from p_0, p_1, and p_2 decay [509]. This information is useful to provide inputs to nuclear structure and decay models in the low-mass region.

A new ANC value for the $^{13}N_{gs} \rightarrow$p+^{12}C was determined by analyzing the reaction ^{12}C(^{10}B,^{9}Be)^{13}N and including the possibility of having a proton transfer from the

projectile to the target, or an ^{3}He transfer from the target to the projectile [510]. With such a value the direct contribution to the ^{12}C(p,γ)^{13}N reaction at astrophysical energy was redetermined, together with an improved description of the parameters characterizing the resonant part of the S-factor. The resulting reaction rate at $T \leq 0.35$ GK is 10% larger than the one recommended in the NACRE II compilation [511].

New spectroscopic data for excited states of ^{14,15}N isotopes above the α threshold were deduced in Ref. [417] by a comprehensive R-matrix fit of experimental data involving α+^{10}B, α+^{11}B collisions and p+^{14}C and n+^{14}N scattering and charge exchange reactions data. Some states in both the isotopes show quite large dimensionless reduced partial widths for the α decay, pointing out the possible occurrence of clustering effects above the α threshold; the existence of such clustered states leads to an enhancement of the rates of α-capture reactions on boron isotopes that could have a sizeable impact in the nucleosynthesis process in first-generation stars.

The multichannel algebraic scattering (MCAS) technique was used to calculate the spectra of the set of mass-15 isobars, including ^{15}N, seeking for a consistent Hamiltonian for clusterization with a neutron and a proton separately, coupled to core nuclei [499].

A microscopic three-cluster model, developed for exotic light nuclei, was recently applied to ^{17}N, described as two neutrons surrounding a ^{15}N core [358]. This method allowed to calculate some spectroscopic properties, such as r.m.s. radii and $E2$ transition probabilities.

13.1 Some observations

Similarly to the boron case, also nitrogen isotopes are still poorly known from the point of view of nuclear clustering. It is worth noting the recent comprehensive R-matrix analysis of α+B scattering and reaction data at low energies, pointing out the occurrence of states with large α partial widths: among them, a 3^- state at 12.689 MeV in ^{14}N almost saturates the α Wigner limit and should deserve some further investigation. New experiments of this type, also involving unstable boron isotopes, could help to unveil cluster structures also in very neutron-rich nitrogen isotopes.

14 Clustering in oxygen isotopes

14.1 Clustering in proton-rich Oxygen isotopes

The ^{11}O decay properties were subject of recent investigations [512, 513]; in particular, in Ref. [513] the partial widths of sequential (^{11}O$\rightarrow$ p+^{10}N $\rightarrow$ p+p+^{9}C) and simultaneous (^{11}O$\rightarrow$ ^{2}He+^{9}C) decay modes were calculated in the frame of a potential model, and the obtained simultaneous decay width is comparable the sequential one.

An analysis of the spectroscopy of the proton-rich ^{12}O nucleus was performed with the invariant mass method using the HIRA hodoscope and knock-out reactions induced by a radioactive ^{13}O beam on a ^{9}Be target [508]. The second 2^+ state at

4.775 MeV was discovered from the analysis of 2p+^{10}C correlations; furthermore, it was pointed out that states at higher excitation energies could have a non-negligible probability of decaying by fission in ^{6}Be+^{6}Be. The obtained experimental data were compared with predictions of the Gamow Coupled Channel model, describing ^{12}O as made by two protons interacting with a deformed ^{10}C core [514]. Subsequently, the effects of two-proton correlations in the decay of proton-rich ^{11,12}O isotopes were theoretically discussed in Ref. [512] by using a realistic time-dependent approach. In such isotopes, di-proton and cigar-like structures merge together during the tunneling phase of the decay; the resulting energy and angular correlations are in agreement with the experimental ones [528].

Also ^{13}O excited states were investigated experimentally with the HIRA detector, by looking at particle correlations coming from particle-unbound states populated in inelastic scattering of ^{13}O beam at about 70 MeV/nucleon. Several high-lying excited states were observed by analyzing the invariant mass spectra of p+^{12}N and 2p+^{11}C. Some of these states are not predicted in no-core shell model calculations, while their energy position and J^{π} values seem in agreement with AMD calculations performed for the mirror nucleus ^{13}B [515] and pointing out the formation of rotational bands built on molecular-like cluster structures.

The occurrence of linear chain states with π- and σ-bonding at large excitation energies in ^{14}O was suggested in [493] with the AMD model; a comparison with analog results for the mirror nucleus ^{14}C clearly indicates the presence of the Thomas–Ehrman shift for the exotic states having the σ-bond linear chain configuration.

14.2 Clustering in ^{16}O

Being a self-conjugate nucleus, ^{16}O attracted a lot of attention during the last 5-year period. From the theoretical point of view, several works tried to investigate the structure of ^{16}O in connection with the possible occurrence of clustering effects, even in its ground state. Hartree–Fock calculations based on the Skyrme energy density functional, reported in Ref. [516], indicated the presence of a pronounced 4α cluster structure with tetrahedral symmetry. The same leading symmetry was at the basis of the ACM calculations of Ref. [517]: evidence of such symmetry is particularly pronounced from the properties of the ground state band, while it is weaker for the excited bands A_1, E, F_2. We recall here that A, E, F (in some text, $T = F$) indicate the so-called *character* of a vibration mode in an object with a given symmetry [168].

The possible evolution of cluster configurations in ^{16}O, from the most simple α+^{12}C decomposition to a more complex tetrahedral or even condensate structure has been investigated in the framework of a "container picture" of the nucleus [518, 519]. The structure of low-lying states in ^{16}O was investigated also by using the Skyrme model in Ref. [520]; the theoretical level scheme substantially agrees with the data, and the model point out a tetrahedral structure for the ground state. Interestingly, the model predicts a structure for the 0_2^+ state at 6.05 MeV as the superposition of a tetrahedral and a *square* configuration. The effects of stabilization of α cluster tetrahedral 0^+ structures occurring in ^{16}O due to the tensor interaction was discussed in Ref. [521]; at relatively large α–α of about 2 fm, the contribution of the tensor interaction to the

0^+ energy (and therefore to the stability of the underlying cluster structure) is not negligible, being about − 20 MeV.

The AMD-VAP and AMD-GCM calculations reported in Ref. [522] confirm the presence of tetrahedral 4α and α+^{12}C configurations arising naturally from nucleon degrees of freedom in the AMD model; the ordering of ^{16}O states into rotational bands having such structures is also discussed. Variation After Projection method was also applied to investigate the possible formation of linear chain states in ^{16}O at large excitation energies [523]: the predicted 0^+ band-head should have about 33 MeV excitation energies and the band is predicted to terminate with the $J^\pi = 6^+$ state. An interesting possibility to obtain information on the α cluster arrangement in ^{16}O could also come from photonuclear reactions; in Ref. [524], the reaction $^{16}\mathrm{O}(\gamma, np)^{14}\mathrm{N}$ was theoretically investigated with the Quantum Molecular Dynamics approach, and several multi-particle correlations (e.g. the p, n opening angle or the hyper-radius distributions) seem to be sensitive to the shape of the ^{16}O target nucleus.

Obviously, the cluster structure of ^{16}O could have a deep impact also in the nuclear dynamic field, by influencing several aspects of nuclear reactions and decay. For example, the spatial manifestation of an α cluster on the surface of ^{16}O was investigated by interpreting α-transfer angular distributions with DWBA calculations, where the ^{12}C-α wave function of the relative motion was microscopically derived using two different approaches: OCM model and five-body calculations [525]. From calculations, it was suggested that several details of the wave function can be determined from the ratio of the first and second maxima of the angular distributions.

Low-energy α+^{12}C elastic scattering collisions can be useful to determine structure properties of ^{16}O. For example, in Ref. [526], a phase shift analysis of elastic scattering data in the $\approx$ 2.5 to 4.0 MeV region with calculations performed with an Effective Field Theory, allowed to determine the Asymptotic Normalization Constants (ANC) for the bound states of ^{16}O, which are needed to better understand the details of the astrophysical important $^{12}\mathrm{C}(\alpha, \gamma)$ reaction. Also the new Δh method, based on the complex analysis of the behavior of the denominator of the re-normalized scattering amplitude [527], allowed to estimate the ANCs for the ground state and the second 0^+ state in ^{16}O. Two different methods of analytical continuation of the scattering data were implemented in Ref. [529], and the correspondingly determined ANC range of values for the 0_2^+ state in ^{16}O was discussed. Resonances in α+^{12}C elastic scattering data were analyzed in terms of the Jost functions method in Ref. [530]. α+^{12}C elastic scattering data at higher energies (13-60 MeV) were described by using a realistic double-folding potential in Ref. [531]; to simultaneously describe the elastic scattering angular distributions and the existence of rotational bands in ^{16}O, it was needed to add a dynamical polarization potential to the bare folding potential.

On the nuclear astrophysical side, the Cluster Effective Field Theory was used to determine the astrophysical factor for the radiative proton capture by ^{15}N, passing through some low-energy resonances in ^{16}O [532]; even if the zero-energy astrophysical factor is close to the extrapolations based on R-matrix analysis of experimental data, the resonance parameters obtained by the EFT approach are, for some cases, quite different from the R-matrix one.

Isoscalar monopole and dipole excitations of ^{16}O were studied within the AMD framework in Ref. [533]; sizable transition strengths for such modes were found

at energies lower than the giant resonance region, and some peculiar dipolar mode appears at low energy (as the vortical mode for tetrahedral 4α structure in the 1^-_1 state). A comparison of AMD calculations to experimental data of elastic and inelastic α+^{12}C data is reported in Ref. [534] with a detailed discussion of the isoscalar dipole and monopole excitations for the 1^-_1 state and the second and third 0^+ states in ^{16}O.

Effects of clusterization in ^{16}O can also be observed by analyzing collective flow parameters obtained in heavy-ion collisions at Fermi energies [535] and also at the ultra-relativistic regime [536], where it seems possible, in central collisions, to distinguish between the occurrence of a tetrahedral α-cluster structure with respect to an ordinary soft-sphere.

From the experimental point of view, in the last 5 years, there was a considerable interest toward the search for a possible state in ^{16}O with properties analog to the ones of the Hoyle state in ^{12}C. By fulfilling the Ikeda rule, such state should be located close to the 4α disintegration threshold (i.e., 14.44 MeV), and in fact the largest part of the experimental investigations focused their attention in that energy region. In Ref. [537] the inelastic scattering of 200 MeV α particles on ^{16}O was investigated at 0° by using the K600 magnetic spectrometer at iThembaLab; the decay products (protons and αs) coming from the decay of unbound states in ^{16}O were detected by an array of silicon detectors. The detailed study of angular correlations pointed out for the first time the existence of a previously unresolved state at $\approx$ 15 MeV, very close in energy to the sixth 0^+ state at about 15.1 MeV, which was considered by several theoretical works as the analog of the Hoyle state. The presence of the close-lying state at smaller energy allows to solve previously reported inconsistencies in the width of the states in the 15 MeV region; in particular, the value of the total width determined for the sixth 0^+ state is slightly smaller than previously published values, and therefore in better agreement with the presence of a long-lived structure predicted for a Hoyle-like state.

Another experiment, performed in inverse kinematics by colliding a ^{20}Ne beam on a ^{4}He gas target [538], studied the multi-particle correlations in 4α events. Despite the limited statistics and energy resolution, the decay patterns of a state at 15.2 MeV, which could correspond to the 0^+_6 state of ^{16}O, were determined experimentally. In particular, they found that, despite the large statistical uncertainties, the decay probabilities of this state toward the ^{8}Be+^{8}Be channel versus the ^{4}He+^{12}C$_{\text{Hoyle}}$ channel are almost equal, in qualitative agreement with the hypothesis of a pronounced 4α structure for this state. However, more recent results obtained from a complete kinematics inelastic scattering α+^{16}O experiment [539], allowing to populate states in ^{16}O at energies above the 4α threshold and to perform many-particle correlations in 5α events, only hardly populated the 15.1 MeV state, making difficult to extract the properties of such state despite the noticeable performances (in terms of energy resolution and efficiency) of the experimental setup. The hunt for the analog of the Hoyle state in ^{16}O is therefore still open.

New results from α transfer experiments populating several ^{16}O bound and unbound states were discussed in Ref. [540]. The spectroscopic amplitudes for the transitions toward the states at 0, 6.05+6.13, 6.92, 7.13, 10.34 MeV, and the ANC values for ^{16}O bound states, were obtained in the framework of the Coupled Reaction Channel

approach, typically used in above-barrier transfer reactions where break-up effects can be present.

A detailed analysis [541] of elastic scattering angular distributions (including backward angles) at bombarding energies $\approx$ 100 to 300 MeV with Coupled Reaction Channel method, inspected the possibility of interference between direct elastic scattering and elastic transfer amplitudes, by considering a leading cluster nature of ^{16}O as α+^{12}C, with the ^{12}C in the ground state or in the excited state at 4.44 MeV. Clustering description of the wave functions of colliding ^{12}C and ^{16}O nuclei was used in the study of supernumerary bows in the analysis of angular distributions for ^{16}O+^{12}C inelastic scattering events [542].

14.3 Clustering in neutron-rich Oxygen isotopes

The spectroscopy of low-energy states of neutron-rich oxygen isotopes $^{18-23}$O was theoretically predicted using ab initio no core shell model and the inside-nonlocal outside-Yukawa (INOY) interaction in Ref. [543]; in this frame, the INOY interaction allows to get the effects of three-body forces without the need of explicitly adding them in the model. Neutron-neutron correlations in the decay of the very neutron-rich ^{26}O were theoretically discussed in Ref. [512] by using a realistic time-dependent approach.

Concerning ^{17}O, the MCAS method was combined to a vibrational model [544] to describe the spectroscopy of low-lying states in ^{17}O and the elastic scattering n+^{16}O data down to almost zero energy ($\approx$ 1 keV). In Ref. [545], spectroscopic amplitudes of ^{17}O states were calculated with the shell model and included in the complex coupling scheme of a two-neutron transfer reaction involving ^{13}C and ^{18}O.

The spectroscopic factors S_α for the cluster decomposition of ^{17}O in α+^{13}C were experimentally determined in Ref. [546] by analyzing, with the Coupled Channel Born Approximation technique, the angular distributions of the ^{13}C(^{11}B,^{7}Li)^{17}O α-transfer reaction at 45 MeV. Interestingly, the largest S_α values are seen for the sub-threshold $1/2^+$ state at 6.356 MeV, being 0.39 or 0.72, depending on the number N of nodes present in the radial wave functions. The obtained Coulomb-modified ANC values are however weakly dependent on N, and are in agreement with previous values reported in the literature. It is worth noting that the accurate knowledge of this ANC value is important for the careful determination of the rate of the astrophysically important ^{13}C(α,n)^{16}O reaction at very low energies [547].

Also the ^{18}O isotope has been the subject of recent investigations. AMD calculations pointed out the possible existence of several different types of clustering phenomena in such a nucleus, going from the more common (and compact) α+^{14}C configuration to the α+^{12}C+2n configuration in the σ orbit, up to the presence of linear 4α chain structures at very large excitation energies, with a huge moment of inertia [548]. It was also shown that the cluster states with the α+^{12}C+2n configuration should preferentially decay by emitting ^{6}He. In another work based on AMD [562], it was pointed out that the monopole and dipole transitions between 0^+ and 1^- states are enhanced when states with a pronounced α+^{14}C cluster configuration are involved, while they are more suppressed when the molecular-like 0^+_4 state, of the type α+^{12}C+2n, is involved. Low-

energy dipole excitations were discussed in [549] with the β-AMD+K-VAP model; it was suggested also that the second 1^- state in ^{18}O could have a pronounced α+^{14}C cluster structure. An interesting study, performed with the OCM, compared the 0^+ energies for bound and unbound states (above the α threshold) in the mirror couple of nuclei ^{18}O and ^{18}Ne; the reduction of the Coulomb energy shift for states above the threshold, originated by the cluster structure in ^{18}C, has some traits similar to the Thomas–Ehrman shift effect seen for the $s_{1/2}$ analog states in ^{17}O (0.871 MeV) and ^{17}F (0.495 MeV) [564].

From the experimental point of view, new data on excited states of ^{18}O in the 7–19 MeV region were obtained in a multi-nucleon transfer experiment [550], and the branching ratios of α decay of several observed states were deduced by performing missing-mass and invariant mass analyses of experimental data. The study of the angular correlation for the decay of the 10.28 MeV state confirmed the 4^+ assignment previously done in the literature with resonant elastic scattering data. The good energy resolution achieved in the experiment allowed to resolve two states in the region of 11.7 MeV excitation energy, where the presence of the 6^+ member of the positive-parity α+^{14}C cluster band was suggested by several theoretical calculations and also by previous resonant elastic scattering experiment [551]; a 6^+ assignment for the observed 11.72 MeV state would lead to a very large dimensionless reduced partial width $\theta_\alpha^2 \simeq 0.56$, in agreement with the presence of a cluster state. Another experiment, making use of the Munich Q3D spectrometer coupled with high segmentation solid state detectors, investigated the α decay branching ratio of ^{18}O states populated with the ^{12}C(^{7}Li,p)^{18}O reaction [552]. The analysis of the so-called "Catania plots" [156] permits to discriminate carefully the α decay events from the others, thus allowing the determination of the α decay branching ratios. The very small experimental values of the dimensionless reduced partial widths θ_α^2 observed for several states that were suggested to be members of the second and fourth 0^+ states in ^{18}O make it difficult to confirm the existence of such cluster bands. A subsequent work [553] determined also the neutron and gamma branching ratios, confirming the small θ_α^2 values in the whole excitation energy region ≈ 7 to 16 MeV, with the exception of two 6^+ states at 11.7 MeV (in agreement with the findings of [550] discussed before) and 12.56 MeV. Further experimental investigations are therefore needed to clarify the existence of cluster bands in ^{18}O.

14.4 Some observations

^{16}O has had a special role in nuclear cluster physics since its beginnings [30]. From a theoretical point of view, several models agree on the occurrence of a tetrahedral α structure for this self-conjugate nucleus even in its ground state. The situation is however less clear from the experimental point of view: a good number of experimental states would match the J^π sequences predicted by ACM by assuming the T_d symmetry, but further data would be very useful to fix better this hypothesis. The question of the existence of a "Hoyle-like" state in ^{16}O close to the 4α threshold is still open: despite the recent experimental efforts discussed in the above section, the small yields observed at 0° for 0^+ states at around 15 MeV populated with α inelastic scattering events, make

very difficult to study the properties (decay pattern, widths) of such states, and call for new experiments performed, for example, with active target systems. Concerning the other isotopes of oxygen, it is interesting to underline the recent theoretical suggestion of a Thomas–Ehrman-like effect in states of mirror nuclei involving oxygen isotopes that could be useful as a guidance to unveil exotic molecular configurations due to α clustering. Unfortunately, from the experimental point of view, the occurrence of cluster bands in ^{18}O is still far from being understood: the recent high-resolution experiments indicate serious difficulties in revealing several members of the molecular bands. Considering the excellent performance obtained in such experiments, it is hard to imagine that new experiments could shed further light on this problem; perhaps we have to rethink from the basis some hidden aspects of ^{18}O structure.

15 Clustering in Fluorine isotopes

The level scheme of low-energy states in the chain of fluorine isotopes $^{18-24}$F was theoretically predicted by ab initio no-core shell model calculations in Ref. [543].

The spectroscopy of ^{19}F states above the α decay threshold was specifically studied in recent times by various resonant elastic scattering experiments. The derived resonance parameters can have an impact on the determination of several reaction rates involved in the fluorine nucleosynthesis in stars; this a question still debated in nuclear astrophysics (see, e.g. [554, 555]). A first experiment, performed with the TTIK method at LNS-Catania, reported new data for elastic scattering excitation functions of α+^{15}N at several angles in the domain of excitation energy $E_x \approx 5.5$–9.5 MeV [556]. Such data, together with data of p+^{18}O previously published in the literature, were analyzed by performing a comprehensive R-matrix fit; the obtained dimensionless reduced partial widths for α decay show very large values for several states, pointing out the occurrence of strong clustering phenomena. Further, the existence of a new high-spin state ($13/2^+$, 9.374 MeV) was suggested.

Since the structure of states very close to the α threshold in ^{19}F was still debated, a new experiment of TTIK resonant elastic scattering [557] was optimized to obtain the excitation functions in the $E_x \approx 5.2$–5.7 MeV region, uncovered by previous experiments both in direct and indirect kinematics. From the R-matrix analysis of data, the emergence of clustering in ^{19}F states at an energy close to the threshold is clearly seen. The near-threshold states of ^{19}F at 5.333 MeV ($1/2^+$) and 5.488 MeV ($3/2^+$) appear as spin–orbit partners coming from the coupling of the ($1/2^-$) ground state of ^{15}N core with a p-wave relative motion of an α cluster. Furthermore, a comparison with near-threshold states in ^{20}Ne with prominent α+^{16}O configuration point out the strong similarities of α cluster structure between the two nearby ^{19}F, ^{20}Ne nuclides. A subsequent R-matrix re-analysis of α+^{15}N scattering data, based on the previous work and also to other literature data, reported a detailed revision of the spectroscopy of ^{19}F above the α threshold [558] and some previous high-spin assignments of Ref. [556] were changed. The new level scheme so obtained for ^{19}F was used as a starting input to perform R-matrix fit of the α+^{15}O elastic scattering literature data [559] involving the mirror ^{19}Ne compound nucleus.

15.1 Some observations

The involvement of near-threshold states in ^{19}F in reactions useful to explain the fluorine nucleosynthesis in stars led to recent experimental efforts in determining the spectroscopic parameters of such states from R-matrix analysis of compound nucleus reaction data. Since states with sizeable α-cluster structures have been seen close to the threshold, it could be interesting to deepen their spectroscopical characteristics also by invariant mass analysis of correlated α+^{15}N fragments emitted in heavy-ion collisions at intermediate energies. In general, however, the occurrence of clustering in unstable fluorine isotopes is poorly known, and this would call for detailed studies both theoretically and experimentally. In particular, special attention should be given to the ^{18}F isotope that, similarly to ^{19}F, has $|Q_\alpha| = 4.415$ MeV, well lower than its one-nucleon separation energy (5.607 MeV): this peculiar trend of energy thresholds could signal the occurrence of cluster structures in this proton-rich isotope.

16 Clustering in neon isotopes

16.1 Clustering in proton-rich Ne isotopes

The spectroscopy of states above the α threshold ($|Q_\alpha| = 3.528$ MeV) in the ^{19}Ne proton-rich isotope has a large interest since the properties of such states can strongly determine the behavior of the astrophysically important ^{15}O$(\alpha, \gamma)^{19}$Ne reaction. This reaction is in fact involved in accreting neutron star processes leading to huge energy emission through X-ray burst (see also, e.g., [560]). Information on resonance positions, spin-parity assignments and partial width determination can be obtained by analyzing α+^{15}O elastic scattering excitations functions, and this has been recently accomplished and discussed in Ref. [559]—thanks to an inverse kinematic experiment. The R-matrix fit of the excitation function at 180° in the center of mass points out the need of including seven new states never reported before; such new states have a correspondent partner in the mirror nucleus ^{19}F. The values of θ_α^2 reported for states at the lowermost energies are quite large (e.g. 0.98 for the 5.704 MeV, $5/2^-$ state), and large θ_α^2 values are seen also for states above the proton threshold $S_p = 6.410$ MeV, pointing out the occurrence of α clustering in ^{19}Ne in a wide energy domain.

As discussed in the previous paragraph, in Ref. [558] the revised spectroscopy of the mirror nucleus ^{19}F was used as starting input for the R-matrix fit of α+^{15}O elastic scattering data of Ref. [559]. As a result, some J^π assignments, previously performed in [559], especially at the highest energies, were changed and several new resonances, with Γ_α values typically smaller than the ones of [559], were reported.

A potential model calculation of energy shifts between levels in the mirror nuclei ^{19}Ne,^{19}F shows an interesting change of sign if one considers single-particle states or cluster states; such behavior, which seems to be present also in the experimental data, could represent a new way to probe the single-particle versus cluster nature of a given state. Finally, in a recent theoretical work [561] the shifted Deng-Fan potential was used to reproduce the rotational bands with α+^{15}O cluster structure; in the frame of this local cluster potential model, the calculated lifetimes for the $7/2^-$ and $9/2^-$ states

at 4.14 and 4.20 MeV (14.3 and 35.8 fs, respectively), involved in the $^{15}O(\alpha, \gamma)^{19}Ne$ reaction, agree well with experimental data.

Very recent data on α clustering in the ^{18}Ne isotope have been obtained, thanks to the analysis of a $^{14}O+^{4}He$ resonant elastic scattering experiment, performed with the TTIK method and the TexAT active target device [563]. Several states in the excitation energy window 8-17 MeV show reduced partial widths γ_α^2 larger that 10% of the Wigner limit; three of them are at or above the Wigner limit. In general, a good correspondence with states in the mirror nucleus ^{18}O was found. A possible *superradiance* mechanism, conceptually similar to the quantum optics superradiance effect, was suggested in Ref. [565] to explain the existence of highly clustered states in ^{18}Ne and ^{18}O.

16.2 Clustering in ^{20}Ne

The old suggestion of the formation of a bipyramidal structure of 5α particles in ^{20}Ne, and the corresponding D_{3h} symmetry, was recently re-considered in the theoretical frame of the ACM. A reasonable description of form factors, radii and electromagnetic transition rates and moments for ^{20}Ne was obtained. Interestingly, all the nine normal vibrational modes predicted by applying the D_{3h} symmetry to the bipyramid structure seem to occur in the known experimental level scheme, giving support to this model [566]. The structure of ^{20}Ne was also interpreted in the frame of a quartet model in Ref. [567], and good agreement with experimental data was found. In this model, it is supposed that, for a nucleus made by a doubly magic core plus a quartet of valence nucleons (2p+2n), the quartet intrinsic wave function would change its nature from a shell model configuration to a pure cluster configuration when a fixed critical radius is overcome.

The presence of cluster configurations in low positive and negative parity states in ^{20}Ne was discussed with the energy density functional theory in [568]; the $K^\pi = 0_1^\pm$ opposite parity bands are well reproduced by the calculations, and also the transition probabilities *within* a band ($E2$) and *between* the bands ($E3$) reasonably reproduce the experimental data. A good description of the $B(E2\downarrow)$ reduced transition strengths for the $K = 0_1^+$ band is obtained also with a local potential cluster model in Ref. [569].

The evolution of clustering in ^{20}Ne at finite temperatures was studied in [570] with the Relativistic Hartree–Bogoliubov theory; in particular, the presence of pairing effects at finite temperature delays the dissolution of cluster structures up to the critical temperatures for the shape phase transition of ^{20}Ne.

Different cluster vibration modes at low energies have been studied in the framework of the relativistic energy density functional in Ref. [571]. The instability toward particle emission in highly excited ^{20}Ne nuclei formed in heavy-ion reactions, with the consequent emission of intermediate mass fragments and clusters, was investigated with the quantum mechanical fragmentation theory in Ref. [572]. In the high energy domain, new theoretical investigations of α particle knock-out induced by fast protons were reported in Refs. [573, 574]; the analysis of experimental data of the energy sharing distribution with Distorted Wave Impulse Approximation calculations

coupled to structure models would represent a useful tool to probe α clustering effects in the surface of the target.

Effects of clustering in the inelastic scattering of protons and α particles on ^{20}Ne were studied with the VAP+AMD model in Ref. [575]. Here, the $K^\pi = 0_1^\pm$ bands are predicted to have α+^{16}O structure, while the $K^\pi = 2^-$ band has a pronounced ^{12}C+2α structure. The comparison of calculations with experimental inelastic scattering data indicates the possible mixing of the $K^\pi = 0_1^-$ cluster component in the 3_1^- state, member of the $K^\pi = 2^-$ band. The determination of the overlap between the α+^{16}O cluster configuration and the wave function of states in ^{20}Ne was calculated, for the first time, in the ab initio symmetry-adapted no-core shell model [576]. The deduced Γ_α of the lowermost 1^- resonance in ^{20}Ne is in good agreement with experimental data; ANC values for the ground state and the 4_1^+ state close to the α threshold were deduced for the first time in a no-core shell model calculation. Such theoretical values were used to calculate the reaction rate of the ^{16}O(α, γ)^{20}Ne in the temperature range $T = 1$–10 GK.

From the experimental side, a new experiment of α+^{16}O resonant elastic scattering in inverse kinematics was performed in Astana [577]; excitation functions in the $E_x \simeq 5.5$–9.6 MeV were reported at several angles in the center of mass, from $\theta_{cm} = 107°$ to $\theta_{cm} = 172°$. A R-matrix fit of data allowed an accurate determination of the energy position and widths of the very broad 0_4^+ and 2_4^+ α cluster states at about 8.77 and 8.79 MeV. To describe their pronounced clustering nature, such states must include configurations from the fp shell and from higher oscillator shells, and this is still a puzzling question since such contributions are predicted to be very small below 15 MeV excitation energy from the traditional shell model Hamiltonian.

The spectroscopic properties of natural parity states in ^{20}Ne were investigated also in Ref. [231] by studying low-energy ^{19}F(p,α)^{16}O reactions leading to the ^{16}O in the ground state (α_0 channel) or in the first excited 0^+ state (α_π channel). A comprehensive R-matrix fit of such reaction data and of p+^{19}F elastic scattering data allowed a revision of resonance parameters in the excitation energy region $E_x \simeq 13$–16 MeV, and a better determination of the reaction rate down to astrophysical energies for both the ^{19}F(p,α)^{16}O reaction channels studied. In particular, a 2^+ state at 13.095 MeV, which was suggested to have a strong α+^{16}O(0_2^+) configuration [578], can contribute to enhancing the reaction rate of the α_π channel in the $T \approx 0.2$–0.3 GK domain.

16.3 Clustering in neutron-rich Ne isotopes

For the isotopic chain $^{20-30}$Ne, the structural properties and their evolution with the mass number were investigated with ab initio calculations using no-core shell model and projected GCM approaches [579].

Concerning the cluster structure of ^{21}Ne, its energy level scheme (and also the one of the mirror nucleus ^{21}Na) was analyzed in terms of the Cluster Shell Model in Ref. [580]. In this approach, the intrinsic states of ^{21}Ne are calculated by solving the Schrodinger equation for a potential having the structure of a bi-pyramid, as predicted by the ACM for the self-conjugate ^{20}Ne core. Several particle and hole bands experimentally observed can be described by the CSM calculations. However, states in a bi-pyramidal

potential are expected to have characteristics similar to those of states determined from an ellipsoidal potential with the Nilsson model. In this context, it is very important to investigate peculiar features of vibrational bands: for a bi-pyramid potential, one would expect nine vibration modes, while in the ellipsoidal potential, one expect three vibration modes (β, single degenerate and γ, double degenerate). Two of these vibrational bands are clearly seen in the experimental data, the $K^\pi = 3/2^+$ (with band-head at 5.549 MeV) and the $K^\pi = 3/2^+$ (with band-head at 5.826 MeV); since with the Nilsson model, we expect a *single beta* vibration band with $K^\pi = 3/2^+$, the experimental data give support to the clustered view of the ^{21}Ne structure.

From the experimental point of view, the spectroscopy of α unbound states in ^{21}Ne was investigated by a novel resonant elastic scattering experiment of ^{17}O+^{4}He with the Inverse Kinematic Method [581]. The excitation functions obtained at several angles cover the excitation energy region $E_x \approx 9-12$ MeV. A comprehensive R-matrix fit of data allowed determining the parameters for 35 states of the ^{21}Ne compound nucleus. The occurrence of a very broad $5/2^+$, $\ell = 0$ state at $\simeq 11$ MeV, with a pronounced α structure, was reported from the analysis, pointing out that the occurrence of broad cluster states is not a trait specific of self-conjugate nuclei, but can occur also in non-self-conjugate ones. Furthermore, the determination of the Γ_α decay widths for states close to the α threshold is of importance to refine the rate determination of the ^{17}O(α,n)^{20}Ne reaction, involved in the nucleosynthesis based on s-process inside fast-rotating massive stars at low metallicity [582].

16.4 Some observations

The known level scheme of ^{20,21}Ne seems to fit well the predictions based on ACM and CSM models, predicting a trigonal bipyramid of α particles as the leading cluster structure. This represents an interesting starting point to deepen the structure of all Ne isotopes. Some open questions that could be addressed in future would concern the nature of very broad cluster states seen at relatively low excitation energies in ^{20}Ne; indeed, the occurrence of very broad states was reported also in ^{21}Ne, and it could be interesting to see if similar states are present in other Ne isotopes. The $^{19-22}$Ne isotopic chain is characterized by quite low $|Q_\alpha|$ values, and such values are smaller than the one-nucleon separation energy (with the exception of ^{21}Ne, where the two values differ for just ≈ 0.5 MeV): this fact could qualitatively indicate the presence of sizable cluster structures, and would suggest new experiments to explore them. Finally, the spectroscopy of states very close to the α threshold in ^{19}Ne would deserve some additional investigations because of their strong involvement in the astrophysically important ^{15}O$(\alpha, \gamma)^{19}$Ne reaction. Also in this case, apart from the "more conventional" compound nucleus reactions already used in the literature, it could be interesting to study the invariant mass spectroscopy of α+^{15}O fragments produced in heavy-ion collisions and to analyze the decay patterns of the observed resonances: new-generation multi-detector arrays (HiRA, FAZIA, CHIMERA, etc.) can safely identify in charge and mass the ^{15}O among the other oxygen isotopes, allowing to perform such type of studies.

17 Conclusions

In this review article, we discuss some aspects of the formation of α-clusters in light nuclei. In the first part of the work, we describe in detail the historical evolution of cluster models for the description of the structure and dynamics of nuclei. In this context, we evidence the logical development leading to the introduction of clustering in nuclear physics, its strong connections with other branches of knowledge, the strenuous efforts made to investigate experimentally the spectroscopy of light nuclear systems, and even some unconventional biographical traits of the first pioneers of this field, with the hope that they could serve as an introduction for more accurate and more extensive historical works. Then, we examine several classes of models, which try to describe the cluster structure of light nuclei; to this end, we point out both their strength points and limits. In detail, we describe the principles on the basis of: (i) microscopic models (RGM, GCM, OCM); (ii) the quartet model for the description of high-energy excitations in self-conjugate nuclei; (iii) the development of Molecular Dynamics models and their applications both to structure and dynamics calculations; (iv) the deformed Harmonic Oscillator model predictions; (v) the development of Algebraic Cluster models and their symmetry implications. Subsequently, we discuss the implication of clustering in nuclei in the nuclear astrophysics context, with particular emphasis on the structure of the Hoyle state in ^{12}C and its implications in the triple-α process, which is crucial to the production of carbon in red giant stars. In Sect. 5, we give an overview of the formation of molecular-like states in light nuclei due to strong α-clustering effects in non-self-conjugate systems, a part of nuclear physics that shines for its strong connections with molecular physics and physical chemistry, emblematic of the countless contacts that nuclear physics research activities pursued with other research fields (not only in physics).

In Sect. 6, we discuss several experimental techniques adopted to probe clustering in light nuclei, with particular emphasis on formation experiments, where a compound nucleus is formed, and production experiments, typically involving direct reaction mechanisms, where clustering is studied from the decay properties of reaction products by means of correlation techniques. An overview of the main theories describing the mechanisms at the basis of both the techniques and typical applications to study clustering in light nuclei has been also discussed.

Then, in the last part of the article, we go through a large series of theoretical and experimental works, published in the 5-year period 2017–2022, discussing general properties of clustering in light nuclei or specific clustering effects present on a given isotope. We decided to order all the data for nuclides going from Helium to Neon isotopes in separated subsections, believing that this choice would make more fluid the reading. The extremely large bibliography associated with this section (about 300 works) points out the excellent "health conditions" of this sector of nuclear physics. This was certainly due to the availability of new radioactive beams, the development of very refined detection setups with cutting-edge performances, the implementation of powerful analysis programs, and the strong evolution and enhancement of theoretical models. In addition, we should not forget that the glowing conditions of nuclear cluster physics are mainly due to the strong work of the researchers involved in this research field.

As a short summary of such a huge work, it appears evident the strong theoretical effort to try to describe, in a coherent way and starting by first principles, the occurrence of clustering in light nuclei and the possible implications that symmetries could have on particular geometrical configurations of the α-clusters. Furthermore, we assisted to a "rush" in performing high-precision experiments designed to unveil rare processes involving cluster structure of nuclei (a typical example is given by ^{12}C properties). Also the research on the spectroscopy of nuclear states that, at least for light nuclei, seemed to be a bit abandoned during the final part of the 20th century, had an explosion in recent times because of its fundamental importance to understanding α-clustering in nuclei. Despite the strong progress made in understanding the clustering properties of nuclei, several questions remain still open in this research field. Among them, a general reconciliation of the large number of models toward a more unifying view of clustering in light nuclei; the resolution of several tensions present in experimental measurements of spectroscopical quantities having an impact both on nuclear clustering and nuclear astrophysics; the occurrence of boson condensation in nuclei triggered by α-cluster structures; a comprehensive understanding of the level scheme of light nuclei and their collective excitations. We believe that they will be surely at the basis of further investigations in the next decades.

Acknowledgements The authors are indebted to all the colleagues with whom they had the opportunity to work and discuss during the last 15 years, and, in particular, to all the members of the Chimera, Indra, and Nucl-ex collaborations. One of us (I.L.) was introduced to the physics of nuclear clustering during a series of unforgettable lessons given at the University of Catania by *late* Prof. Domenico Vinciguerra, while the notes of such lectures often served as a stimulus for both the authors during their activities. We want to thank him for having transferred to us, directly or indirectly, the curiosity on this aspect of nuclear physics. We gratefully acknowledge the help from Dr. Luigi Redigolo (University of Catania) during the preparation of figures for the present work.

Funding Open access funding provided by Università degli Studi di Napoli Federico II within the CRUI-CARE Agreement.

Open Access This article is licensed under a Creative Commons Attribution 4.0 International License, which permits use, sharing, adaptation, distribution and reproduction in any medium or format, as long as you give appropriate credit to the original author(s) and the source, provide a link to the Creative Commons licence, and indicate if changes were made. The images or other third party material in this article are included in the article's Creative Commons licence, unless indicated otherwise in a credit line to the material. If material is not included in the article's Creative Commons licence and your intended use is not permitted by statutory regulation or exceeds the permitted use, you will need to obtain permission directly from the copyright holder. To view a copy of this licence, visit http://creativecommons.org/licenses/by/4.0/.

References

1. V. Kukulin et al., *Clusters as Subsystems in Light Nuclei* (Vieweg+Teubner Verlag, Wiesbaden, 1983)
2. A. Arima, S. Kubono, *Treatise on Heavy Ion Science*, vol. 1 (Plenum Press, New York, 1984)
3. C. Beck, *Clusters in Nuclei*, vol. 1 (Springer, 2010)
4. C. Beck, *Clusters in Nuclei*, vol. 2 (Springer, Berlin, 2012), p.848
5. C. Beck, *Clusters in Nuclei*, vol. 3 (Springer, Berlin, 2014), p.875
6. W. Catford, Clustering in nuclei from n/z=1 to n/z=2 (1999). arXiv:1302.3849
7. W. von Oertzen, M. Freer, Y. Kanada-En'yo, Phys. Rep. **432**, 43 (2006)
8. M. Freer, H.O.U. Fynbo, Prog. Part. Nucl. Phys. **78**, 1 (2014)
9. M. Freer et al., Rev. Mod. Phys. **90**, 035004 (2018)

10. M.F. L'Annunziata, Radioactivity (second edition), in *Radioactivity (Second Edition)*, 2nd edn., ed. by M.F. L'Annunziata (Elsevier, New York, 2016), pp.621–638
11. G. Gamow, Proc. R. Soc. **A126**, 630 (1930)
12. E. Fermi, Z. Phys. **36**, 902 (1926)
13. C.F.V. Weizsäcker, Z. Phys. **96**, 431 (1935)
14. W. Heisenberg, Z. Phys. **96**, 473 (1935)
15. H.A. Bethe, R.F. Bacher, Rev. Mod. Phys. **8**, 82 (1936)
16. C.F.V. Weizsäcker, Z. Nat. **A3**, 370 (1948)
17. W. Wefelmeier, Z. Angew. Phys. **107**, 332 (1937)
18. W. Wefelmeier, Ann. Phys. **36**, 373 (1939)
19. L. Meitner, O.H.S. Hahn, Z. Phys. **106**, 249 (1937)
20. M. Orna, M. Fontani, Substantia **3**(Suppl. 5), 59 (2019)
21. H. Andersen, Stud. Hist. Phil. Mod. Phys. **21**, 463 (1996)
22. W. Shea, *Otto Hahn and the Rise of Nuclear Physics*, vol. 875 (Reidel Publ. Comp, Dordrecht, 1983)
23. H. Hocker, Z. Nat. **A3**, 365 (1948)
24. J.A. Wheeler, Phys. Rev. **52**, 1083 (1937)
25. L. Elton, *Introduction to Nuclear Theory* (Pitman, London, 1966)
26. U. Fano, Naturwiss **25**, 602 (1937)
27. L. Rosenfeld, *Nuclear Forces* (North Holland, Amsterdam, 1948)
28. D.R. Inglis, Phys. Rev. **60**, 837 (1941)
29. L.R. Hafstad, E. Teller, Phys. Rev. **54**, 681 (1938)
30. D.M. Dennison, Phys. Rev. **57**, 454 (1940)
31. W. Wefelmeier, Naturwiss **25**, 525 (1937)
32. L. Hafstad, E. Teller, Phys. Rev. **54**, 681 (1938)
33. J.M. Blatt, W.F. Weisskopf, *Theoretical Nuclear Physics* (Wiley, New York, 1955)
34. J.A. Wheeler, Phys. Rev. **52**, 1107 (1937)
35. P.I. Dee, C.W. Gilbert, Proc. R. Soc. Lond. Ser. A **154**, 279 (1936)
36. E. Feenberg, E. Wigner, Phys. Rev. **51**, 95 (1937)
37. S. Devons, Proc. R. Soc. Lond. Ser. A **172**, 559 (1939)
38. J.A. Wheeler, Phys. Rev. **59**, 16 (1941)
39. W.F. Hornyak, T. Lauritsen, P. Morrison, W.A. Fowler, Rev. Mod. Phys. **22**, 291 (1950)
40. G. Bernardini, D. Bocciarelli, Atti Acc. Lincei **24**, 132 (1936)
41. H. Maier-Leibnitz, Z. Angew. Phys. **101**, 478 (1936)
42. W. Burcham, S. Devons, Proc. R. Soc. A **137**, 555 (1939)
43. J. Streib, W. Fowler, C. Lauritsen, Phys. Rev. **59**, 253 (1941)
44. G. Gamow, C. Critchfield, *Theory of Atomic Nucleus and Nuclear Energy Sources* (Clarendon Press, Oxford, 1949)
45. B.O. Grönblom, R.E. Marshak, Phys. Rev. **55**, 229 (1939)
46. H. Margenau, Phys. Rev. **59**, 37 (1941)
47. H. Wergeland, Nor. Vidensk. Selsk. Skrift. **1**, 1 (1941)
48. E.W. Titterton, Nature **168**, 590 (1951)
49. T. San-Tsiang, H. Zah-Wei, R. Chastel, L. Vigneron, Phys. Rev. **71**, 382 (1947)
50. A. Davydov, *Theory of the Atomic Nuclei*, 1st edn. (Nauka, Moscow, 1958)
51. W.H. Guier, H.W. Bertini, J.H. Roberts, Phys. Rev. **85**, 426 (1952)
52. G. Harries, Proc. Phys. Soc. Lond. A **67**, 153 (1954)
53. E. Salpeter, Phys. Rev. **88**, 547 (1952)
54. D.N. Dunbar, R.E. Pixley, W.A. Wenzel, W. Whaling, Phys. Rev. **92**, 649 (1953)
55. C.W. Cook, W.A. Fowler, C.C. Lauritsen, T. Lauritsen, Phys. Rev. **107**, 508 (1957)
56. D.M. Dennison, Phys. Rev. **96**, 378 (1954)
57. H. Morinaga, Phys. Rev. **101**, 254 (1956)
58. K. Wildermuth, T. Kanellopoulos, Nucl. Phys. **7**, 150 (1958)
59. B.F. Bayman, A. Bohr, Nucl. Phys. **9**, 596 (1958)
60. J.P. Elliott, Proc. R. Soc. Lond. Ser. A **245**, 128 (1958)
61. G. Igo, Phys. Rev. Lett. **1**, 72 (1958)
62. J.O. Rasmussen, Phys. Rev. **113**, 1593 (1959)
63. H.J. Mang, Phys. Rev. **119**, 1069 (1960)
64. A. Zuker, B. Buck, J. McGrory, Phys. Rev. Lett. **21**, 39 (1968)

65. W. Bauhoff, H. Schultheis, R. Schultheis, Phys. Rev. C **29**, 1046 (1984). https://doi.org/10.1103/PhysRevC.29.1046
66. J.J. Griffin, J.A. Wheeler, Phys. Rev. **108**, 311 (1957)
67. D.M. Brink, A. Weiguny, Nucl. Phys. A **120**, 59 (1968)
68. D.M. Brink, H. Friedrich, A. Weiguny, C.W. Wong, Phys. Lett. B **33**, 143 (1970)
69. W.D.M. Rae, A.C. Merchant, J. Zhang, Phys. Lett. B **321**, 1 (1994)
70. Y.A. Kudeyarov, Z. Matthies, V.G. Neudachin, Y.F. Smirnov, Nucl. Phys. **65**, 529 (1965)
71. K. Ikeda et al., Prog. Theor. Phys. Suppl. E **68**, 464 (1968)
72. S.K. Allison, P.G. Murphy, E. Norbeck, Phys. Rev. **102**, 1182 (1956)
73. E. Norbeck, Phys. Rev. **105**, 204 (1957)
74. H.W. Fulbright, Annu. Rev. Nucl. Part. Sci. **29**, 161 (1979)
75. K.P. Artemov, Goldberg et al., Phys. Lett. B **37**, 61 (1971)
76. A. Cunsolo, A. Foti, G. Pappalardo, G. Raciti, N. Saunier, E.F. Silveira, Nuovo Cimento A Ser. **40**, 293 (1977)
77. A. Cunsolo, A. Foti, G. Imme, G. Pappalardo, G. Raciti, N. Saunier, Phys. Rev. C **21**, 2345 (1980)
78. D.A. Bromley, J.A. Kuehner, E. Almqvist, Phys. Rev. Lett. **4**, 365 (1960)
79. E. Almqvist, D.A. Bromley, J.A. Kuehner, Phys. Rev. Lett. **4**, 515 (1960)
80. G. Michaud, E.W. Vogt, Phys. Lett. B **30**, 85 (1969)
81. B. Imanishi, Phys. Lett. B **27**, 267 (1968)
82. H.C. Britt, A.R. Quinton, Phys. Rev. **124**, 877 (1961)
83. J.M. Alexander, L. Winsberg, Phys. Rev. **121**, 529 (1961)
84. P. Darriulat, G. Igo, H.G. Pugh, H.D. Holmgren, Phys. Rev. **137**, 315 (1965)
85. S. Ali, A.R. Bodmer, Nucl. Phys. **80**, 99 (1966)
86. E. Epelbaum, H. Krebs, T.A. Lähde, D. Lee, U.-G. Meißner, Eur. Phys. J. A **49**, 82 (2013)
87. P. Adsley et al., Phys. Rev. Lett. **129**, 102701 (2022)
88. P. Hodgson, *Nuclear Reactions and Nuclear Structure* (Clarendon Press, Oxford, 1971)
89. C. Gruhn, N. Wall, Nucl. Phys. **81**, 161 (1966)
90. H.C. Bryant, N. Jarmie, Ann. Phys. **47**, 127 (1968)
91. T. Honda, Y. Kudo, H. Ui, Nucl. Phys. **44**, 472 (1963)
92. N.C. Schmeing, Nucl. Phys. A **142**, 449 (1970)
93. L. Pauling, Proc. Natl. Acad. Sci. **54**, 989 (1965)
94. M. MacGregor, Nuovo Cimento A **36**, 113 (1976)
95. J.R. Nix, Annu. Rev. Nucl. Part. Sci. **22**, 65 (1972)
96. V.M. Strutinsky, Nucl. Phys. A **95**, 420 (1967)
97. G. Leander, S.E. Larsson, Nucl. Phys. A **239**, 93 (1975)
98. Y. Abe, J. Hiura, H. Tanaka, Progress Theoret. Phys. **49**, 800 (1973)
99. A.C. Fonseca, J. Revai, A. Matveenko, Nucl. Phys. A **326**, 182 (1979)
100. A. Arima, V. Gillet, J. Ginocchio, Phys. Rev. Lett. **25**, 1043 (1970)
101. R. Middleton, J.D. Garrett, H.T. Fortune, Phys. Rev. Lett. **27**, 950 (1971)
102. P. Cuzzocrea et al., Lett. Nuov. Cim. **28**, 515 (1980)
103. P. Sperr et al., Phys. Rev. Lett. **37**, 321 (1976)
104. K.W. McVoy, M.E. Brandan, Nucl. Phys. A **542**, 295 (1992)
105. D.T. Khoa, W. von Oertzen, H.G. Bohlen, S. Ohkubo, J. Phys. G Nucl. Part. Phys. **34**, R111 (2007)
106. M. Riou, Rev. Mod. Phys. **37**, 375 (1965)
107. N.S. Chant, P.G. Roos, Phys. Rev. C **15**, 57 (1977)
108. P.G. Roos et al., Phys. Rev. C **15**, 69 (1977)
109. T.A. Carey, P.G. Roos, N.S. Chant, A. Nadasen, H.L. Chen, Phys. Rev. C **29**, 1273 (1984)
110. J.P. Genin, J. Julien, M. Rambaut, C. Samour, A. Palmeri, Vinciguerra, Phys. Lett. B **52**, 46 (1974)
111. J. Tanaka et al., Science **371**, 260 (2021)
112. J. Kahlbow, Eur. Phys. J. A **59**, 128 (2023)
113. M. Furic et al., Phys. Lett. B **39**, 629 (1972)
114. I. Slaus et al., Phys. Rev. C **8**, 444 (1973)
115. D. Miljanic et al., Phys. Lett. B **50**, 330 (1974)
116. J. Kasagi, T. Nakagawa, N. Sekine, T. Tōhei, H. Ueno, Nucl. Phys. A **239**, 233 (1975)
117. N. Arena et al., Lett. Nuovo Cim. **17**, 231 (1976)
118. S. Barbarino et al., Nuovo Cimento A Ser. **53**, 327 (1979)
119. M. Lattuada, F. Riggi, C. Spitaleri, D. Vinciguerra, Nuovo Cimento A Ser. **83**, 151 (1984)

120. L. Colli-Milazzo, G.M. Marcazzan-Braga, Phys. Lett. B **38**, 155 (1972)
121. J. England, *Techniques in Nuclear Structure Physics* (MacMillan, London, 1974)
122. J.E. Spencer, H.A. Enge, Nucl. Inst. Methods **49**, 181 (1967)
123. N. Nakanishi, K. Matsuda, Nucl. Inst. Methods **57**, 245 (1967)
124. C.A. Wiedner et al., Nucl. Inst. Methods **105**, 205 (1972)
125. D. Aleksandrov et al., JETP Lett. **40**, 909 (1984)
126. S. Gales, E. Hourani, M. Hussonnois, J.P. Schapira, L. Stab, M. Vergnes, Phys. Rev. Lett. **53**, 759 (1984)
127. A. Sandulescu, D. Poenaru, W. Greiner, Sov. J. Part. Nucl. **11**, 528 (1980)
128. P.B. Price, Annu. Rev. Nucl. Part. Sci. **39**, 19 (1989)
129. R.G. Lovas, R.J. Liotta, A. Insolia, K. Varga, D.S. Delion, Phys. Rep. **294**, 265 (1998)
130. R. Bonetti, A. Guglielmetti, Roman. Rep. Phys. **59**, 301 (2007)
131. T.M. Cormier et al., Phys. Rev. Lett. **38**, 940 (1977)
132. R. Stokstad et al., Phys. Rev. Lett. **28**, 1523 (1972)
133. R.R. Betts, B.B. Back, B.G. Glagola, Phys. Rev. Lett. **47**, 23 (1981)
134. R.R. Betts, A.H. Wuosmaa, Rep. Prog. Phys. **60**, 819 (1997)
135. T.M. Cormier et al., Phys. Rev. Lett. **40**, 924 (1978)
136. H. Morgenstern et al., Phys. Rev. Lett. **52**, 1104 (1984)
137. F. Amorini et al., Phys. Rev. C **58**, 987 (1998)
138. D. Dell'Aquila, B. Gnoffo, I. Lombardo, F. Porto, Phys. Lett. B **837**, 137642 (2023)
139. V.V. Samarin, Phys. Atom. Nucl. **81**, 486 (2018)
140. M.S. Asnain, M. Shuaib, I. Majeed, M.K. Sharma, V.R. Sharma, A. Yadav, D.P. Singh, P.P. Singh, U. Gupta, R.N. Sahoo, A. Sood, M. Kaushik, S. Kumar, R. Kumar, B.P. Singh, R. Prasad, Phys. Rev. C **104**, 034616 (2021)
141. S. Marsh, W.D.M. Rae, Phys. Lett. **153B**, 21 (1985)
142. E. Da Silveira, Proc. XIV Winter Meet. Nucl. Phys. (Bormio) **12**, 293 (1976)
143. M. Harada, R. Tamagaki, H. Tanaka, Progress Theoret. Phys. **29**, 933 (1963)
144. D.M. Brink, J.J. Castro, Nucl. Phys. A **216**, 109 (1973)
145. A. Péghaire et al., Nucl. Instrum. Methods Phys. Res. **A295**, 365 (1990)
146. R.T. de Souza, N. Le Neindre, A. Pagano, K.H. Schmidt, Eur. Phys. J. A **30**, 275 (2006)
147. A.R. Bodmer, Q.N. Usmani, Nucl. Phys. A **468**, 653 (1987)
148. O. Shigeto, H. Toru, A. Yoshinori, Nucl. Phys. A **514**, 613 (1990)
149. E. Hiyama et al., Prog. Theor. Phys. **97**, 881 (1997)
150. E. Hiyama, T. Yamada, Prog. Part. Nucl. Phys. **63**, 339 (2009)
151. J. Aichelin, Phys. Rep. **202**, 233 (1991)
152. H. Feldmeier, Nucl. Phys. A **515**, 147 (1990)
153. Y. Kanada-En'yo, M. Kimura, A. Ono, Progress Theoret. Exp. Phys. **2012**, 01A202 (2012)
154. M. Papa et al., Phys. Rev. C **64**, 024612 (2001)
155. K. Artemov et al., Sov. J. Nucl. Phys. **52**, 408 (1990)
156. E. Costanzo, M. Lattuada, S. Romano, D. Vinciguerra, M. Zadro, Nucl. Instrum. Methods Phys. Res. **A295**, 373 (1990)
157. E. Costanzo et al., Phys. Rev. C **49**, 985 (1994)
158. E.H.M. Heijne et al., Nucl. Inst. Methods **178**, 331 (1980)
159. M. Freer, Phys. Rev. C **49**, R1751 (1994)
160. A.H. Wuosmaa et al., Phys. Rev. Lett. **68**, 1295 (1992)
161. A.H. Wuosmaa et al., Phys. Rev. C **41**, 2666 (1990)
162. R. Nouicer et al., Phys. Rev. C **60**, 041303 (1999)
163. E. Uegaki, Y. Abe, Phys. Lett. B **231**, 28 (1989)
164. E. Uegaki, Y. Abe, Phys. Lett. B **340**, 143 (1994)
165. W. von Oertzen, Z. Phys. A **354**, 37 (1996)
166. D. Scharnweber, W. Greiner, U. Mosel, Nucl. Phys. A **164**, 257 (1971)
167. J. Maruhn, W. Greiner, Z. Angew. Phys. **251**, 431 (1972)
168. P.W. Atkins, *Physical Chemistry*, iii edn. (Oxford University Press, Oxford, 1986)
169. W. von Oertzen, Z. Phys. A **357**, 355 (1997)
170. M. Milin, W. von Oertzen, Eur. Phys. J. A **14**, 295 (2002). https://doi.org/10.1140/epja/i2001-10199-6
171. A. Tohsaki et al., Phys. Rev. Lett. **87**, 192501 (2001)

172. J. Cseh, Phys. Lett. B **281**, 173 (1992)
173. P.O. Hess, G. Lévai, J. Cseh, Phys. Rev. C **54**, 2345 (1996)
174. R. Bijker, F. Iachello, Ann. Phys. **298**, 334 (2002)
175. P. Danielewicz, Q. Pan, Phys. Rev. C **46**, 2002 (1992)
176. W. Reisdorf et al., Nucl. Phys. A **612**, 493 (1997)
177. H. Takemoto, H. Horiuchi, A. Ono, Phys. Rev. C **57**, 811 (1998)
178. Pawłowski et al., Eur. Phys. J. A **9**, 371 (2000)
179. S. Kowalski et al., Phys. Rev. C **75**, 014601 (2007)
180. M. Beyer, S.A. Sofianos, C. Kuhrts, G. Röpke, P. Schuck, Phys. Lett. B **488**, 247 (2000)
181. M. Schmidt, G. Röpke, H. Schulz, Ann. Phys. **202**, 57 (1990)
182. T.K. Nayak et al., Phys. Rev. Lett. **62**, 1021 (1989)
183. T.K. Nayak et al., Phys. Rev. C **45**, 132 (1992)
184. J. Takahashi et al., Phys. Rev. Lett. **78**, 30 (1997)
185. S.J. Sanders, ASd. Toledo, C. Beck, Phys. Rep. **311**, 487 (1999)
186. R.K. Gupta et al., Phys. Rev. C **56**, 3242 (1997)
187. C. Beck et al., Eur. Phys. J. A **2**, 281 (1998)
188. J. Hiura, I. Shimodaya, Progress Theoret. Phys. **30**, 585 (1963). https://doi.org/10.1143/PTP.30.585
189. P. Descouvemont, J. Phys. G Nucl. Particle Phys. **19**, S141 (1993)
190. S. Saito, S. Okai, R. Tamagaki, M. Yasuno, Progress Theoret. Phys. **50**, 1561 (1973). https://doi.org/10.1143/PTP.50.1561
191. A. Solovyev et al., J. Phys. Conf. Ser. **569**, 012020 (2014)
192. H. Horiuchi, Progress Theoret. Phys. **53**, 447 (1975)
193. A. DeRosa, E. Perillo, P. Cuzzocrea, G. Inglima, E. Rosato, M. Sandoli, G. Spadaccini, Nuovo Cimento A Ser. **44**, 433 (1978)
194. M. Sambataro, N. Sandulescu, Phys. Rev. Lett. **88**, 061303 (2013)
195. M. Sambataro, N. Sandulescu, Phys. Rev. Lett. **115**, 112501 (2015)
196. A. Ono, J. Randrup, Eur. Phys. J. A **30**, 109 (2006)
197. Y. Kanada-En'yo, H. Horiuchi, Phys. Rev. C **68**, 014319 (2003)
198. H. Horiuchi, Y. Kanada-En'yo, Nucl. Phys. A **616**, 394c (1997)
199. M. Freer, Rep. Prog. Phys. **70**, 2149 (2007)
200. M. Freer, R.R. Betts, A.H. Wuosmaa, Nucl. Phys. A **587**, 36 (1995)
201. W.D.M. Rae, Int. J. Mod. Phys. A **3**, 1343 (1988)
202. F. Iachello, Phys. Rev. C **23**, 2778 (1981)
203. J. Cseh, G. Levai, Ann. Phys. **230**, 165 (1994)
204. T.K. Wheldon, J. Phys. Conf. Ser. **569**, 012010 (2014)
205. D. Marin-Lambarri et al., Phys. Rev. Lett. **113**, 012502 (2014)
206. R.F.I. Bijker, Phys. Rev. Lett. **112**, 152501 (2014)
207. C.E. Rolfs, W.S. Rodney, *Cauldrons in the Cosmos: Nuclear Astrophysics*, 5th edn. (The University of Chicago Press, Chicago, 1997)
208. C. Iliadis, *Nuclear Physics of Stars*, 2nd edn. (Wiley-VCH Verlag GmbH & Co. KGaA, Weinheim, 2015)
209. D. Jenkins, O. Kirsebom, Phys. World **26**, 23 (2013)
210. E. Opik, Proc. R. Irish Acad. A **54**, 49 (1951)
211. F. Hoyle et al., Phys. Rev. **92**, 1095c (1953)
212. F. Hoyle, Astrophys. J. Suppl. Ser. **1**, 121 (1954)
213. N. Nguyen, F. Nunes, I. Thompson, Phys. Rev. C **87**, 054615 (2013)
214. K. Nomoto, F.-K. Thielemann, S. Miyaji, Astron. Astrophys. **149**, 239 (1985)
215. K. Langanke, M. Wiescher, F. Thielemann, Z. Phys. A Atom. Nuclei **324**, 147 (1986)
216. C. Angulo et al., Nucl. Phys. A **656**, 3 (1999)
217. N. Nguyen, F. Nunes, I. Thompson, E. Brown, Phys. Rev. Lett. **109**, 141101 (2012)
218. E. Garrido, R. de Diego, D.V. Fedorov, A.S. Jensen, Eur. Phys. J. **A47**, 102 (2011). https://doi.org/10.1140/epja/i2011-11102-8
219. K. Yabana, Y. Funaki, Phys. Rev. C **85**, 055803 (2012). https://doi.org/10.1103/PhysRevC.85.055803
220. K. Ogata, M. Kan, M. Kamimura, Prog. Theor. Phys. **122**, 1055 (2009)
221. P.G. Prada Moroni, O. Straniero, Astrophys. J. **581**, 585 (2002)
222. I. Domínguez, P. Höflich, O. Straniero, Astrophys. J. **557**, 279 (2001)

223. G. Imbriani, M. Limongi, L. Gialanella, F. Terrasi, O. Straniero, A. Chieffi, Astrophys. J. **558**, 903 (2001)
224. R.J. deBoer, J. Görres, M. Wiescher, R.E. Azuma, A. Best, C.R. Brune, C.E. Fields, S. Jones, M. Pignatari, D. Sayre, K. Smith, F.X. Timmes, E. Uberseder, Rev. Mod. Phys. **89**, 035007 (2017)
225. G.E. Brown, A.M. Green, Nucl. Phys. **75**, 401 (1966)
226. P. Descouvemont et al., Nucl. Phys. A **430**, 426 (1984)
227. K. Langanke et al., Nucl. Phys. A **439**, 384 (1985)
228. P. Descouvemont, Nucl. Phys. A **470**, 309 (1987)
229. M. Dufour, P. Descouvemont, Phys. Rev. C **78**, 015808 (2008)
230. A. Volya, Y.M. Tchvilsky, Phys. Rev. C **91**, 044319 (2015)
231. I. Lombardo et al., Phys. Rev. C **100**, 044307 (2019)
232. J. Slater, *Quantum Theory of Matter*, 1st edn. (McGraw-Hill, New York, 1968)
233. J.M. Blatt, V.F. Weisskopf, *Theoretical Nuclear Physics*, 1st edn. (Wiley, New York, 1962)
234. N. Itagaki, S. Okabe, Phys. Rev. C **61**, 044306 (2000)
235. M.T.S. Bernheim, D. Vinciguerra, Nucl. Phys. A **97**, 488 (1969)
236. D. Vinciguerra, T. Stovall, Nucl. Phys. A **132**, 410 (1969)
237. Y. Kanada-En'yo, H. Horiuchi, A. Doté, J. Phys. G Nucl. Particle Phys. **24**, 1499 (1998)
238. D. Suzuki et al., Phys. Rev. C **87**, 054301 (2013)
239. N. Soić et al., Europhys. Lett. **34**, 7 (1996)
240. Y. Kanada-En'yo, Phys. Rev. C **75**, 024302 (2007). https://doi.org/10.1103/PhysRevC.75.024302
241. T. Kawabata et al., Phys. Rev. C **70**, 034318 (2004). https://doi.org/10.1103/PhysRevC.70.034318
242. T. Kawabata et al., Phys. Lett. B **646**, 6 (2007)
243. N. Soic et al., Nucl. Phys. A **742**, 271 (2004)
244. I. Ragnarsson, S. Åberg, H.B. Hakansson, R.K. Sheline, Nucl. Phys. A **361**, 1 (1981)
245. T. Yoshida, N. Itagaki, T. Otsuka, Phys. Rev. C **79**, 034308 (2009)
246. N. Furutachi, M. Kimura, Phys. Rev. C **83**, 021303 (2011)
247. Y. Chiba, M. Kimura, J. Phys. Conf. Ser. **569**, 012047 (2014)
248. T. Yamada, Y. Funaki, Phys. Rev. C **92**, 034326 (2015)
249. T. Suhara, Y. Kanada-En'Yo, Phys. Rev. C **82**, 044301 (2010)
250. P. Descouvemont, Nucl. Phys. A **675**, 559 (2000)
251. D. Bazin et al., Phys. Rev. C **57**, 2156 (1998)
252. N. Itagaki, S. Okabe, K. Ikeda, I. Tanihata, Phys. Rev. C **64**, 014301 (2001). https://doi.org/10.1103/PhysRevC.64.014301
253. T. Baba, Y. Chiba, M. Kimura, Phys. Rev. C **90**, 064319 (2014)
254. M. Gai et al., Phys. Rev. Lett. **50**, 239 (1983)
255. W.D.M. Rae, R.K. Bhowmik, Nucl. Phys. A **427**, 142 (1984)
256. A. Cunsolo, A. Foti, G. Immè, G. Pappalardo, G. Raciti, N. Saunier, Phys. Rev. C **24**, 476 (1981)
257. B. Buck, H. Friedrich, A.A. Pilt, Nucl. Phys. A **290**, 205 (1977)
258. W. von Oertzen et al., Eur. Phys. J. A **43**, 17 (2010)
259. E.D. Johnson et al., Eur. Phys. J. A **42**, 135 (2009)
260. R.D. Lawson, F.J.D. Serduke, H.T. Fortune, Phys. Rev. C **14**, 1245 (1976)
261. H.T. Fortune, Eur. Phys. J. A **48**, 63 (2012)
262. G. Lévai, Phys. Rev. C **88**, 014328 (2013)
263. M. Dufour, P. Descouvemont, Nucl. Phys. A **726**, 53 (2003)
264. M. von Tresckow et al., Phys. Lett. B **821**, 136624 (2021)
265. H.A. Enge, *Introduction to Nuclear Physics*, 1st edn. (Addison-Wesley Publishing Company, Massachusetts, 1981)
266. B.L. Cohen, *Concepts of Nuclear Physics*, 1st edn. (McGraw-Hill Book Company, New York, 1971)
267. T.-Y. Wu, T. Ohmura, *Quantum Theory of Scattering*, 1st edn. (Dover Publications Inc., New York, 2011)
268. M. Abramowitz, I. Stegun, Nat. Bur. St. Appl. Math **55**, 1 (1972)
269. A. Messiah, *Mecanique Quantique*, 1st edn. (Dunod, Paris, 1959)
270. J. Marion, F. Young, *Nuclear Reaction Analysis*, 1st edn. (North Holland, Amsterdam, 1968)
271. A.M. Lane, R.G. Thomas, Rev. Mod. Phys. **30**, 257 (1958)
272. E. Wigner, Phys. Rev. **70**, 606 (1946). https://doi.org/10.1103/PhysRev.70.606
273. E. Wigner, L. Eisenbud, Phys. Rev. **72**, 29 (1947). https://doi.org/10.1103/PhysRev.72.29
274. G. Rogachev et al., J. Phys. Conf. Ser. **569**, 012004 (2014)

275. R. Azuma et al., Phys. Rev. C **81**, 045805 (2010). https://doi.org/10.1103/PhysRevC.81.045805
276. H. Herndl et al., Phys. Rev. C **44**, R952 (1991)
277. Y. Yamashita, Y. Kudo, Prog. Theor. Phys. **90**, 1303 (1993)
278. N. Austern, *Direct Nuclear Reaction Theories*, i edn. (Wiley-Interscience, New York, 1970)
279. T. Tamura, Rev. Mod. Phys. **37**, 679 (1965)
280. Z. Mao, H. Fortune, A. Lacaze, Phys. Rev. C **53**, 1197 (1996)
281. T.A. Carey, P.G. Roos, N.S. Chant, A. Nadasen, H.L. Chen, Phys. Rev. C **23**, 576 (1981)
282. A. Nadasen et al., Phys. Rev. C **59**, 760 (1999)
283. A. Shotter, J. Phys. Soc. Jpn. (suppl.) **58**, 145 (1989)
284. M. Freer, Nucl. Instrum. Methods Phys. Res. A **383**, 463 (1996)
285. A. Artyukh et al., Nucl. Exp. Tech. **1**, 19 (2009)
286. R.H. Dalitz, Philos. Mag. Ser. **744**, 1068 (1953)
287. E. Fabri, Il Nuovo Cimento **11**, 479 (1954)
288. K.L. Laursen, H.O.U. Fynbo, O.S. Kirsebom, K.S. Madsbøll, K. Riisager, Eur. Phys. J. A **52**, 271 (2016)
289. H.T. Fortune, Eur. Phys. J. A **54**, 51 (2018)
290. C.W. Johnson et al., J. Phys. G Nucl. Phys. **47**, 123001 (2020)
291. Y.A. Berezhnoy, V.P. Mikhailyuk, Eur. Phys. J. A **53**, 125 (2017)
292. Z.M.M. Mahmoud et al., Phys. Rev. C **105**, 044609 (2022)
293. G. Röpke, D.N. Voskresensky, I.A. Kryukov, D. Blaschke, Nucl. Phys. A **970**, 224 (2018)
294. G. Röpke, Phys. Rev. C **101**, 064310 (2020)
295. A. Pakou, O. Sgouros, V. Soukeras, J. Casal, K. Rusek, Eur. Phys. J. A **58**, 8 (2022)
296. J. He, S. Zhang, Y.-G. Ma, J. Chen, C. Zhong, Eur. Phys. J. A **56**, 52 (2020)
297. S. Zhang, Y.G. Ma, J.H. Chen, W.B. He, C. Zhong, Eur. Phys. J. A **54**, 161 (2018)
298. M. Rybczyński et al., Phys. Rev. C **97**, 034912 (2018)
299. A.A. Zaitsev, D.A. Artemenkov, V.V. Glagolev, M.M. Chernyavsky, N.G. Peresadko, V.V. Rusakova, P.I. Zarubin, Phys. Lett. B **820**, 136460 (2021)
300. L. Satarov et al., J. Phys. G. Nucl. Part. Phys. **44**, 125102 (2017)
301. D. DeMartini, E. Shuryak, Nucl. Phys. A **1016**, 122336 (2021)
302. Y. Kanada-En'yo et al., Phys. Rev. C **106**, 054312 (2022)
303. V.V. Baran, D.S. Delion, J. Phys. G Nucl. Phys. **45**, 035106 (2018)
304. M. Sambataro, N. Sandulescu, Eur. Phys. J. A **53**, 47 (2017)
305. M. Sambataro, N. Sandulescu, Phys. Lett. B **820**, 136476 (2021)
306. J. Ebran et al., J. Phys. G. Nucl. Part. Phys. **44**, 103001 (2017)
307. V.V. Samarin, Eur. Phys. J. A **58**, 117 (2022)
308. D. Hove, E. Garrido, P. Sarriguren, D.V. Fedorov, H.O.U. Fynbo, A.S. Jensen, N.T. Zinner, J. Phys. G Nucl. Phys. **45**, 073001 (2018)
309. A. Afanasjev, H. Abusara, Phys. Rev. C **97**, 024329 (2018)
310. P. Descouvemont, Eur. Phys. J. A **57**, 29 (2021)
311. M. Freer, R. Canavan, T. Marsh, J. Souter, Eur. Phys. J. A **57**, 102 (2021)
312. M. Freer, T. Marsh, J. Souter, J. Phys. G Nucl. Phys. **49**, 055105 (2022)
313. J. Casal, L. Fortunato, E.G. Lanza, A. Vitturi, Eur. Phys. J. A **57**, 14 (2021)
314. P.O. Hess, Eur. Phys. J. A **54**, 25 (2018)
315. P.O. Hess, J.R.M. Berriel-Aguayo, L.J. Chávez-Nuñez, Eur. Phys. J. A **55**, 15 (2019)
316. G. Stellin, K.-H. Sppagesel, U.-G. Meißner, Eur. Phys. J. A **58**, 208 (2022)
317. C.A. Bertulani, T. Frederico, M.S. Hussein, Phys. Lett. B **774**, 247 (2017)
318. B.W. Asher et al., Eur. Phys. J. A **57**, 272 (2021)
319. M. Shuaib, V.R. Sharma, A. Yadav, M.K. Sharma, P.P. Singh, D.P. Singh, R. Kumar, R.P. Singh, S. Muralithar, B.P. Singh, R. Prasad, J. Phys. G Nucl. Phys. **44**, 105108 (2017)
320. G. Tian et al., Phys. Rev. C **95**, 044613 (2017)
321. G. Tian et al., Phys. Rev. C **97**, 034610 (2018)
322. K. Fossez et al., Phys. Rev. C **98**, 061302(R) (2018)
323. D.M. Rodkin et al., Phys. Rev. C **104**, 044323 (2021)
324. C. Spitaleri, S. Typel, C.A. Bertulani, A.M. Mukhamedzhanov, T. Kajino, M. Lattuada, A. Cvetinović, S. Messina, G.L. Guardo, N. Soić, M. Milin, S.S. Perrotta, C. Li, P. Čolović, G. D'Agata, D. Dell'Aquila, C.G. Fatuzzo, M. Gulino, S.Q. Hou, M. La Cognata, D. Lattuada, D. Nurkić, R.

Popočovski, N. Skukan, S. Szilner, O. Trippella, M. Uroić, N. Vukman, Eur. Phys. J. A **57**, 20 (2021)
325. B. Laurent et al., J. Phys. G Nucl. Phys. **46**, 03LT02 (2019)
326. S.K. Pandit, A. Shrivastava, K. Mahata, N. Keeley, V.V. Parkar, R. Palit, P.C. Rout, K. Ramachandran, A. Kumar, S. Bhattacharyya, V. Nanal, S. Biswas, S. Saha, J. Sethi, P. Singh, S. Kailas, Phys. Lett. B **820**, 136570 (2021)
327. S. Pandit et al., Phys. Rev. C **96**, 044616 (2017)
328. K. Cook et al., Phys. Rev. Lett. **122**, 102501 (2019)
329. J. Lei, A. Moro, Phys. Rev. C **95**, 044605 (2017)
330. M. Ichimura, N. Austern, C.M. Vincent, Phys. Rev. C **32**, 431 (1985)
331. C. Li et al., Phys. Rev. C **95**, 035804 (2017)
332. A. Rudchik et al., Phys. Rev. C **103**, 044614 (2021)
333. A.T. Rudchik et al., Phys. Rev. C **106**, 014615 (2022)
334. L.A. Souza et al., Phys. Rev. C **104**, 034623 (2021)
335. D. Chattopadhyay et al., Phys. Rev. C **98**, 014609 (2018)
336. A. Gómez-Camacho et al., Phys. Rev. C **97**, 054609 (2018)
337. M. Hassanain et al., Phys. Rev. C **97**, 044610 (2018)
338. U. Umbelino et al., Phys. Rev. C **106**, 054602 (2022)
339. V. Zagatto et al., Phys. Rev. C **95**, 064614 (2017)
340. D. Chattopadhyay et al., Phys. Rev. C **97**, 051601(R) (2018)
341. K. Cook et al., Phys. Rev. C **97**, 021601(R) (2018)
342. Q. Zhao, B. Zhou, M. Kimura, H. Motoki, S.-H. Shin, Eur. Phys. J. A **58**, 25 (2022)
343. P. Fraser et al., Phys. Rev. C **96**, 014619 (2017)
344. W. Horiuchi, T. Furumoto, Nucl. Phys. A **1011**, 122204 (2021)
345. L. Hlophe et al., Phys. Rev. C **96**, 064003 (2017)
346. O. Kiss et al., Phys. Rev. C **106**, 034325 (2022)
347. J. Lei et al., Phys. Rev. C **98**, 051001(R) (2018)
348. I.J. Shin, Y. Kim, P. Maris, J.P. Vary, C. Forssén, J. Rotureau, N. Michel, J. Phys. G Nucl. Phys. **44**, 075103 (2017)
349. T. Yamagata et al., Phys. Rev. C **95**, 044307 (2017)
350. S. Costa, S. Ferroni, V. Wataghin, R. Malvano, Phys. Lett. **4**, 308 (1963)
351. S. Satsuka et al., Phys. Rev. C **100**, 024334 (2019)
352. B.-S. Huang, Y.-G. Ma, Phys. Rev. C **103**, 054318 (2021)
353. A. Pakou et al., Phys. Rev. C **95**, 044615 (2017)
354. A. Solovyev et al., Phys. Rev. C **99**, 054618 (2019)
355. M. Vorabbi et al., Phys. Rev. C **100**, 024304 (2019)
356. M.V. Egorov, Nucl. Phys. A **986**, 175 (2019)
357. W.H. Ma et al., Phys. Rev. C **103**, L061302 (2021)
358. P. Descouvemont, Phys. Rev. C **99**, 064308 (2019)
359. R.M. Id Betan, Nucl. Phys. A **959**, 147 (2017)
360. B. Zhou, M. Kimura, Q. Zhao, S.-H. Shin, Eur. Phys. J. A **56**, 298 (2020)
361. S. Li et al., Phys. Rev. C **101**, 064307 (2020)
362. A.V. Nesterov, Y.A. Lashko, V.S. Vasilevsky, Nucl. Phys. A **1016**, 122325 (2021)
363. D. Chattopadhyay et al., Phys. Rev. C **102**, 021601(R) (2020)
364. Y.J. Li, Z.H. Li, Y.B. Wang, Y.P. Shen, Nucl. Phys. A **1022**, 122444 (2022)
365. X. Zhang, K.M. Nollett, D.R. Phillips, J. Phys. G Nucl. Phys. **47**, 054002 (2020)
366. M. Poudel, D.R. Phillips, J. Phys. G Nucl. Phys. **49**, 045102 (2022)
367. A.V. Dobrovolsky et al., Nucl. Phys. A **989**, 40 (2019)
368. M. Munch, Kirsebom O. Sølund, J.A. Swartz, K. Riisager, H.O.U. Fynbo, Phys. Lett. B **782**, 779 (2018)
369. H. Matsuno et al., Phys. Rev. C **98**, 054306 (2018)
370. H. Zhang et al., Phys. Rev. C **105**, 054317 (2022)
371. D. Bai, Z. Ren, Phys. Rev. C **101**, 034311 (2020)
372. T. Fukui, J. Phys. G Nucl. Phys. **49**, 055102 (2022)
373. S. Chakraborty et al., Phys. Rev. C **106**, 034610 (2022)
374. D.M. Rodkin, Y.M. Tchuvil'sky, Phys. Lett. B **788**, 238 (2019)
375. G. Stellin, S. Elhatisari, U.-G. Meißner, Eur. Phys. J. A **54**, 232 (2018)

376. A. Arazi et al., Phys. Rev. C **97**, 044609 (2018)
377. R. Kaur et al., Phys. Rev. C **98**, 064612 (2018)
378. H. Kumawat et al., Phys. Rev. C **106**, 024602 (2022)
379. M. Kaushik et al., Eur. Phys. J. A **57**, 320 (2021)
380. R. Kharab, A. Kumari, Nucl. Phys. A **981**, 62 (2019)
381. V. Vasilevsky et al., Phys. Rev. C **96**, 034322 (2017)
382. Rocca V. Della, R. Bijker, F. Iachello, Nucl. Phys. A **966**, 158 (2017)
383. Rocca V. Della, F. Iachello, Nucl. Phys. A **973**, 1 (2018)
384. V. Starastsin et al., Eur. Phys. J. A **57**, 334 (2021)
385. Y. Hirayama, T. Shimoda, H. Miyatake, H. Izumi, A. Hatakeyama, K.P. Jackson, C.D.P. Levy, M. Pearson, M. Yagi, H. Yano, Phys. Rev. C **91**, 024328 (2015)
386. D.R. Tilley, J.H. Kelley, J.L. Godwin, D.J. Millener, J.E. Purcell, C.G. Sheu, H.R. Weller, Nucl. Phys. A **745**, 155 (2004)
387. B.A. Urazbekov et al., J. Phys. G Nucl. Phys. **46**, 105110 (2019)
388. E. Leistenschneider et al., Phys. Rev. C **98**, 064601 (2018)
389. S.B. Dubovichenko, N.A. Burkova, A.V. Dzhazairov-Kakhramanov, Nucl. Phys. A **1000**, 121842 (2020)
390. T. Furumoto, T. Suhara, N. Itagaki, Phys. Rev. C **104**, 034613 (2021)
391. Y. Kanada-En'yo et al., Phys. Rev. C **102**, 014607 (2020)
392. Y. Kanada-En'yo, Y. Shikata, Phys. Rev. C **95**, 064319 (2017)
393. R.J. Charity et al., Phys. Rev. C **105**, 014314 (2022)
394. K. Amos, L. Canton, P.R. Fraser, S. Karataglidis, J.P. Svenne, D. van der Knijff, Eur. Phys. J. A **53**, 72 (2017)
395. Y.A. Lashko, G.F. Filippov, V.S. Vasilevsky, Nucl. Phys. A **958**, 78 (2017)
396. J.G. Johansen et al., J. Phys. G Nucl. Phys. **44**, 044009 (2017)
397. S. Upadhyayula et al., Phys. Rev. C **101**, 034604 (2020)
398. D. Dell'Aquila et al., Phys. Rev. C **93**, 024611 (2016)
399. M. Dan, R. Chatterjee, M. Kimura, Eur. Phys. J. A **57**, 25 (2021)
400. K. Amos, S. Karataglidis, L. Canton, P.R. Fraser, K. Murulane, Eur. Phys. J. A **58**, 181 (2022)
401. K. Fossez, W. Nazarewicz, Y. Jaganathen, N. Michel, M. Ploszajczk, Phys. Rev. C **93**, 011305(R) (2016)
402. A. Macchiavelli et al., Phys. Rev. C **97**, 011302(R) (2018)
403. M.Y. Lyu et al., Phys. Rev. C **99**, 064610 (2019)
404. Q. Zhao et al., Phys. Rev. C **106**, 054313 (2022)
405. J. Chen et al., Phys. Rev. C **103**, 12 (2021)
406. J. Chen et al., Phys. Lett. B **781**, 412 (2018)
407. C. Morse et al., Phys. Lett. B **780**, 227 (2018)
408. M. Freer et al., Phys. Lett. B **775**, 58 (2017)
409. Q. Zhao et al., Phys. Rev. C **97**, 054323 (2018)
410. N. Itagaki et al., Phys. Rev. C **102**, 024332 (2020)
411. S. Lei et al., Eur. Phys. J. A **58**, 58 (2022)
412. V.K. Lukyanov et al., Eur. Phys. J. A **53**, 31 (2017)
413. A. Gula et al., Phys. Rev. C **106**, 065801 (2022)
414. S. Kuvin et al., Phys. Rev. C **96**, 041301(R) (2017)
415. B. Maas et al., Phys. Rev. Lett. **122**, 182501 (2019)
416. Y.P. Shen et al., Phys. Lett. B **797**, 134820 (2019)
417. M. Wiescher, O. Clarkson, R.J. deBoer, P. Denisenkov, Eur. Phys. J. A **57**, 24 (2021)
418. T.N. Massey et al., Phys. Rev. C **105**, 054612 (2022)
419. A. Di Pietro et al., Phys. Lett. B **832**, 137256 (2022)
420. Q. Zhao, Y. Suzuki, J. He, B. Zhou, M. Kimura, Eur. Phys. J. A **57**, 157 (2021)
421. A.V. Dobrovolsky et al., Nucl. Phys. A **1008**, 25 (2021)
422. H.T. Fortune, Eur. Phys. J. A **54**, 12 (2018)
423. S. Ehlatisari et al., Phys. Rev. Lett. **119**, 222505 (2017)
424. V. Guimaraes et al., Phys. Rev. C **100**, 034603 (2019)
425. C. Spitaleri et al., Phys. Rev. C **95**, 035801 (2017)
426. G.G. Rapisarda et al., Eur. Phys. J. A **54**, 12 (2018)
427. I. Lombardo et al., J. Phys. G Nucl. Part. Phys. **43**, 045109 (2016)

428. J.H. Kelley et al., Nucl. Phys. A **880**, 88 (2012)
429. M. Wiescher et al., Phys. Rev. C **95**, 044617 (2017)
430. Z. Li et al., Phys. Rev. C **107**, 25 (2023)
431. D. Dell'Aquila, Clustering in light nuclear systems: a multi-method approach. Ph.D. thesis, Università degli Studi di Napoli "Federico II" and Univeristé Paris-Sud (Paris-Saclay) (2018)
432. B. Van Kolk et al., Phys. Rev. C **105**, 055802 (2022)
433. G. Kaur et al., Phys. Rev. C **105**, 024609 (2022)
434. J. Okołowicz, M. Płoszajczak, W. Nazarewicz, Phys. Rev. C **107**, L021305 (2023)
435. T. Ichikawa, N. Itagaki et al., Phys. Rev. C **105**, 024314 (2022)
436. N. Itagaki et al., Phys. Rev. C **98**, 044306 (2018)
437. R. Katsuragi et al., Phys. Rev. C **98**, 044303 (2018)
438. B. Zhou et al., Phys. Rev. C **99**, 051303(R) (2019)
439. A. Dreyfuss et al., Phys. Rev. C **95**, 044312 (2017)
440. P. Marevic et al., Phys. Rev. C **99**, 034317 (2019)
441. Y. Funaki, M. Isaka, E. Hiyama, T. Yamada, K. Ikeda, Phys. Lett. B **773**, 336 (2017)
442. P.H.C. Lau, N.S. Manton, Phys. Rev. Lett. **113**, 125 (2014)
443. J.I. Rawlinson, Nucl. Phys. A **975**, 122 (2018)
444. C.J. Halcrow, J.I. Rawlinson, Phys. Rev. C **102**, 12 (2020)
445. Y. Kanada-En'yo et al., Phys. Rev. C **97**, 014303 (2018)
446. S.-I. Ando, Phys. Rev. C **100**, 015807 (2019)
447. L. Fortunato, Phys. Rev. C **99**, 031302(R) (2019)
448. S. Adachi et al., Phys. Rev. C **97**, 014601 (2018)
449. T. Otsuka et al., Nat. Commun. **13**, 25 (2022)
450. R. Smith, M. Gai, M.W. Ahmed, M. Freer, H.O.U. Fynbo, D. Schweitzer, S.R. Stern, Phys. Rev. C **101**, 021302 (2020)
451. J. Bishop et al., Phys. Rev. C **102**, 041303(R) (2020)
452. T.K. Rana et al., Phys. Lett. B **793**, 130 (2019)
453. R. Smith, T. Kokalova, C. Wheldon, J.E. Bishop, M. Freer, N. Curtis, D.J. Parker, Phys. Rev. Lett. **119**, 132502 (2017). https://doi.org/10.1103/PhysRevLett.119.132502
454. D. Dell'Aquila et al., Phys. Rev. Lett. **119**, 132501 (2017)
455. L. Morelli et al., J. Phys. **G43**, 045110 (2016)
456. M. Itoh et al., Phys. Rev. Lett. **113**, 102501 (2014)
457. T.K. Rana et al., Phys. Rev. C **88**, 021601(R) (2013)
458. O.S. Kirsebom et al., Phys. Rev. Lett. **108**, 202501 (2012)
459. J. Manfredi et al., Phys. Rev. C **85**, 037603 (2012). https://doi.org/10.1103/PhysRevC.85.037603
460. M. Ito, Phys. Rev. C 97 (2018) 044608
461. A. Raduta et al., Phys. Lett. B **705**, 65 (2011)
462. T. Kibédi et al., Phys. Rev. Lett. **125**, 25 (2020)
463. A.W. Obst, W.J. Braithwaite, Phys. Rev. C **13**, 2033 (1976)
464. R.G. Markham et al., Nucl. Phys. A **270**, 489 (1976)
465. H.B. Mak et al., Phys. Rev. C **12**, 1158 (1975)
466. C.N. Davids et al., Phys. Rev. C **11**, 2063 (1975)
467. D. Chamberlin et al., Phys. Rev. C **9**, 2394 (1974)
468. I. Hall, N.W. Tanner, Nucl. Phys. **53**, 673 (1964)
469. P.A. Seeger et al., Astrophys. J. **137**, 704 (1963)
470. D.E. Alburger et al., Phys. Rev. C **124**, 193 (1961)
471. J. Refsgaard, H.O.U. Fynbo, O.S. Kirsebom, K. Riisager, Phys. Lett. B **779**, 414 (2018)
472. H. Zheng, A. Bonasera, M. Huang, S. Zhang, Phys. Lett. B **779**, 460 (2018)
473. A. Baishya et al., Phys. Rev. C **104**, 024601 (2021)
474. T.K. Eriksen et al., Phys. Rev. C **102**, 024320 (2020)
475. J. Bishop et al., Nat. Commun. **13**, 2151 (2022)
476. M. Beard, S.M. Austin, R. Cyburt, Phys. Rev. Lett. **119**, 112701 (2017)
477. M. Tsumura et al., Phys. Lett. B **817**, 136283 (2021)
478. G. Cardella et al., Phys. Rev. C **104**, 064315 (2021)
479. A. Tumino et al., Phys. Lett. B **750**, 59 (2015)
480. J. Bishop et al., Phys. Rev. C **103**, L051303 (2021)
481. G. Cardella et al., Nucl. Phys. A **1020**, 122395 (2022)

482. K.C.W. Li et al., Phys. Lett. B **827**, 136928 (2022)
483. M. Munch, H.O. Uldall Fynbo, Eur. Phys. J. A **54**, 138 (2018)
484. O.S. Kirsebom, A.M. Howard, M. Munch, S. Sablok, J.A. Swartz, H.O.U. Fynbo, Eur. Phys. J. A **56**, 179 (2020)
485. M. Kuhlwein, K. Lytje, H.O.U. Fynbo, A. Gad, E. Jensen, O.S. Kirsebom, M. Munch, J. Refsgaard, K. Riisager, Phys. Lett. B **825**, 136857 (2022)
486. A. Demyanova, V. Starastsin, A. Ogloblin, A. Danilov, S. Dmitriev, W. Trzaska, P. Heikkinen, T. Belyaeva, S. Goncharov, V. Maslov, Y. Sobolev, Y. Gurov, B. Chernyshev, N. Burtebaev, D. Janseitov, S. Khlebnikov, Eur. Phys. J. A **57**, 204 (2021)
487. R. Bijker, F. Iachello, Phys. Rev. Lett. **122**, 162501 (2019)
488. S. Shin et al., Phys. Rev. C **103**, 054313 (2021)
489. I. Lombardo et al., Phys. Rev. C **97**, 034320 (2018)
490. A.P.D. Ramirez et al., Nucl. Phys. A **1023**, 122446 (2022)
491. M. Nassurlla et al., Eur. Phys. J. A **57**, 231 (2021)
492. T. Baba, M. Kimura, Phys. Rev. C **95**, 064318 (2017)
493. T. Baba, M. Kimura, Phys. Rev. C **99**, 021303(R) (2019)
494. M. Kumar Raju et al, Phys. Lett. B **777** 250 (2018)
495. Y. Kanada-En'yo et al., Phys. Rev. C **101**, 014317 (2020)
496. A. Fritsch et al., Phys. Rev. C **93**, 014321 (2016)
497. H. Yamaguchi et al., Phys. Lett. B **766**, 11 (2017)
498. J. Li et al., Phys. Rev. C **95**, 021303(R) (2017)
499. P.R. Fraser et al., Phys. Rev. C **100**, 024609 (2019)
500. Y. Sun et al., Phys. Rev. C **99**, 024605 (2019)
501. T. Baba, M. Kimura, Phys. Rev. C **97**, 054315 (2018)
502. Y. Chiba and M. Kimura, Phys. Rev. C 101 (2020) 024317
503. T. Baba et al., Phys. Rev. C **102**, 041302(R) (2020)
504. D.D. Zhang et al., Phys. Rev. C **105**, 024322 (2022)
505. Y. Liu et al., Phys. Rev. Lett. **124**, 192501 (2020)
506. J.X. Han et al., Phys. Rev. C **105**, 044302 (2022)
507. X. Pereira-López et al., Phys. Lett. B **811**, 135939 (2020)
508. T.B. Webb et al., Phys. Rev. C **100**, 024306 (2019)
509. K. Chipps et al., Phys. Rev. C **95**, 044319 (2017)
510. S.V. Artemov et al., Eur. Phys. J. A **58**, 24 (2022)
511. Y. Xu, K. Takahashi, S. Goriely, M. Arnould, M. Ohta, H. Utsunomiya, Nucl. Phys. A **918**, 61 (2013)
512. S.M. Wang, W. Nazarewicz, R.J. Charity, L.G. Sobotka, J. Phys. G Nucl. Phys. **49**, 10LT02 (2022)
513. H. Fortune et al., Phys. Rev. C **96**, 014317 (2017)
514. S. Wang et al., Phys. Rev. C **99**, 054302 (2019)
515. Y. Kanada-En'yo, Y. Kawanami, Y. Taniguchi, M. Kimura, Progress Theoret. Phys. **120**, 917 (2008)
516. X.B. Wang, G.X. Dong, Z.C. Gao, Y.S. Chen, C.W. Shen, Phys. Lett. B **790**, 498 (2019)
517. R. Bijker, F. Iachello, Nucl. Phys. A **957**, 154 (2017)
518. Y. Funaki, Phys. Rev. C **97**, 021304(R) (2018)
519. Y. Funaki, Eur. Phys. J. A **57**, 14 (2021)
520. C. Halcrow et al., Phys. Rev. C **95**, 031303(R) (2017)
521. N. Itagaki, A. Toshaki, Phys. Rev. C **97**, 014304 (2018)
522. Y. Kanada-En'yo, Phys. Rev. C **96**, 034306 (2017)
523. Y. Suzuki, W. Horiuchi, Phys. Rev. C **95**, 044320 (2017)
524. B.-S. Huang, Y.-G. Ma, W.-B. He, Eur. Phys. J. A **53**, 119 (2017)
525. T. Fukui, Y. Kanada-En'yo, K. Ogata, T. Suhara, Y. Taniguchi, Nucl. Phys. A **983**, 38 (2019)
526. S.-I. Ando, Phys. Rev. C **97**, 014604 (2018)
527. Y.V. Orlov, Nucl. Phys. A **1014**, 122257 (2021)
528. R.J. Charity et al, Phys. Rev. C **104** 024325 (2021)
529. L.D. Blokhintsev, A.S. Kadyrov, A.M. Mukhamedzhanov, D.A. Savin, Eur. Phys. J. A **58**, 257 (2022)
530. P. Vaandrager, S.A. Rakityansky, Nucl. Phys. A **992**, 121627 (2019)
531. Y. Kucuk, A. Soylu, L.C. Chamon, Nucl. Phys. A **994**, 121665 (2020)
532. S. Son et al., Phys. Rev. C **106**, 055807 (2022)
533. Y. Kanada-En'yo, Y. Shikata, Phys. Rev. C **100**, 014301 (2019)
534. Y. Kanada-En'yo, K. Ogata, Phys. Rev. C **99**, 064601 (2019)

535. C.-C. Guo et al., Phys. Rev. C **99**, 044607 (2019)
536. Y.-A. Li et al., Phys. Rev. C **102**, 054907 (2020)
537. K. Li et al., Phys. Rev. C **95**, 031302(R) (2017)
538. M. Barbui et al., Phys. Rev. C **98**, 044601 (2018)
539. S. Manna et al., European Physical Journal A **57**, 286 (2021)
540. S. Adhikari et al., J. Phys. G Nucl. Part. Phys. **44**, 015102 (2017)
541. N. Phuc et al., Phys. Rev. C **98**, 024613 (2018)
542. S. Ohkubo et al., Phys. Rev. C **96**, 024607 (2017)
543. A. Saxena, P.C. Srivastava, J. Phys. G Nucl. Phys. **47**, 055113 (2020)
544. J. Svenne et al., Phys. Rev. C **95**, 034305 (2017)
545. D. Carbone et al., Phys. Rev. C **95**, 034603 (2017)
546. S. Mezhevych et al., Phys. Rev. C **95**, 034607 (2017)
547. B. Guo et al., Astrophys. J. **756**, 193 (2012)
548. T. Baba, M. Kimura, Phys. Rev. C **100**, 064311 (2019)
549. Y. Shikata, Y. Kanada-En'yo, Phys. Rev. C **103**, 034312 (2021)
550. B. Yang et al., Phys. Rev. C **99**, 064315 (2019)
551. M.L. Avila et al., Phys. Rev. C **90**, 024327 (2014)
552. S. Pirrie et al., Phys. Rev. C **102**, 064315 (2020)
553. S. Pirrie et al., Eur. Phys. J. A **57**, 150 (2021)
554. S. Cristallo et al., Astron. Astrophys. **570**, A46 (2014)
555. M. LaCognata et al., Astrophys. J. **805**, 128 (2015)
556. M. LaCognata et al., Phys. Rev. C **99**, 034301 (2019)
557. A. Volya et al., Phys. Rev. C **105**, 014614 (2022)
558. V.Z. Goldberg, Phys. Rev. C **105**, 014615 (2022)
559. D. Torresi et al., Phys. Rev. C **96**, 044317 (2017)
560. M. Wiescher, J. Görres, E. Uberseder, G. Imbriani, M. Pignatari, Annu. Rev. Nucl. Part. Sci. **60**, 381 (2010)
561. M. Sajedi, Z. Kargar, Nucl. Phys. A **1015**, 122314 (2021)
562. T. Baba and M. Kimura, Phys. Rev. C **102** 024317 (2020)
563. M. Barbui et al., Phys. Rev. C **106**, 054310 (2022)
564. M. Nakao et al, Phys. Rev. C 98 (2018) 054318
565. A. Volya, M. Barbui, V.Z. Goldberg, G.V. Rogachev, Commun. Phys. **5**, 322 (2022)
566. R. Bijker, F. Iachello, Nucl. Phys. A **1006**, 122077 (2021)
567. D. Bai et al., Phys. Rev. C **99**, 034305 (2019)
568. P. Marević, J.P. Ebran, E. Khan, T. Nikšić, D. Vretenar, Phys. Rev. C **97**, 024334 (2018)
569. T.T. Ibrahim et al., Phys. Rev. C **99**, 064332 (2019)
570. E. Yuksel et al., Phys. Rev. C **106**, 054309 (2022)
571. F. Mercier et al., Phys. Rev. C **103**, 024303 (2021)
572. M. Kaur et al., Phys. Rev. C **95**, 014611 (2017)
573. K. Yoshida et al., Phys. Rev. C **98**, 024614 (2018)
574. K. Yoshida et al., Phys. Rev. C **100**, 044601 (2019)
575. Y. Kanada-En'yo, K. Ogata, Phys. Rev. C **101**, 064308 (2020)
576. A.C. Dreyfuss et al., Phys. Rev. C **102**, 044608 (2020)
577. D. Nauruzbayev et al., Phys. Rev. C **96**, 014322 (2017)
578. C. Laymon et al., Phys. Rev. C **45**, 576 (1992)
579. M. Frosini et al., Eur. Phys. J. A **58**, 63 (2022)
580. R. Bijker, F. Iachello, Nucl. Phys. A **1010**, 122193 (2021)
581. A.K. Nurmukhanbetova et al., Phys. Rev. C **100**, 062802(R) (2019)
582. A. Best et al., Phys. Rev. C **87**, 045805 (2013)